COMENIUS UNIVERSITY IN BRATISLAVA
FACULTY OF MATHEMATICS PHYSICS AND INFORMATICS

AND

UNIVERSITY OF SCIENCE AND TECHNOLOGY LILLE 1

The Lattice Dynamics of Lead Chalcogenides

2011

Ondrej Kilián Mgr.

UNIVERSITY OF SCIENCE AND TECHNOLOGY LILLE 1

École doctoral Sciences Pour L'Ingénieur Université Lille Nord-de-France - 072

The Lattice Dynamics of Lead Chalcogenides

Dissertation Thesis

Jury:

Dr. Valerio OLEVANO	Prof. Peter BALLO
RNDr. Anton ŠURDA	Prof. Štefan MATEJČÍK
Prof. Stefan ROTTER	Prof. Thomas PICHLER
Prof. Jozef NOGA	Doc. Pavol BAŇACKÝ

Date of defence:	September 2011
Study programme:	Electronics and communication engineering
Study field:	Physics
Department:	Department of Experimental Physics Faculty of Mathematics Physics and Informatics Comenius University, Bratislava Slovakia Department ISEN, Physics Group Institute of Electronics, Microelectronics, and Nanotechnology, CNRS-UMR 8520, Lille, France
Director of thesis:	Pavel Veis prof. RNDr CSc. (FMPI CU) Ludger Wirtz Dr. habil., CNRS CR1 (IEMN, USTL)

Lille 2011

Ondrej Kilián Mgr.

COMENIUS UNIVERSITY IN BRATISLAVA
FACULTY OF MATHEMATICS PHYSICS
AND INFORMATICS

registration number:
812df134-a5b5-4940-9c69-dfde9150c01d

The Lattice Dynamics of Lead Chalcogenides

Dissertation Thesis

Study programme:	Plasma Physics
Study field:	4.1.6 Plasma Physics
Department:	Department of Experimental Physics Faculty of Mathematics Physics and Informatics Comenius University, Bratislava Slovakia Department ISEN, Physics Group Institute of Electronics, Microelectronics, and Nanotechnology, CNRS-UMR 8520, Lille, France
Director of thesis:	Pavel Veis prof. RNDr CSc. (FMPI CU) Ludger Wirtz Dr. habil., CNRS researcher CR1 (IEMN)

Bratislava 2011

Ondrej Kilián Mgr.

Univerzita Komenského v Bratislave
Fakulta matematiky, fyziky a informatiky

ZADANIE ZÁVEREČNEJ PRÁCE

Meno a priezvisko študenta: Mgr. Ondrej Kilián
Študijný program: fyzika plazmy (Jednoodborové štúdium, doktorandské III. st., denná forma)
Študijný odbor: 4.1.6. fyzika plazmy
Typ záverečnej práce: dizertačná
Jazyk záverečnej práce: anglický

Názov: The Lattice Dynamics of Lead Chalcogenides

Literatúra: W. Jantsch, A. Bussmann-Holder, H. Bilz, and P. Vogl, Dynamical Properties of IV-VI Compounds, Springer Tracts in Modern Physics Vol. 99 (Springer, Berlin Heidelberg, 1983).

Cieľ: The goal of the thesis is to understand the anomalous behaviour of the longitudinal optical mode of lead salts at the Brillouin-zone center for which previously several conflicting theories were developped. Furthermore, the goal is to accompany Raman spectroscopy measurements of lead salt nanocrystals as a function of the crystal diameter.

Anotácia: Anotation: We present calculations of the phonon dispersion relations for the three lead chalcogenides PbS, PbSe, and PbTe using density-functional theory. The pronounced minimum of the transverse optical branch at Gamma due to the near-ferroelectricity of the lead chalcogenides is qualitatively reproduced. In addition, we find a pronounced dip in the longitudinal optical branch at the zone-center which we explain as a "near Kohn anomaly" which is associated with the small electronic band-gap at the high- symmetry point L. Furthermore, we explain the dependence of the Raman spectra of lead salt nanocrystals on the diameter. Our calculations help to understand electron-phonon coupling in these materials which play an important role in infra-red detection and, possibly, in future light emitting and harvesting devices.

Školiteľ: prof. RNDr. Pavel Veis, CSc.
Školiteľ: Dr. Ludger Wirtz

Spôsob sprístupnenia elektronickej verzie práce:
bez obmedzenia

Dátum zadania: 22.10.2010

Dátum schválenia: 22.10.2010

prof. RNDr. Štefan Matejčík, DrSc.
garant študijného programu

študent

školiteľ, školiteľ

Acknowledgment

I would like to thank all the people who helped me during my studies and especially to my tutors who supported me on my crusade:

Ludger Wirtz *Pavel Veis*
Christophe Delerue *Viktor Martišovitš*

Abstract - English

Key words: *ab-initio calculations, lead chalcogenides, phonons, phonon confinement*

We present *ab-initio* phonon dispersion relations for the three lead chalcogenides PbS, PbSe, and PbTe. The acoustic branches are in very good agreement with inelastic neutron-scattering data. Also calculations of the specific heat give good agreement with experimental data. The pronounced minimum of the transverse-optical (TO) branch at Γ due to the near ferroelectricity of the lead chalcogenides is qualitatively reproduced. In addition, we find a pronounced dip in the longitudinal-optical (LO) branch at Γ. This dip was previously explained as the effect of "free carriers" due to the presence of impurities. The calculations demonstrate that it persists also in the case of pure lead chalcogenides. We explain the dip as a "near Kohn anomaly" which is associated with the small electronic band gap at the high-symmetry point L. We show that this band-gap can be reduced to zero upon compression of the crystal lattice constant by 1.8%. In this case, the conduction and valence bands at L display a linear crossing, the TO and LO mode at Γ are degenerate, and a very pronounced Kohn anomaly in the LO mode occurs. Furthermore, we have given theoretical and computational support for the interpretation of the diameter dependence of the Raman spectra of lead selenide nanocrystals. The first order Raman peak at about 136cm^{-1} and its second order overtone at twice this wave number move up in energy with decreasing nanocrystal radius. We interpret this anomalous behavior in terms of quantum confinement of the longitudinal optical (LO) phonon. This interpretation is validated by *ab-initio* calculations of the phonons of PbSe slabs with up to fifteen layers, taking into account the effects of dielectric embedding. The LO mode perpendicular to the slab shifts indeed upwards with decreasing layer thickness. Our work provides the starting point for the investigation of electron-phonon coupling in bulk and nanocrystalline lead chalcogenides, which should help to better understand the photon absorption mechanisms and the use of these materials in light-harvesting and light-emitting devices.

Abstract - French

Mots-clefs : calculs ab-initio, chalcogénures de plomb, phonons, confinement de phonons

Nous présentons ici les dispersions de phonons calculées de manière Ab-initio pour les trois chalcogénures de plomb PbS, PbSe et PbTe. Les branches acoustiques obtenues sont en très bon accord avec les expériences d'IXS ("Inelastic Neutron Scattering" – spectroscopie par diffraction inélastique de neutrons). La chaleur spécifique calculée concorde elle aussi avec les résultats expérimentaux. Enfin, le minimum particulièrement marqué de la branche optique transverse (TO) en Gamma induit par la quasi-ferroélectricité est reproduit de manière qualitative. Par ailleurs, nous observons dans nos calculs une chute prononcée sur la branche optique longitudinale (LO) en Gamma. Par le passé, cette baisse était associée à l'écrantage du champs électrique (associé au mode LO) par des porteurs libres suite à la présence d'impuretés. Mais nos calculs montrent que cela persiste même dans le cas de cristaux parfaits de chalcogénures de plomb. Nous expliquons cette chute comme une "quasi-Anomalie de Kohn" associée au faible gap électronique au point de haute symétrie L. Nous montrons que ce gap peut être réduit à zéro à la suite d'une compression de 1.8% de la constante de maille du cristal. Dans ce cas, les bandes de conduction et de valence montrent un croisement linéaire, les modes TO et LO en Gamma sont dégénérés, et une Anomalie de Kohn très forte apparaît sur le mode LO. Nos travaux apportent par ailleurs un support théorique pour l'interprétation des spectres Raman en fonction du diamètre des nanocristaux de séléniure de plomb (PbSe). En effet, le pic Raman de premier ordre se situe aux alentours de 136 cm^{-1} (et le pic de second ordre est situé au double de cette fréquence). Ils se décalent vers le haut avec la réduction du diamètre du nanocristal. Nous interprétons ce comportement inhabituel comme un confinement quantique du phonon optique longitudinal (LO). Cette hypothèse est validée par les calculs ab-initio des phonons de films de PbSe, avec une épaisseur allant jusqu'à 15

couches. Ces calculs tiennent compte des effets causés par l'environnement diélectrique. Le mode LO orienté perpendiculairement aux films est en effet décalé vers le haut en fréquences lorsque l'épaisseur des couches se réduit. Notre travail propose un point de départ à l'investigation du couplage électron-phonon dans le matériau massif et dans les nanocristaux de chalcogénures de plomb. Ceci pourra contribuer à une meilleure compréhension des mécanismes d'absorption de photons et à l'utilisation de ces matériaux pour les dispositifs d'émission et d'absorption de lumière.

Abstract - Slovak

Kľúčové slová: *ab-initio výpočty, olovnaté chalkogenidy, fonóny, uväznenie fonónov*

V tejto práci prezentujeme *ab-initio* disperzné vzťahy fonónov troch olovnatých chalkogenidov PbS, PbSe a PbTe. Akustické vetvy sa veľmi dobre zhodujú s výsledkami neelastického rozptylu neutrónov, rovnako ako výpočty špecifického tepla, ktoré zodpovedajú experimentálnym dátam. Kvalitatívne popisujeme výrazné minimum transverzálnej optickej (TO) vetvy v bode Γ, ktoré je spôsobené kvázi ferroelektrickými vlastnosťami olovnatých chalkogenidov. Taktiež sme zaznamenali výrazný pokles longitudinálnej optickej vetvy (LO) v bode Γ. Pôvod anomálie bola pripisovaný voľným nosičom, ktoré pochádzajú z prítomnosti nečistôt v materiáli. Naše výpočty ukazujú, že obrátený pík pretrváva aj v prípade čistých olovnatých chalkogenidov. Pokles LO módu vysvetľujeme ako „kvázi Kohnovú anomáliu“, ktorá súvisí s úzkym zakázaným pásmom v bode vysokej symetrie L. Ukázali sme, že zakázané pásmo môžeme zredukovať na nulu zmenšením mriežkovej konštanty o 1,8%. Vodivostné a valenčné pásmo potom vykazujú lineárne kríženie, TO a LO módy sú v bode Γ degenerované a v LO vetve vznikne silná Kohnová anomália. Okrem toho sme prispeli teóriou a výpočtami k interpretácii závislosti Ramanovho spektra nanokryštálov PbS od ich priemeru. Energia Ramanovho píku prvého rádu 136cm^{-1} a druhého rádu stúpne s klesajúcim polomerom nanokryštálu. Toto nezvyčajné správanie vysvetľujeme v rámci kvantového uväznenia longitudinálneho optického (LO) fonónu, čo sme overili *ab-initio* výpočtami fonónov PbSe dosiek v rozmedzí 6-15 vrstiev. Frekvencia LO módu, ktorý je kolmý k posunu dosiek, stúpa s klesajúcou hrúbkou vrstiev. Naša práca predstavuje počiatočný bod pre ďalší výskum elektrón-fonónovej interakcie v masíve a nanokryštáloch olovnatých chalkogenidov, pričom môže dopomôcť k tomu, aby sme lepšie pochopili mechanizmus fotónovej absorpcie týchto materiálov použitých v zariadeniach pohlcujúcich, alebo emitujúcich svetlo.

Table of Contents

Table of Contents

Introduction

Lead chalcogenides are outstanding materials with a complex nature and very interesting properties. They offer a great potential for modern technology. But, surprisingly, even at present time, their electronic and vibrational properties are not yet fully understood.

Lead chalcogenides (PbS, PbSe, PbTe) are IV-VI materials with a narrow electronic band gap between 280 and 410 meV in the bulk phase[1], making them a good medium for infrared optoelectronic devices. Through the 20th century they were leading materials in the IR detector technology covering the spectral range from 1.5–5μm and exhibiting high detection ability even at room temperature, exceeding thus other materials in performance and practical applications (mostly in army technology). The large potential of IV-VI rock salt structures initiated intensive research of their properties through the middle of the last century and efficient crystal growth procedures[2,3] were developed. Historically, the main focus was on PbTe as it has a very high dielectric constant (ε=32.6[4]), near ferroelectric behavior (manifesting itself in the low frequency of the transverse optical mode[5]) and it's ternary alloys have very interesting properties. E.g., in lead tin telluride ($Pb_{1-x}Sn_xTe$) one can manipulate the gap by changing the compound ratio[6] and thus tune the spectral detection range. And in the $Pb_{1-x}Ge_xTe$ compound, already a small admixture of germanium (x=0.005) leads to a ferroelectric phase transition from the rock-salt structure (at high temperature) to the rhombohedral configuration (at low temperature)[7]. The potential of lead chalcogenides, however, does not end with the IR technology of the 20th century. Their nanocrystalline form, discovered around three decades ago[8,9], opens a wide field of applications in light emission and light harvesting.

The small electronic band gap of the lead salts (280 – 410meV at room temperature)[1], a large exciton diameter[10] (e.g., 20nm in PbS and 46nm in PbSe) and small effective electron and hole masses lead to pronounced quantum confinement effects[10,11] in nanocrystals of the lead salts. Through quantum confinement, the gap of the nanocrystal

can be tuned by changing the size of the crystal. For instance, PbS nanodots have a variable gap from 0.67eV to 1.08eV in the crystal size range of 8nm–4nm[12]. During the fabrication process of nanocrystals one can precisely control their size and shape[13] and thus prepare a medium with exact optical properties, like a recently constructed[14] infrared diode laser based on PbSe/PbEuTe quantum dots. In addition to the size tunable optical properties, nanocrystals display strong luminescence. Thanks to these properties lead salt nanocrystals found quickly applications as infra-red colorant dye, as it's very convenient to use one strongly fluorescent medium for several colors instead of different rare earth ions (Erbium, Thulium, Ytterbium…).

The transition from bulk to nanocrystals brought also into play several important effects, originally with marginal occurrence becoming dominant in the NC phase. Recent studies[15] indicate that PbSe nanocrystals might be good candidates for high-efficient solar cells. Impact ionization (an electron-hole pair with large energy decays into several electron-hole pairs with lower energy) becomes more probable at the nano level and efficient carrier multiplication occurs. This could lead to solar cells based on lead salt nanocrystals with high energy conversion rate, theoretically up to 60,3%[15]. The potential of lead chalcogenides nanocrystals in optoelectronics, colorant technology or solar energy conversion stimulated in recent years the scientific community and lots of efforts was made to understand these promising materials. However there are still gaps in the exact understanding of all properties of their nanocrystalline and bulk phase. In order to fully understand the de-excitation of hot carriers – in particular, the ratio of radiative versus non-radiative decay channels and the mechanisms of line broadening – it is necessary to learn more about the electron-phonon coupling in lead chalcogenides. While high-quality calculations of the electronic bands are available (Ref.[16] and references therein), the understanding of the phonon dispersion of the lead chalcogenides is much less complete. Experimentally, phonon dispersion relations of PbS, PbSe, and PbTe were obtained by inelastic neutron scattering measurements[17,18,19]. Simulations of the phonon dispersions have been done so far mainly on the level of the semi-empirical shell model[20,21,22,23]. The three compounds have, as expected, a similar phonon dispersion and display an interesting

phonon softening of the longitudinal optical (LO) mode around the Γ point. Different explanations were proposed for the LO dip. Cowley and Dolling[22] attributed the dip to screening by free carriers in the crystal. A term for free carrier doping was consequently introduced in the recent semi-empirical phonon calculations by Upadhyaya *et al.*[20]. Maksimenko and Mishchenko[23] explain the LO dip by the dipolar pseudo-Jahn-Teller effect[21]. Recent *ab-initio* calculations of the phonon dispersions of PbS, PbSe, and PbTe[24] displayed a minimum of the LO mode at Γ which (for PbSe and PbTe) turned into a strongly pronounced dip when spin-orbit coupling was taken into account. The reason for the strong dip enhancement, however, remained open.

In this work we present a systematic *ab-initio* study of the phonon dispersion relations of the three lead chalcogenides. The small gap and the near-ferroelectric behavior demand a careful choice of calculation parameters such as sampling grid and pseudopotentials. Our calculations reproduce quantitatively the acoustic modes. The anomalies of LO and TO (transverse optical) modes are qualitatively reproduced in the calculations (since they are strongly temperature dependent[23], anharmonic effects would have to be taken into account in order to quantitatively reproduce the measurements which were performed at room temperature). Our calculations show that a pronounced LO dip is present in the pure materials even without free carrier doping. We explain this dip in analogy to the Kohn anomalies[25] that occur in the semi-metal graphene[26]. Furthermore, we demonstrate that *ab-initio* calculations can reproduce very well the specific heat of PbS, PbSe, and PbTe and compare with recent calculations[24,27] that include the effect of spin-orbit effects. We also present *ab-initio* LO phonon frequency calculations for PbSe slabs of various thickness. These calculations explain recent Raman spectroscopy experiments[28] in which the diameter dependence of the peaks was measured and blue shift of the dominant (LO mode related) peak with decreasing nanocrystal radius was observed.

Outline:

The thesis is organized into IV. chapters. In chapter "I. Lead chalcogenides" we introduce the three materials we have been studying, presenting their main characteristics, short history and a separate sub chapter for nanocrystals. In "II. Calculation Methods" we explain the theoretical background and calculation methods in the framework of density functional theory. Furthermore we show several concepts and procedures used in computational physics to enhance the calculations. The results of our work are summarized in chapter "III. Results and discussion"; we show our *ab-initio* calculated dispersion relations for lead chalcogenides, compare them to neutron scattering experimental data and propose an explanation of the LO mode softening of the gamma phonon in terms of a "near-Kohn" anomaly. Furthermore, we use the obtained phonon dispersions to calculate specific heat and compare it to experimental data. In the final part we present calculations of optical frequencies of gamma phonon of PbSe slabs and compare them to recent Raman-spectroscopy data of PbSe nanocrystals. We also present a study on the choice of k-point sampling used in the calculation process of the phonon dispersions which influences the correct results for the longitudinal optical mode at Γ. The thesis end with" IV. Conclusion", where we summarize our work and present future perspectives based on this work.

I. Lead chalcogenides

I.1 Origin and short history

Lead chalcogenides (PbS, PbSe, PbTe) are IV-VI narrow gap semiconductor compounds with rock salt crystal structure. In nature they are found as *galena* (PbS), *clausthalite* (PbSe) and *altaite* (PbTe)[29]. The oldest known is *galena*, lead sulfide (PbS), a silvery lead gray mineral which often contains large amount of silver and therefore is very important for silver mining. Lead selenide (PbSe) is a lead-gray mineral discovered in the locality of Clausthal-Zellerfeld in the Harz Mountains (1832) in Germany and therefore named *clausthalite*. In a similar way lead telluride (PbTe), a yellowish white mineral, received his name *altaite* after the Altai Mountains in central Asia in 1845.

galena

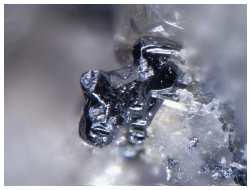

clausthalite

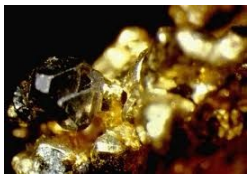

altaite

	Lead Sulfide (PbS)	Lead Selenide (PbSe)	Lead Telluride (PbTe)
name of the mineral	galena	clausthalite	altaite
elements	sulfur 16, lead 82	selenium 34, lead 82	tellurium 16, lead 82
crystalline structure	fcc	fcc	fcc
lattice constant	5.9362 Å [30]	6.1260 Å[31]	6.4620 Å[32]
gap	410 meV	280 meV	310 meV

***Table I.1**: Material properties of lead chalcogenides*

In the history of mankind we can trace their usage already to Ancient Egypt, 5500 years ago, when galena was mixed in *kohl*, soot with other ingredients, which women traditionally applied on their eyelids and eyelashes as mascara[33]. Surprisingly galena is still used in 1/3 of kohl despite the known toxicity of lead[34].

kohl

In modern science, lead chalcogenides made their name in several fundamental discoveries. In 1847 a German physicist, *Ferdinand Braun,* discovered the electrical point-contact rectification effect. He measured the characteristics of certain electrolytes and crystals and by probing a galena crystal with a thin wire he noticed that the current flowed only in one direction. He presented this semi-conductor device in 1876 in Leipzig, but it had no useful application until the 1900's in first radio devices.

Ferdinand Braun

During 1894-1898 *Sir Jagadish Chandra Bose* developed the so called *Galena detector* and demonstrated it in the Royal Institution Discourse in 1900. It was composed of a lead sulfide crystal, two wires in point contact (cat whiskers) connected in series with a source, and a galvanometer. It was the first radiation detector and the first semiconductor device in the world.

Sir Jagadish Chandra Bose

Lead sulfide came into play during the Second World War as the base medium for the first usable IR detectors, practically starting the mass implementation of IR technology. The PbS detectors were sensitive in the infrared region of 1.5–3μm and therefore deployed in various military devices, like night vision or early missile guidance systems. In the 40's and 50's new materials were developed and investigated for applications in IR detection

technology. The other two lead salts (PbSe, PbTe) were implemented increasing the detection capability to 3–5μm. Typical lead salt detectors were polycrystalline and relatively easy to produce by vacuum evaporation and chemical deposition from a solution, followed by a post-growth sensitisation process[3]. At the same time detectors based on InSb (one of the first newly discovered III–V semiconductor compounds) were developed with spectral range similar to PbS and PbSe. In the beginning of 60's Lawson *et all.*[35] introduced a new revolutionary type of narrow gap semiconductor materials – *ternary alloys* – with HgCdTe (MCT) as the first representative. The new material systems had a tunable gap by changing the ratio of the elements admixture, and thus semiconductor alloys like III–V ($InAs_{1-x}Sb_x$), IV–VI ($Pb_{1-x}Sn_xTe$) and II–VI ($Hg_{1-x}Cd_xTe$) allowed to construct detectors for the whole infrared spectrum. In 1960's photolitography was developed and used to construct an IR sensor array. The technology was first demonstrated in PbS, PbSe and InSb detectors but further applied on the new MCT materials who started to dominate in the IR technology.

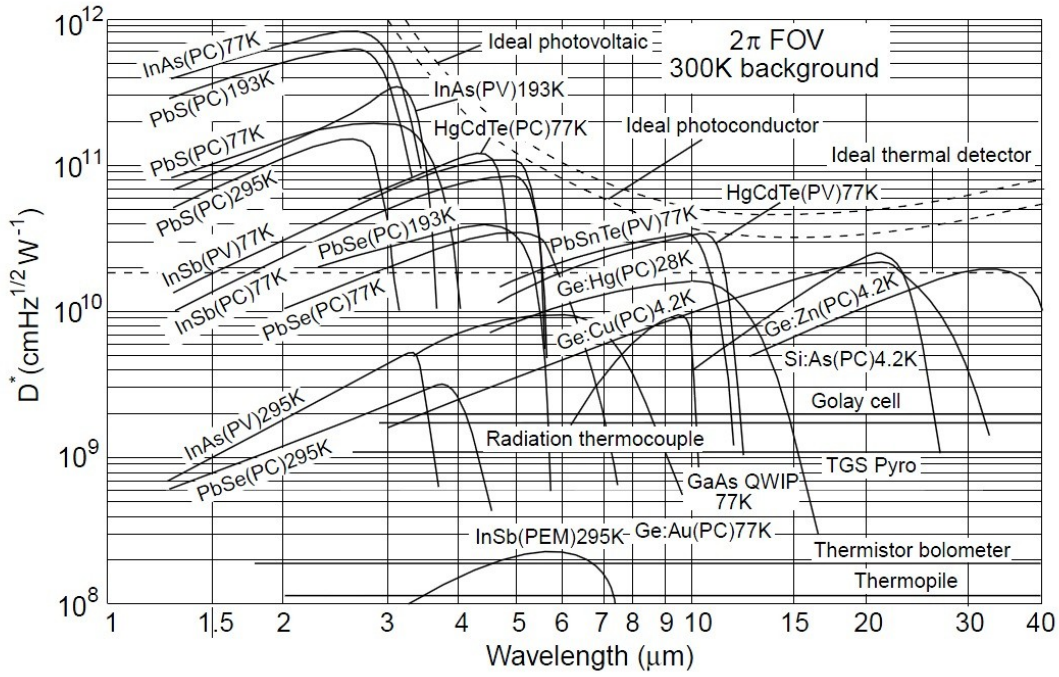

***Figure** I.1: Comparison of commercially avalable infrared detectors by A. Rogalski[36], showing detection D* curves (black lines) over the infra red spectral range operating at indicated temperature. PC denotes photoconductive type of detectors, PV – photovoltaic and PEM – photoelectromagnetic. The dashed curves represent theoretical ideal detectors.*

I.Lead chalcogenides

Lead chalcogenides dominated in the infrared detection technology over the half of the 20th century, mainly implemented in army technology as night vision devices, missile guidance systems and anti-missile detection technology. Their main advantage over other materials with similar detection region (InSb) was a good detection ability even without extensive cooling (see comparison of detectivity D*, a measure of the intrinsic quality of the detector material itself, of IR detectors by A. Rogalski[36] Figure I.1), allowing for example miniaturized night vision devices. Furthermore, cooled lead salts have one of the best detection abilities in their spectral range and a very fast response speed[37].

Mainly because of their potential in infrared technology, lead chalcogenides were heavily studied through the middle of 20th century[38]. The research was focused on optical and electrical properties[4], especially the band structure[39], ohmic transport[40], high-field transport[41], magneto-optic properties[42,43] and electronic states of defects[44,45]. Experiments on lead salts and their ternary alloys revealed several interesting properties. Lead telluride and $Pb_{1-x}Sn_xTe$ compounds had an anomaly high dielectric constant, depending on temperature and alloy composition, pointing to soft-mode behavior and a possible ferroelectric structural transition[5]. Another outstanding property of the $Pb_{1-x}Sn_xTe$ alloy is the fact that by adjusting x, the gap can be tuned and even be brought down to zero[6]. This makes it especially attractive for infrared source and detection technology[46,47,48] as it allows to optimize the medium for a specific wavelength region.

The lead chalcogenides have a very unusual phonon dispersion behavior. Neutron scattering experiments[17,18] showed a pronounced phonon softening of the transverse optical mode and an inverse peak (kink) of the longitudinal optical mode at the center of the Brillouin zone. Cowley and Dolling[23] proposed that this phenomenon is caused by the screening of the macroscopic electric field accompanying the LO mode by free carriers which may have their origin by doping from impurities. An alternative theory was proposed by Maksimenko and Mischenko[23] , explaining the LO mode anomaly as due to the pseudo-Jahn-Teller effect (in absence of free-carrier doping). In a recent semi-empirical calculation of the phonon dispersions of the lead chalcogenides[20] the free carrier doping

was used to improve the fit. The exact origin of the LO dip at Γ has thus remained an open issue and its clarification is a major goal of this thesis.

I.2 Nanocrystals

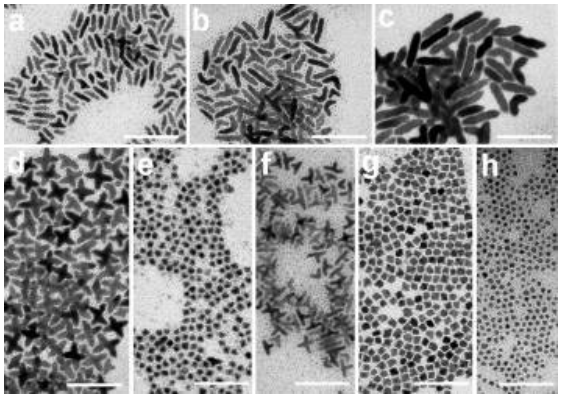

PbSe nanocrystals

In the 80's of the last century a new form of crystals, quantum dots, was discovered by Alexey I. Ekimov[8] (CuCl in glass matrix) and Louis E. Brus[9] (CdS colloidal solutions). Quantum dots, also called nanocrystals, are small crystalline semi-conductors composed of several hundreds to several thousands of atoms, with electric and optical properties tunable by size. Moreover, in some semiconducting materials, specific effects like direct impact ionization that have a small occurrence in bulk material become enhanced in nanocrystals. Thus semiconducting nanocrystals opened a huge field of research and gave rise to new potential applications also for the lead chalcogenides. A possible use of nanocrystals is as colorant dyes in biology and medicine. Furthermore, many optoelectronics applications can be envisioned, e.g., as highly efficient laser diodes. Last but not least, nanocrystals may constitute a new material for solar energy conversion.

a) Quantum confinement

By decreasing the size of a semiconductor until its dimensions are comparable to the de Broglie wavelength of electrons one restricts the electron's movement. This phenomenon is called quantum confinement. It leads to the discretization of the energy

spectrum of the electrons. Energy levels depend on the crystal size which can be controlled very precisely. Thus in the fabrication process of semiconductor nanocrystals, the band gap (and the energy of an emitted or absorbed photon) can be tuned with high accuracy.

The effect of quantum confinement is easily understandable in the model of a "*particle in a box"* or *"infinite quantum well"*. In the simplest case, the *1D box,* we imagine a system, where a particle can move only in one direction and in that direction it's movement is restricted to a certain interval, $x \in (0,L)$, by two infinite potential barriers (Figure [I.2]).

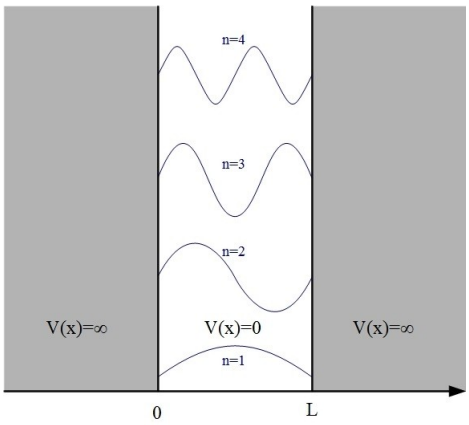

***Figure** I.2: Infinite potential well and first four wavefunctions of a particle in 1D box $\phi_n(x)$*

In Table [I.2] we summarize the solutions of the Schrödinger equation for a free particle and for a particle in a 1D box. The wavefunctions are $\phi_n(x)$ and $\phi_k(x)$ with discrete eigenenergies E_n or a continuum of possible energies $E(k)$, respectively. L is the length of the box, m is the particle's mass, n is a positive integer and k is a real number:

Particle in 1D box	Free particle
$\phi_n(x) = \begin{cases} \sqrt{2/L}\sin(\frac{n\pi}{L}x), & 0<x<L \\ 0, \quad outside\,the\,box \end{cases}$	$\phi_k(x) = \frac{1}{\sqrt{2\pi}} e^{ikx}$
$E_n = \frac{\hbar^2\pi^2}{2mL^2}n^2$	$E(k) = \frac{\hbar^2}{2m}k^2$

***Table** I.2: solutions for free particle and particle in a 1D box, illustrated on Figure [I.2]*

The *particle in a box* example nicely shows the fundamental character of quantum confinement: when we restrict the movement of a free particle, the continuous energy spectrum $E \approx k^2$ becomes discrete $E \approx n^2$, $n=1,2,3,\ldots$. Moreover the energy levels depend directly on the dimensions of the confined space (here $1/L^2$) which is an essential property making nanocrystals so attractive for optoelectronic applications as we can precisely control their size. A good example can be found in recent work on size dependable properties of PbS quantum dots by Moreels *et al.*[12] where they study the relation between the gap of the quantum dot and its size. By fitting experimental data[12,13,49] they show that the gap scales according to

$$E_0(d) = 0.41 + \frac{1}{0.0252\mathrm{d}^2 + 0.283\mathrm{d}}$$

with E_0 representing the gap in *eV* and *d* the diameter of the nanocrystal in *nm* (in the range 3.9-13.3nm). The experimental data[13,49,12] (○,Δ,●) are in accordance with the tight-binding calculations[12,50] (◊,□) both predicting a $\sim 1/d$ dependance, as shown on Figure I.3 (blue line).

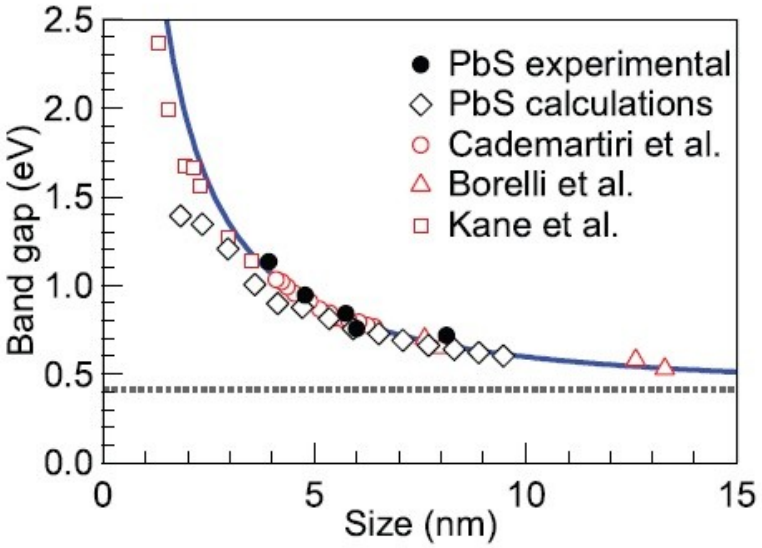

***Figure** I.3: Band gap of PbS nanocrystal as a function of it's size, studied by Moreels et al.[12]. Empirical fit (blue line). Experimental data: Cademartiri et all.[13] (○), Borrelli et all.[49](Δ) and Moreels et al.[12] (●). Tight-binding calculations: Moreels et al.[12] (□), Kane et al.[50] (□). PbS bulk gap walue (dotted line)*

b) Nanocrystal applications

In recent years nanocrystals were used as colorants in biological analysis instead of organic dyes for fluorescent imaging. Nanocrystals are more flexible due to their size tunable optical properties and they are more stable. It's more convenient in experiments to use the same substance as a colorant for various wavelengths as to use different substances for each color like rare earth ions (Erbium, Thulium, Ytterbium…). For exemple CdSe quantum dots emit by fluorescence from blue (diameter 2.5 nm) to red light (diameter 5.5nm)[51,52]. Also due to their high quantum yield they are brighter than the classical colorants. Another advantage is the low cost of their fabrication and their non toxicity in some cases. In spite of mentioned advantages of nanocrystals their use for florescent imaging was first hampered, because they were insoluble in aqueous media. This drawback was solved by a surface treatment of the CdSe nanodots; various layers were added to form composed soluble nanocrystals, for instance CdSe/CdS or CdSe/ZnS[53,54,55]. Another obstacle could be the toxicity of q-dots which could disturb *in-vivo* experiments. However toxicity wasn't observed in live animals even in embryos under standard conditions[56].

***Figure** I.4: CdSe NC colorants*[52]

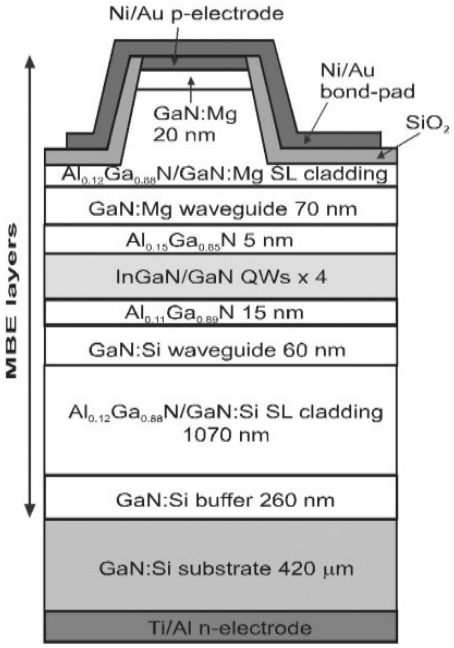

***Figure** I.5: blue LED based on InGaN q-dots presented by N. Nakamura et all..*[57]

Nanocrystals are quasi zero-dimensional therefore the density of state is sharper. This implies superior optical and transport properties, which makes them good adepts for diode lasers. By synthesis of InGaN quantum dots it was possible to build an efficient miniaturized blue laser[57,58] and implement them as the Blu-ray Disc technology[59], a high information density medium that surpasses the well-known DVD by a factor of five.

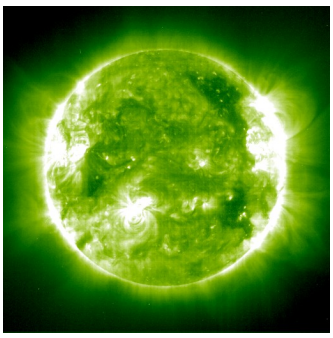

Nowadays the conventional solar cells convert from 15% to 30% of the light they absorb into electrical energy. Theoretically the maximum conversion efficiency is 43,9%. This calculation was based on the hypothesis that only a part of the absorbed photon's energy is used to create an electron-hole pair (exciton) which can recombine by passing through an external electrical circuit. The excess energy is lost in interactions between the electron and the crystal lattice. The carrier multiplication effect uses this excess energy to excite more electrons and thus we could surpass the maximum conversion limit. Carrier multiplication by impact ionization is an effect, when one photon excites two or more electrons in the conduction band. A photon with energy at least twice the gap excites an electron to a level much higher than the last unoccupied molecular orbital (LUMO). The excited electron descends to a lower energy state and excites another electron into the conduction band. In this manner more of the energy from the impacting photon is converted. Carrier multiplication was observed in bulk materials already in the 50's but it wasn't considered strong enough to yield considerable improvements in solar cells . In 2002 Nozik[67] proposed that impact ionization in NCs could enhance the carrier

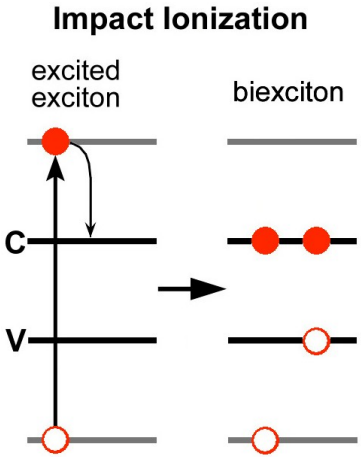

multiplication and end up in higher solar conversion efficiency. In 2004 Klimov and Schaller[15,68] demonstrated that impact ionization occurs in PbSe nanodots with high efficiency and it is a major phenomenon. This could lead to nanocrystal solar cells with power conversion efficiency up to 60,3%. Through the past decade PbSe nanocrystals, as promissing solar technology medium, were intensively studied[60-66] and first prototypes of solar cells were fabricated, the most recent (2010) was a cell with energy conversion factor 4% in laboratory conditions[69].

II. Calculation Methods

II. Calculation Methods

This chapter is devoted to the theoretical background and computational details of our calculations. We will explain how to calculate the equilibrium geometry using density functional theory (DFT) (section II.3) and phonons from the dynamical matrix (section II.1) and how to calculate the dynamical matrix using Density Functional Perturbation Theory (DFPT) (chapter II.4). In order to understand better both theories we give an explanation of what is meant by *ab-initio*, first principles, calculations (section II.2). For historical reasons we present the Schrödinger equation, to show the foundations on which large parts of modern theoretical physics are built. We also review the Hartree-Fock theory for solving many-electron problems.

In the Computational details (section II.5) we will describe the concepts of pseudo-potentials, plane-wave decomposition and special sampling of Brillouin zone and their implementations in the calculations of dynamical matrix with DFT+DFPT.

II.1 Equilibrium geometry, phonons and dynamical matrix.

Our main task was to calculate phonons of lead chalcogenides and as an indispensable part of the investigation we studied the equilibrium geometry of the system. In order to obtain phonons we have to know the so called dynamical matrix. Let us briefly introduce the theory.

The starting point of our calculations is the Schrödinger Equation for the electrons moving in the field of the ions.

$$H_{BO}(\vec{r},\vec{R})\varphi(\vec{r},\vec{R})=E_{BO}(\vec{R})\varphi(\vec{r},\vec{R}) \quad \text{[II.1]}$$

The corresponding Hamiltonian H_{BO} depends on the set of all the nulcear coordinates $\vec{R}$ and acts on the electronic variables:

$$H_{BO}(\vec{r},\vec{R})=-\frac{\hbar^2}{2\mathrm{m}}\sum_i\frac{\partial^2}{\partial\vec{r}_i^{\,2}}+\frac{e^2}{2}\sum_{i\neq j}\frac{1}{|\vec{r}_i-\vec{r}_j|}-\sum_{iI}\frac{Z_I e^2}{|\vec{r}_i-\vec{R}_I|}+\frac{e^2}{2}\sum_{I\neq J}\frac{Z_I Z_J}{|\vec{R}_I-\vec{R}_J|}, \quad \text{[II.2]}$$

where $\vec{R}_I$ is the position of the I-th nucleus, m is the electron mass ($9.9105\text{x}10^{-31}$kg), Z_I is the charge of the I-th nucleus and $-e$ is the charge of an electron ($1.60225\text{x}10^{-19}$C). In the so-called *Born-Oppenheimer approximation*, we assume that the electrons are moving in

the field of fixed nuclei (whose masses are four order of magnitude larger than the electron mass). $E_{BO}(\vec{R})$, the ground-state energy of the system as a function of the nuclear coordinatets is called the *Born-Oppenheimer energy surface* and constitutes the "potential landscape" in which the nuclei move.

The system is at equilibrium when all the forces acting on the nuclei become zero. The geometry of the system at equilibrium is then given by these equations:

$$\vec{F}_I \equiv -\frac{\partial E_{BO}\left(\vec{R}_I\right)}{\partial \vec{R}_I} = 0$$

[II.3]

The vibration frequencies ω are determined from the eigenvalues of the Hessian of the Born-Oppenheimer energy surface, scaled by the nuclear masses:

$$\det\left|\frac{1}{\sqrt{M_I M_J}} \frac{\partial^2 E_{BO}\left(\vec{R}\right)}{\partial \vec{R}_I \partial \vec{R}_J} - \omega^2\right| = 0$$

[II.4]

This Hessian is also referred to as ***dynamical matrix*** or matrix of the interatomic force constants.

The dynamical matrix as a key element for our phonon investigation can be obtained by either semi-empirical methods or by *ab-initio* calculations. The basic idea of semi-empirical methods lies in creating a physically motivated model with several parameters and then fitting these parameters to experimental data. On the other hand we

can calculate *ab-initio* the interatomic force constants which means just by using the fundamental laws of physics and the base information of atomic structure, without any fitting parameters.

The Hellmann-Feynman theorem, dynamical matrix and electronic density.

A standard way to proceed in the investigation of crystal properties is to express the dynamical matrix using the Hellmann-Feynman theorem, as presented in the work of De Cicco and Johnson (1969)[70] and by Pick, Cohen, and Martin (1970)[71]. The **Hellmann-Feynman**[72] theorem, separately proven by H. Hellmann in 1937 and by R.P. Feynman in 1939, is a very useful mathematical tool in quantum mechanics as it gives a relation between the derivative of the total energy with respect to a parameter and the expectation value of the derivative of the Hamiltonian with respect to that same parameter:

$$\frac{d E_\lambda}{d \lambda} = \int \psi^*(\lambda) \frac{d H_\lambda}{d \lambda} \psi(\lambda) d\tau \qquad \text{[II.5]}$$

Where E_λ is the eigenenergy of the wavefunction $\psi(\lambda)$ and H_λ is the Hamiltonian operator, all depending on the continuous parameter λ. The $d\tau$ represents integration over the domain of the wavefunction.

We use the Hellmann-Feynman theorem to relate the gradient of the Born-Oppenheimer energy surface $E_{BO}(\vec{R})$ and the gradient of the corresponding Hamiltonian $H_{BO}(\vec{R})$:

$$\frac{\partial E_{BO}(\vec{R})}{\partial \vec{R}_I} = \int \psi^*(\vec{R}, \vec{r}) \frac{\partial H_{BO}}{\partial \vec{R}_I} \psi(\vec{R}, \vec{r}) d\vec{r} \qquad \text{[II.6]}$$

Where $\psi(\vec{R},\vec{r})$ is the ground state wave function of the Hamiltonian H_{BO} and the vector with the positions of the nuclei, $\vec{R}$ **,** is the continuous parameter. In the Born-Oppenheimer Hamiltonian the terms for the kinetic energy of the electrons and the term for the electron-electron Coulomb interactions are independent of the nuclear positions and therefore vanish from the derivative $\partial H_{BO}/\partial \vec{R}_I$. The remaining terms, depending on $\vec{R}$, are the electron-nucleus interaction term $V_{\vec{R}}(\vec{r})$ and the term describing the Coulomb repulsion between different nuclei, $E_N(\vec{R})$:

$$V_{\vec{R}}(\vec{r}) = -\sum_{iI} \frac{Z_I e^2}{|\vec{r}_i - \vec{R}_I|} \qquad E_N(\vec{R}) = \frac{e^2}{2}\sum_{I\neq J} \frac{Z_I Z_J}{|\vec{R}_I - \vec{R}_J|}$$

[II.7]

The expression for the derivative of the total energy $\partial E(\vec{R}_I)/\partial \vec{R}_I$ can be written as follows, where $n(\vec{R},\vec{r})$ is the ground state electron charge density :

$$\frac{\partial E_{BO}(\vec{R})}{\partial \vec{R}_I} = \int n(\vec{R},\vec{r}) \frac{\partial V_{\vec{R}}(\vec{r})}{\partial \vec{R}_I} d\vec{r} + \frac{\partial E_N(\vec{R})}{\partial \vec{R}_I}$$

[II.8]

Finally the expression for the dynamical matrix is:

$$C := \frac{\partial^2 E_{BO}}{\partial \vec{R}_I \partial \vec{R}_J} = \int n(\vec{R},\vec{r}) \frac{\partial^2 V_{\vec{R}}(\vec{r})}{\partial \vec{R}_I \partial \vec{R}_J} d\vec{r} + \int \frac{\partial n(\vec{R},\vec{r})}{\partial \vec{R}_J} \frac{\partial V_{\vec{R}}(\vec{r})}{\partial \vec{R}_I} d\vec{r} + \frac{\partial^2 E_N(\vec{R})}{\partial \vec{R}_I \partial \vec{R}_J}$$

[II.9]

The main asset of equation [II.9] is the fact, that we can calculate the dynamical matrix ***C*** by knowing only the distribution of the electron charge density $n_R(\vec{r})$, as a function of configuration $\vec{R}$ at the ground state, and knowing the linear response of $n_R(\vec{r})$ to the perturbation of the nuclear geometry $\partial n_R(\vec{r})/\partial \vec{R}_I$. This expression of the dynamical matrix is very helpful for computational physics, because we can calculate the electronic density $n_R(\vec{r})$ and the linear response using density functional theory and density functional perturbation theory as will be shown further in chapters [II.3] and [II.4].

II.2 *Ab-initio* calculations

Ab-initio or first principles calculations are calculations which use only the fundamental laws of physics with only minor approximations to predict electronic, structural or optical properties of a system. A typical *ab-initio* calculation is, for example, solving the Schrödinger equation for the hydrogen atom and obtaining the ground state energy levels, or to calculate phonon dispersion relations using density functional theory. In general, for the quantum-mechanical treatment of many-electron systems, there are two main approaches. The first is the Hartree-Fock approximation proposed in 1930 and the second is the density functional theory by Hohenberg, Kohn and Sham published in 1964. For historical reasons let us briefly introduce the Schrödinger equation and the Hartree-Fock method as they are the roots of on which is built modern computational physics and deserve to be reminded off, then we will proceed to the density functional theory.

The laws of quantum mechanics, according to the Copenhagen interpretation, can be mathematically expressed by the **Schrödinger equation**[73] and by the probability interpretation of the wavefunction.

$$\hat{H}\Psi = -i\hbar\frac{\partial\Psi}{\partial t} \qquad \text{[II.10]}$$

Where $\boldsymbol{H}$ is the Hamiltonian operator representing the energy of the system. Ψ is the wavefunction, a function of electron and nuclear positions, spin and time representing the state of the system. The absolute square of the wavefunction is interpreted as the probability to find an electron at a given coordinate. From this rises the condition, that the

square of the wavefunction must be integrable and finite.

$$\int |\Psi^2| d\tau < \infty \qquad [II.11]$$

The Schrödinger equation is a first order differential equation with respect to the time ***t*** and for a given initial function there exists a unique solution. In other word, by knowing the initial state of a system at time t_0 we know the state of the system at any time ***t***. Unfortunately, the Schrödinger equation can be analytically solved only for a few systems: the harmonic oscillator, the particle in a box, the hydrogen molecular ion, and the hydrogen atom. For other systems, the Schrödinger equation has to be solved numerically. In the case of many-electron systems, this solution can quickly exceed the limits of computational resources. We can, however, use several approximations which allow a simplified solution of the problem.

In computational physics, the **Hartree-Fock** method[74] is, briefly, an approximate method for the determination of the ground-state wavefunction and ground-state energy of a quantum many-body system. The Hartree-Fock method assumes that the exact, N-body wavefunction of the system can be approximated by a single Slater determinant[75] (in the case where the particles are fermions) or by a single product (in the case of bosons) of N spin-orbitals. Solution of these equations yields the Hartree-Fock wavefunction and energy of the system, which are approximations of the exact ones.

More precisely, we want to solve the Schrödinger equation for a many particle wavefunction by introducing a special ansatz in form of Hartree product (example of two particles).

$$\Psi(x_1, x_2) = \chi_1(x_1)\chi_2(x_2) \qquad [II.12]$$

Where ψ is the two-particle wavefunction and χ_1 and χ_2 are one-particle functions corresponding to particle one and two. In the case of electrons (which are fermions), the wavefunction must be antisymmetric and obey the Pauli exclusion principle[76]. In order to anti-symmetrize it we do a linear combination of Hartree products

$$\Psi(x_1,x_2)=\frac{1}{\sqrt{2}}(\chi_1(x_1)\chi_2(x_2)-\chi_1(x_2)\chi_2(x_1))=\frac{1}{\sqrt{2}}det\begin{vmatrix}\chi_1(x_1) & \chi_2(x_1)\\ \chi_1(x_2) & \chi_2(x_2)\end{vmatrix}$$

[II.13]

This product is antisymmetric and becomes zero when the one-particle functions are identical (two identical fermions in a system) and thus satisfies the Pauli exclusion principle. The generalization of such antisymmetric linear combination of Hartree products is the so called Slater determinant:

$$\Psi(x_1,x_2,..,x_N)=\frac{1}{\sqrt{N!}}det\begin{vmatrix}\chi_1(x_1) & \chi_2(x_1) & \cdots & \chi_N(x_1)\\ \chi_1(x_2) & \chi_2(x_2) & \cdots & \chi_N(x_2)\\ \vdots & \vdots & . & \vdots\\ \chi_1(x_N) & \chi_2(x_N) & \cdots & \chi_N(x_N)\end{vmatrix}$$

[II.14]

II.3 Density Functional Theory

"Density functional theory is a clever way to solve Schrödinger equation for a many-body system. In the formulation given by Kohn, Hohenberg and Sham in the 1960's the real system is described by an effective one-body system. To achieve the goal, the complex many-body wave function, which is the solution of Schrödinger equation, is abandoned in favor of the density which only depends in the three spatial coordinates. The energy is just a function of this function, i.e., a density functional." [77]

The basis of density functional theory[78] lies in two theorems stated by Hohenberg and Kohn[79]:

Theorem 1.

"The external potential $v_{ext}(\mathbf{r})$, and hence the total energy, is a unique function of the ground-state electron density."

Theorem 2.

"The ground-state energy can be obtained variationally: the density that minimizes the total energy is the exact ground-state density."

According to these two theorems, we can fully describe a system in its ground-state by only knowing the distribution of the electronic density. The two theorems however don't offer a way to calculate the ground-state density. This was made possible by the new formulation by W. Kohn and L.J. Sham known as density functional theory (DFT). Using

DFT we can transform problem of a system of *N* interacting electron into *N* problems of single electrons moving in a mean field, defined by the Kohn-Sham potential which depends on the electronic density. The Kohn-Sham equations are cast in this form:

$$[\frac{-\hbar^2}{2\mathrm{m}}\frac{\partial^2}{\partial \vec{r}^2}+V_{SCF}(\vec{r})]\psi_n(\vec{r})=\epsilon_n\psi_n(\vec{r})$$

[II.15]

Where $\psi_n(\vec{r})$ are the Kohn-Sham orbitals, ϵ_n are the Kohn-Sham eigenenergies and $V_{SCF}(\vec{r})$ is the Kohn-Sham mean potential (also called the self consistent field). $V_{SCF}(\vec{r})$ is a functional of the electronic density, which is defined as:

$$n(\vec{r})=2\sum_{n=1}^{N/2}\left|\psi_n(\vec{r})^2\right| \qquad [II.16]$$

The potential $V_{SCF}(\vec{r})$ is defined as the sum of the external potential, the Hartree term and the exchange-correlation potential:

$$V_{SCF}(\vec{r})=V(\vec{r})+e^2\int\frac{n(\vec{r}\,')}{|\vec{r}-\vec{r}\,'|}d\vec{r}\,'+v_{xc}(\vec{r})$$

$$v_{xc}(\vec{r}) = \frac{\delta E_{xc}}{\delta n(\vec{r})}$$

[II.17]

The external potential $V(\vec{r})$ is typically a sum of nuclear potentials centered at the atomic positions. In some cases it is the Coulomb attraction of the bare nuclei. In other problems the Coulomb potential (with its singularities) makes the calculation unfeasible and we have to use pseudo-potentials. The Hartree potential can be evaluated by directly integrating or by solving the equivalent differential (Poisson's) equation. For the exchange-correlation potential there exist many approximations. The simplest one is the local-density approximation (LDA)[78] defined as

$$E_{xc}^{LDA} = \int d^3 r \, \epsilon^{HEG}(n)|_{n=n(\vec{r})} \qquad v_{xc}^{LDA}(\vec{r}) = \frac{d}{dn}\epsilon^{HEG}(n)|_{n=n(\vec{r})}$$

[II.18]

where $\epsilon^{HEG}(n)$ is the exchange-correlation energy per unit volume of a homogeneous electron gas of constant density. Here, $\epsilon^{HEG}(n)$ is a simple function of the electronic density and was tabulated using Quantum-Monte Carlo methods by Ceperley and Alder[80]. Another simple approximation of the v_{xc} is the generalized gradient approximation (GGA)[81,82], where the function has similar form, but ε depends not only on n but also on the gradient of the density ∇n.

The solutions of the Kohn-Sham equations yield the Kohn-Sham orbitals and the Kohn-Sham total energy. These are not the exact solutions of the Schrödinger equation of the original interacting-electron system but they give a very precise approximation. The advantage of the Kohn-Sham formulation lies in the fact that we can relatively easily solve the system of the Schrödinger-like differential equations in an iterative way, using modern computational procedures.

The flow chart (Figure. [II.1]) represents the idea of such a computational cycle. One uses an educated initial guess for the density (i.e., sume of atomic densities). With this density, one solves the Kohn-Sham equations and recalculates the new density. If the density has converged, the cycle stops. If not, the new calculated density is used as input for the next calculation. To avoid instabilities in the calculations, the new density for the next cycle is a mixture of the last two (or more) calculated densities. The choice of the initial density strongly influences the calculation time. The better the estimation the faster will be the calculation. For the mixing and for the estimation of the initial density there exist several physically well motivated propositions which lead to fast and precise calculations.

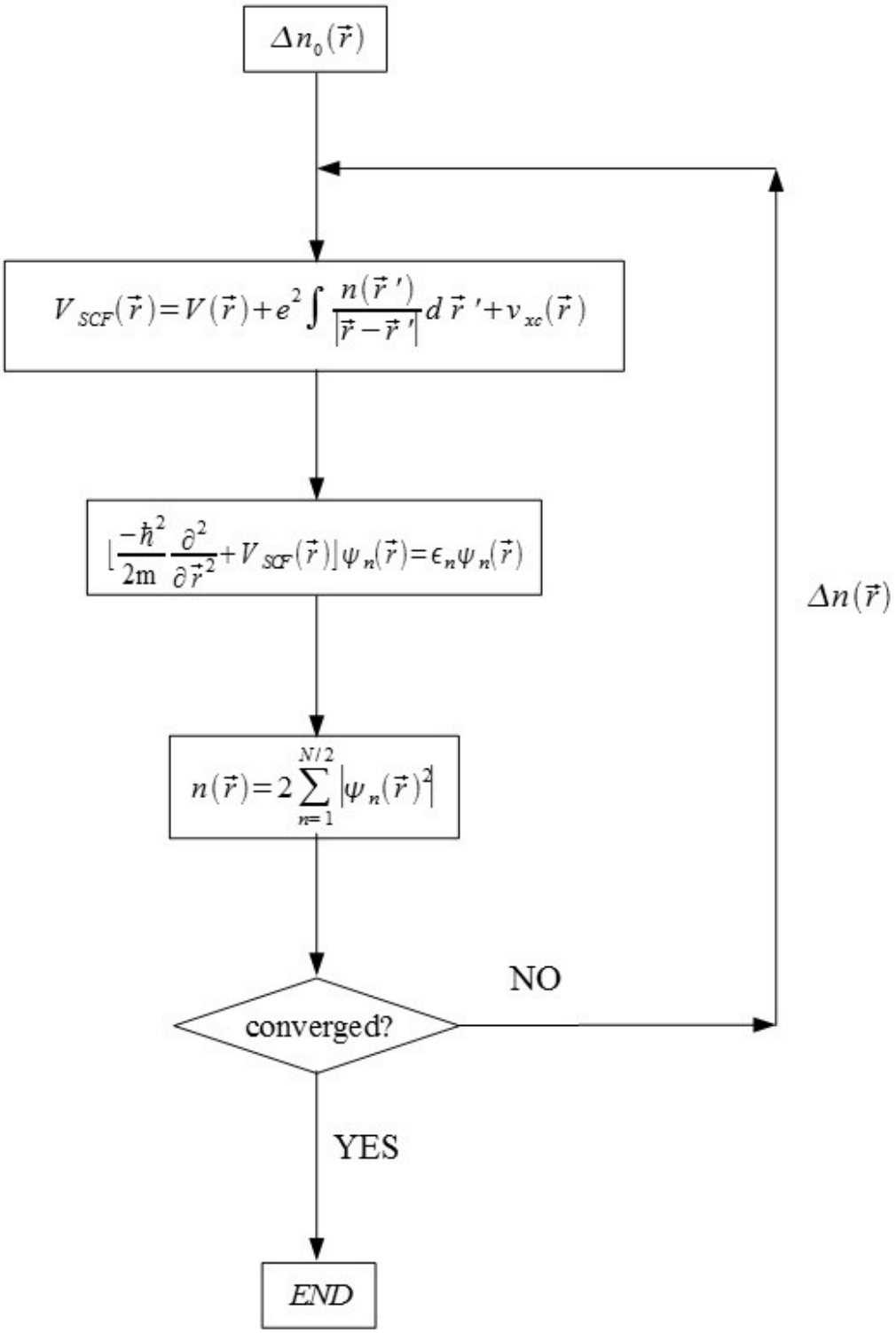

***Figure II.1**: Flow chart of self-consistent computational cycle for the Khon-Sham problem*

II.4 Density Functional Perturbation Theory

To determine the electronic and structural properties of a material within the adiabatic approximation, we have to obtain the dynamical matrix. We will calculate it *ab-initio* using density-functional perturbation theory (DFPT). Using the Hellman-Feynman theorem we can express the dynamical matrix in terms of the electronic density and its linear response to atomic displacement and to the electric-fields. We know how to calculate the electronic density using density-functional theory (DFT). Using a procedure known in literature as density-functional perturbation theory[83] we can calculate the linear response through a set of Kohn-Sham like equations.

Following the procedure explained in the review-article of Baroni at all.[84] we start from Kohn-Sham equations [II.15,II.16,II.17] describing N non-interacting electrons in mean field, solvable in self-consistent way as summarized in flow chart (Figure [II.1]). Then we linearize the Kohn-Sham equations [II.15,II.16,II.17] and use the standard first-order perturbation theory[85]. This leads to an analogue set of self-consistent equations:

$$(H_{SCF} - \epsilon_n)\left|\Delta\psi_n\right\rangle = -(\Delta V_{SCF} - \Delta\epsilon_n)\left|\Delta\psi_n\right\rangle$$

[II.19]

$$\Delta n(\vec{r}) = 4\,\mathrm{Re}\sum_{n=1}^{N/2}\psi_n^*(\vec{r})\,\Delta\psi_n(\vec{r})$$

[II.20]

$$\Delta V_{SCF}(\vec{r}) = \Delta V(\vec{r}) + e^2 \int \frac{\Delta n(\vec{r}')}{|\vec{r}-\vec{r}'|} d\vec{r}' + \frac{d v_{xc}(n)}{dn}\Big|_{n=n(\vec{r})} \Delta n(\vec{r})$$

[II.21]

Where H_{SCF} is the unperturbed Kohn-Sham Hamiltonian [II.15] and $\Delta\psi_n$, ΔV_{SCF} , Δn are first order corrections (linear response) to Kohn-Sham orbitals ψ_n , self consistent field potential V_{SCF} and the electronic density n. The self-consistency of this set lies within the correction ΔV_{SCF} on the right-hand side of equation [II.19], as it depends on Δn [II.21]. In analogy to the computational procedure used in DFT (Figure [II.1]), we can calculate the linear response to the electronic density Δn, using the self-consistent cycle schematically presented in Figure [II.2]:

We calculate ΔV_{SCF} using equation [II.21] with initial arbitrary Δn_0 , then solve the Schrödinger like equation [II.19] and recalculate Δn; equation [II.20]. If Δn hasn't converged we restart the procedure with the new Δn. If it converged then the cycle ends and we have calculated the linear response to the electronic density. As in the case of DFT self-consistent calculations (Figure [II.1]) the speed of the calculations depends on the choice of the initial estimation of the linear-response and on the way the new linear-response is incorporated in subsequent cycle.

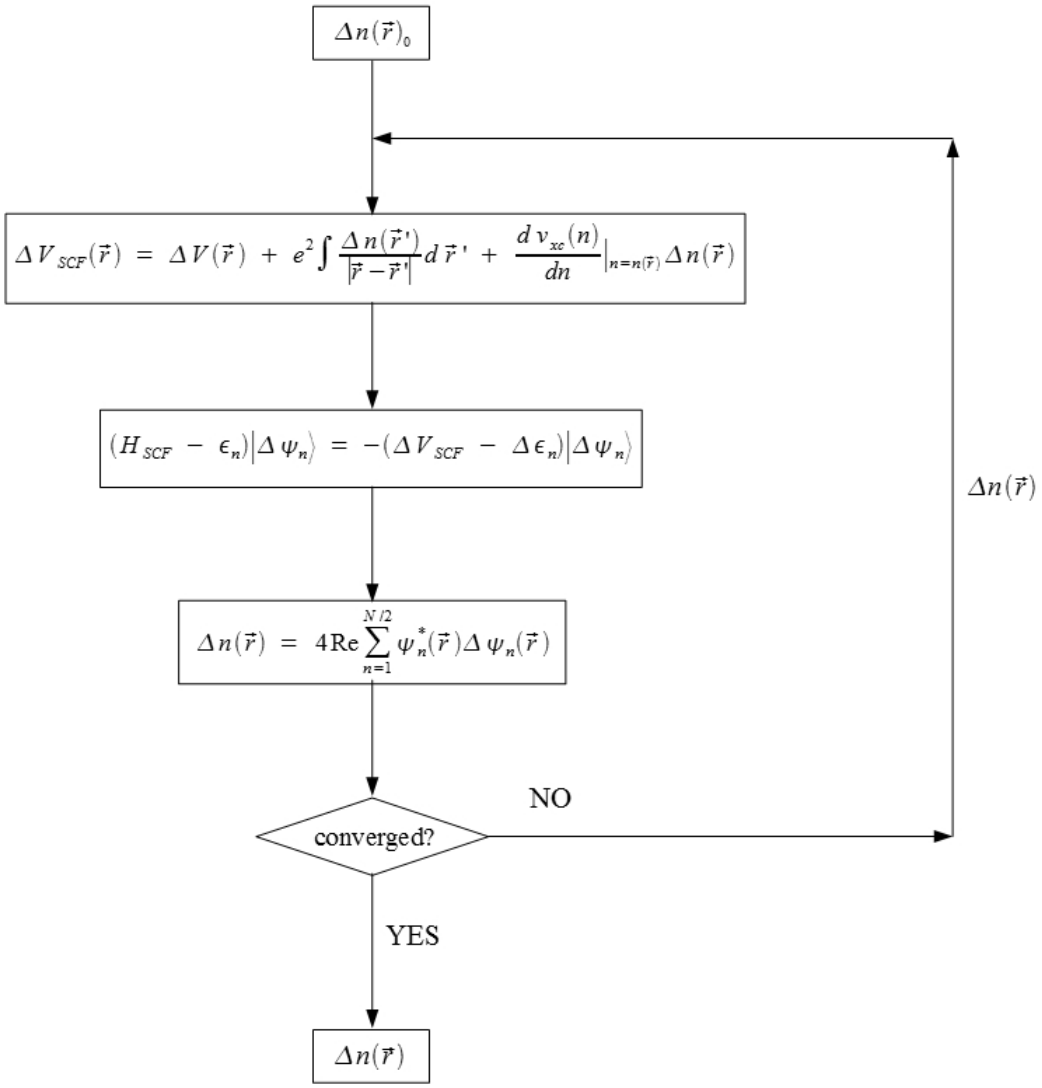

Figure II.2*: Flow chart of self-consistent computational cycle of perturbed Kohn-Sham problem*

II.5 Computational details

This part is devoted to introduction of several concepts and procedures in the computational process which allow to perform efficiently the phonon calculations. Namely we will talk about plane-wave decomposition, pseudo-potentials, k-point sampling of the Brillouin zone and the interpolation and integration.

a) Plane-wave decomposition

Plane-wave decomposition of Kohn-Sham orbitals is an approach which makes it easier to calculate the total energy of solids taking advantage of their structural periodicity [86,87,88]. The plane-wave basis set is orthonormal and the precision of a calculation increases with the number of plane-waves. Accordingly to the size of the basis set the computational time increases. The basis set can be characterized by the energy cut-off which is the maximal kinetic energy of included plane-waves. One has to converge this parameter in order to find the right balance between the desired accuracy of a calculation and the necessary computational time.

Atomic wavefunctions near the core region are highly oscillating and therefore we need a large set of plane-waves to accurately decompose the wavefunction. To bypass this, we adopt the concept of pseudopotentials; we replace the oscillating wavefunction by a smooth pseudo-wavefunction, in such way to conserve the relevant physical information. This allows to considerably reduce the number of plane waves necessary to represent the wave function.

b) Pseudopotentials

Pseudopotentials are a clever approximate description of the real atomic potential making the computational calculations fast and precise enough and at the same time conserving important information such as bonding properties of the atom. The general concept is to replace the oscillating core part of the atomic (molecular) wavefunction by a smooth curve, to simplify the calculations, and leave the outer part of the wavefunction unchanged, as it mostly carries the information about bounding properties of the atom. The general pseudpotential method, which gave very good description of electronic structures of solids, was introduced by Phillips and Kleinman[89,90,91] in 1959 and further developed by Topp and Hopfield[92] in 1973 by adding the norm-conserving property to the pseudopotentials.

The Phillips-Kleinman pseudopotential is derived from the Schrödinger equation for electrons divided into core electrons and valence electrons. The valence orbitals $|\psi_v\rangle$ are then written as a sum of smooth, so called pseudo-wavefunctions $|\varphi_v\rangle$, and an oscillating function:

$$|\psi_v\rangle = |\varphi_v\rangle + \sum_c a_{cv}|\psi_c\rangle$$
$$a_{cv} = -\langle\psi_c|\varphi_v\rangle$$

[II.22]

The pseudo-wavefunctions satisfy then Schrödinger like equation with an energy dependent Hamiltonian:

$$\hat{H}^{PK}(E) = \hat{H} - \sum_c (E_c - E)|\psi_c\rangle\langle\psi_c|$$
$$\hat{w}^{PK}(E) = \hat{v} - \sum_c (E_c - E)|\psi_c\rangle\langle\psi_c|$$

[II.23]

Where $\hat{w}^{PK}$ is the pseudopotential and $\hat{v}$ is the real effective potential in which valence electrons move. In the region near the core of the atom the oscillating $\hat{v}$ is canceled by the second term and makes the pseudo-wavefunction smooth in the core region. This cancellation leads to a very good description of electronic structure of materials. Empirical pseudopotentials based on the Phillips-Kleinman idea are created from an analytic model and then fitted to experimental data. The most used one was proposed by Heine and Abarenkov[93,94,95] and simplified by Ashcroft[96,97].

In 1973 Topp and Hopfield[92] proposed a new approach, so called *norm-conserving* pseudopotentials. They suggested that pseudopotentials should accurately describe the valence charge density. Secondly the pseudo-wavefunction shouldn't have nodal surfaces and the pseudo-energy should match the true valence eigenvalues. Adding this conditions one can better describe the electronic and structural properties.

To obtain such norm-conserving pseudopotential one has to solve the radial Kohn-Sham equation of the free atom taking into account all the electrons in a given reference configuration. Then, using the norm-conserving condition, the pseudo-wavefunction is determined. By inverting the radial Kohn-Sham equation[98] we then calculate the pseudopotential from the pseudo-wavefunction. For the parametrization of pseudo-wavefunctions several approaches were proposed. The most used are the one by Bachelet, Hamann, and Schlüter[99] and by Troullier and Martins[100,101].

When constructing a norm conserving pseudopotential, for example by using the code fhi98PP[102] by M. Fuchs, M. Scheffler[103], one has to set the cut-off radius which is the distance from the nucleus where the pseudo-wavefunction matches the true wavefunction. The r_c is then a parameter which describes the quality of the pseudopotential. The smaller the cut-off radius is, the more realistic is then the pseudo-wavefunction. Harder pseudopotentials are more realistic but have bigger demands on the calculations. Smoother pseudopotentials (bigger r_c) tend to converge fast but are less realistic. So one has to well converge the pseudopotential and find a good compromise between the accuracy of the calculation and the computer time.

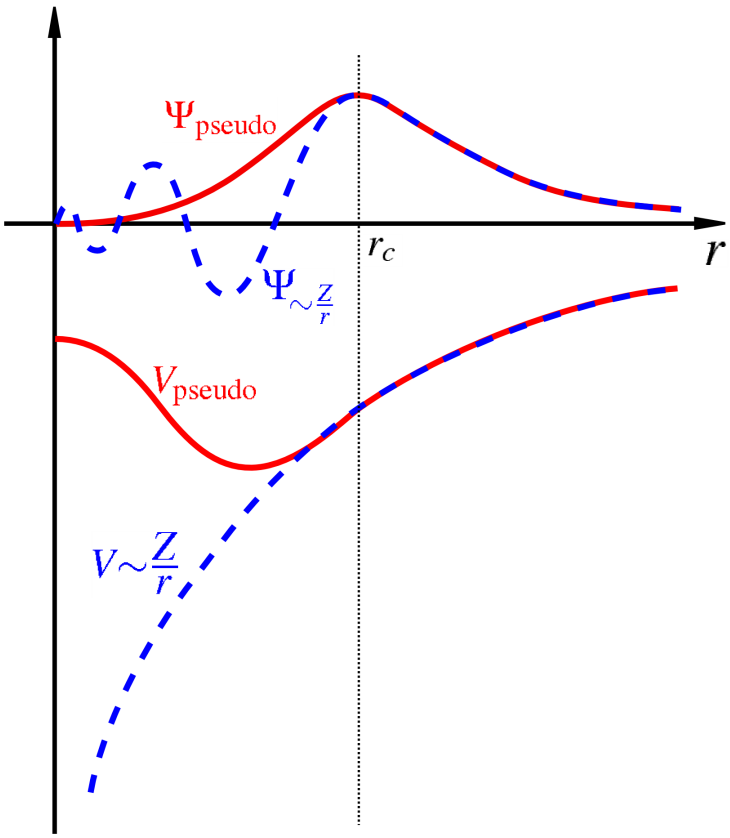

***Figure** II.3: (blue dashed lines): illustration of wavefunction Ψ in Coulombian potential V; (red lines) illustration of wavefunction Ψ_{pseudo}, in pseudopotential V_{pseud}, The wavefunction in pseudopotential is smooth in the core region which is convenient for further calculations. The cut-off radius r_c marks where the pseudopotential and the real potential match.*

c) K-point sampling

In the process of solving numerically the Kohn-Sham equations, we have to integrate periodic functions over the whole first Brillouin zone. Such kind of integrations, very common in computational solid state physics, are typically solved using the approach of Monkhorst and Pack[104]. In 1976 they introduced a universal algorithm for generating sets of special points in the Brillouin zone which provide an efficient method to solve such integrals. We briefly derive the method, as it's a simple but powerful tool for efficient calculations.

Monkhorst-Pack sampling

Let's have a lattice defined, as usual, by primitive translation vectors $\{\vec{t}_1, \vec{t}_2, \vec{t}_3\}$, then the corresponding reciprocal lattice vectors are:

$$\vec{b}_1 = \frac{2\pi}{v}\vec{t}_2 \times \vec{t}_3 \qquad \vec{b}_2 = \frac{2\pi}{v}\vec{t}_3 \times \vec{t}_1 \qquad \vec{b}_3 = \frac{2\pi}{v}\vec{t}_1 \times \vec{t}_2$$

[II.24]

with v as the volume of the primitive unit cell. The Monkhorst-Pack sampling of the reciprocal cell is defined in the following way:

$$\vec{k}_{prs} = u_p \vec{b}_1 + u_r \vec{b}_2 + u_s \vec{b}_3$$

$$u_p = (2\mathrm{p} - q - 1)/2\mathrm{q} \qquad p = 1,2,3,\ldots,q$$

$$u_r = (2\mathrm{r} - q - 1)/2\mathrm{q} \qquad r = 1,2,3,\ldots,q$$

$$u_s = (2\mathrm{s} - q - 1)/2\mathrm{q} \qquad s = 1,2,3,\ldots,q$$

[II.25]

with q as an integer representing the number of special points.

Orthonormal set of functions on the M-P special points:

On the Monkhorst-Pack special grid we can define a set of functions $A_m(\vec{k})$ which are orthonormal under certain restriction on the choice of vectors $\vec{R}$:

$$A_m(\vec{k}) = N_m^{-1/2} \sum_{|\vec{R}| = C_m} \mathrm{e}^{i\vec{k}\cdot\vec{R}}$$

[II.26]

where the sum goes over all vectors $\vec{R}$ from m-th set of vectors C_m related by the operations of lattice point group. Sets C_m, also called stars, are in ascending order beginning with $C_0=0$ with N_m representing the number of terms in m-th set. The condition assuring the orthonormality of the set $A_m(\vec{k})$ is written as follows:

$$\left|R_j^a\right| < q/2, \quad \left|R_j^b\right| < q/2 \qquad (j = 1,2,3)$$

[II.27]

when a and b are integers running from 1 to N_m and N_n and q represents the number of special points.

Integration and interpolation:

Once we have an orthonormal set of functions $A_m(\vec{k})$ in the reciprocal space we can integrate a periodic and totally symmetric function $f(\vec{k})$ in the k-space. We can formally expand the function $f(\vec{k})$ using the orthonormal set $A_m(\vec{k})$:

$$f(\vec{k}) = \sum_{m=1}^{\infty} f_m A_m(\vec{k})$$

[II.28]

where, because of orthonormality of the set A_m on the Brillouin zone, f_m can be cast as follows:

$$f_m = \frac{v}{8}\pi^3 \int_{BZ} d\vec{k}\, A_m^*(\vec{k}) f(\vec{k})$$

[II.29]

Then the integration over the whole Brillouin zone can be expressed:

$$\int_{BZ} d\vec{k}\, f(\vec{k}) = 8\frac{\pi^3}{v} f_1$$

[II.30]

We can also represent an approximation of the functions f_m ($\tilde{f}_m$)

$$\tilde{f}_m = \frac{1}{q^3} \sum_{j=1}^{P(q)} w_j f(\vec{k}) A_m(\vec{k}_j)$$

[II.31]

for a sum over the set $\vec{k}_j$ and for all A_m corresponding to the star satisfying the condition [II.27]. We can thus represent approximately the function $f(\vec{k})$ for any $\vec{k}$:

$$\tilde{f}(\vec{k}) = \sum_m f_m A_m(\vec{k})$$

[II.32]

Similar method for finding such sets of special points was proposed by Chadi and Cohen in 1973[105], early to Monkhorst and Pack. All the sets from Chadi and Cohen can be reproduced by M&P method, which provides additional sets with similar properties.

Conclusion of II.5 chapter:

In this chapter we explained notions and procedures of computational physics which allow to perform the calculations in an efficient way considering the time and resource management and overall precision of the results. Mainly we use the plane-wave decomposition of Kohn-Sham orbitals, we replace the real atomic potential by a pseudo-potential and use Monkhorst-Pack special sampling of the first Brillouin zone to perform numerical integration. We also calculate the dynamical matrix only on several special points in the reciprocal space and use the Fourier interpolation to calculate all the other points we are interested in to save computer resources.

III. Results and discussion

III.1 Phonon Dispersions spectra

In the harmonic approximation, the phonon frequencies as a function of the wave vector **q** are obtained from the equation:

$$\det\left|\frac{1}{\sqrt{M_s M_t}}\ \widetilde{C}_{st}^{\alpha\beta}(\vec{q})-\omega(\vec{q})^2\right|=0$$

[III.1]

The dynamical matrix $\widetilde{C}_{st}^{\alpha\beta}(\vec{q})$ corresponds to the force on atom *t* in direction β linearly induced by a displacement of atom *s* in direction α. We calculate it with density-functional perturbation theory[83,84] as implemented in the code ABINIT[106]. We use the local-density approximation (LDA) for the exchange-correlation functional[78]. The wave functions are expanded in plane waves. Core electrons are replaced by pseudopotentials.

We found that the phonon frequencies are very sensitive to the choice of the lead pseudopotential. In particular, it is important to include the lead *5d* semicore electrons as valence electrons in the calculation. (This is different from the case of pure lead, where the *5d* electrons do not alter the phonon frequencies significantly[107]). The reason lies in the strongly ionic character of the lead chalcogenides; the lead atoms tend to transfer the *6p* valence electrons to the anions. It is then the overlap of the remaining *6s* and *5d* electrons of lead with the *3p* orbitals of the anion that determines the covalent part of the PbX bond (where X stands for the anion S, Se, or Te, respectively). Since the *5d* orbitals contribute to

this bonding, their density should be calculated explicitly and not be substituted by a pseudopotential. We tested different Troullier-Martins pseudopotentials created with the FHI pseudopotential generation code[102,103]. We verified that the corresponding FHI potential for lead and the chalcogens from the ABINIT[106] webpage yielded converged results for the phonon frequencies. The plane-wave energy cutoff is 40 hartree.

It has been observed for ferroelectric materials that *ab-initio* phonon calculations give better agreement with experimental data if they are performed at the experimental lattice constant, rather than at the lattice constant obtained by total energy minimization (see Ref.[108] and references therein). The reason is that the LDA tends to underestimate the lattice constant and in near ferroelectric materials even a small underestimation of 1% strongly influences the ferroelectric instability. Our phonon calculations are performed using the experimental lattice constants at 300K. The experimental lattice constant are given in Table [III.1] together with the values of the optimized lattice constants. Since anharmonic effects are neglected (and very difficult to include on an *ab-initio* level[109]), we do not expect to fully reproduce the temperature dependence of the phonon dispersions.

	DFT-LDA (Å)	Expt. 30 K (Å)	Expt. 300 K (Å)
PbS	5.810	5.909	5.936
PbSe	6.012	6.098	6.124
PbTe	6.318	6.428	6.462

Table III.1*: Calculated lattice constants in comparison with experimental lattice constants (Ref. [111]) at 30K and 300K.*

The influence of the electronic k-point sampling on the phonon dispersion is discussed in the chapter [III.4]. For converged results, we used a (7,3) nested grid, i.e., a 7x7x7 (shifted) Monkhorst-Pack *k*-point sampling with an additional 3x3x3 sampling of the volume element around the high-symmetry point L. In order to obtain the phonons at

arbitrary phonon wave vector ***q***, the dynamical matrix $\widetilde{C}_{st}^{\alpha\beta}(\vec{q})$ is calculated on a 8x8x8 mesh and then Fourier interpolated for arbitrary ***q***. In order to properly reproduce the LO dip around Γ, we calculated the dynamical matrix explicitly for a set of ***q*** points along the high-symmetry lines Δ, Σ, and Λ close to the point Γ.

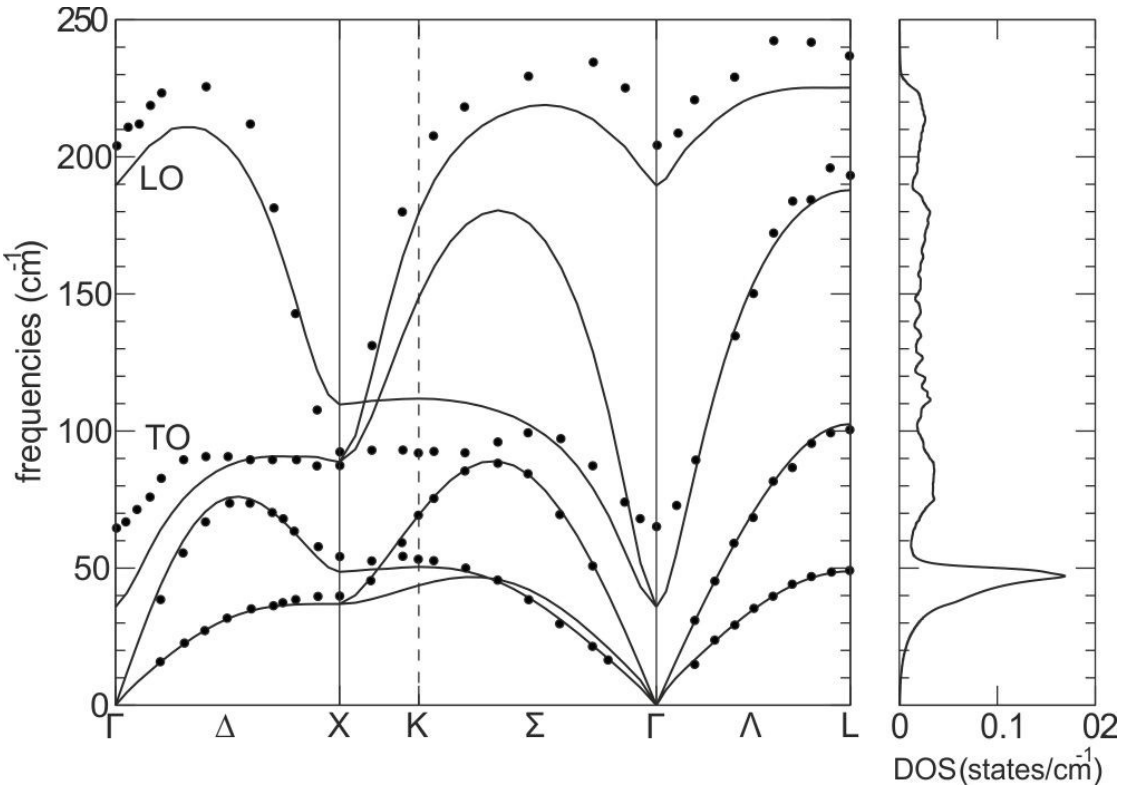

Figure III.1*: Left panel: Calculated phonon dispersion relation of lead sulfide (PbS) lines in comparison with experimental data (Ref.[21]) dots. Right panel: phonon density of states.*

In Figures [III.1-III.3], we present our calculated dispersion relations for PbS, PbSe, and PbTe, respectively, and compare with experimental data from inelastic neutron scattering. We also show the calculated phonon densities of states which will be needed for the calculation of the specific heat. In all three cases, we obtain excellent agreement between theory and experiment for the three acoustic modes. Since the mass of the Pb atoms is much larger than the masses of S, Se, and Te, the acoustic branches correspond almost exclusively to vibrations of lead ions. Consequently, the acoustic-mode dispersion is quantitatively very similar in the three lead chalcogenides. The main difference is a

small frequency lowering that corresponds to increasing lattice constant in the series PbS, PbSe, and PbTe.

The three optical branches correspond to vibrations of the anions. Their maximum frequency scales as $\frac{1}{\sqrt{M_X}}$, where X denotes the anion species. For PbS, the optical modes are so high in energy that they do not intersect with the acoustic modes. For PbSe and PbTe some crossings occur. In all three cases, we observe a remarkably large LO/TO splitting at Γ. For cubic systems, the splitting is given by[84]

$$\omega^2_{\mathrm{LO}} - \omega^2_{\mathrm{TO}} = \frac{4\pi e^2}{\mu\Omega}\frac{(Z^*)^2}{\epsilon}$$

[III.2]

where Z^* is the effective charge, ε is the dielectric constant, e is the electron charge, Ω is the unit-cell volume, and $\mu = \frac{M_{Pb}M_X}{M_{Pb}+M_X}$ is the effective mass. The values for Z and ε are given in Table III.2.

	ϵ	Z*
PbS	19.6	±4.5
PbSe	24.1	±4.9
PbTe	31.7	±6.1

Table III.2*: Values of the dielectric constants and the effective charges of the three lead chalcogenides. Calculations are performed on the DFT-LDA level with the experimental lattice constant at 300 K.*

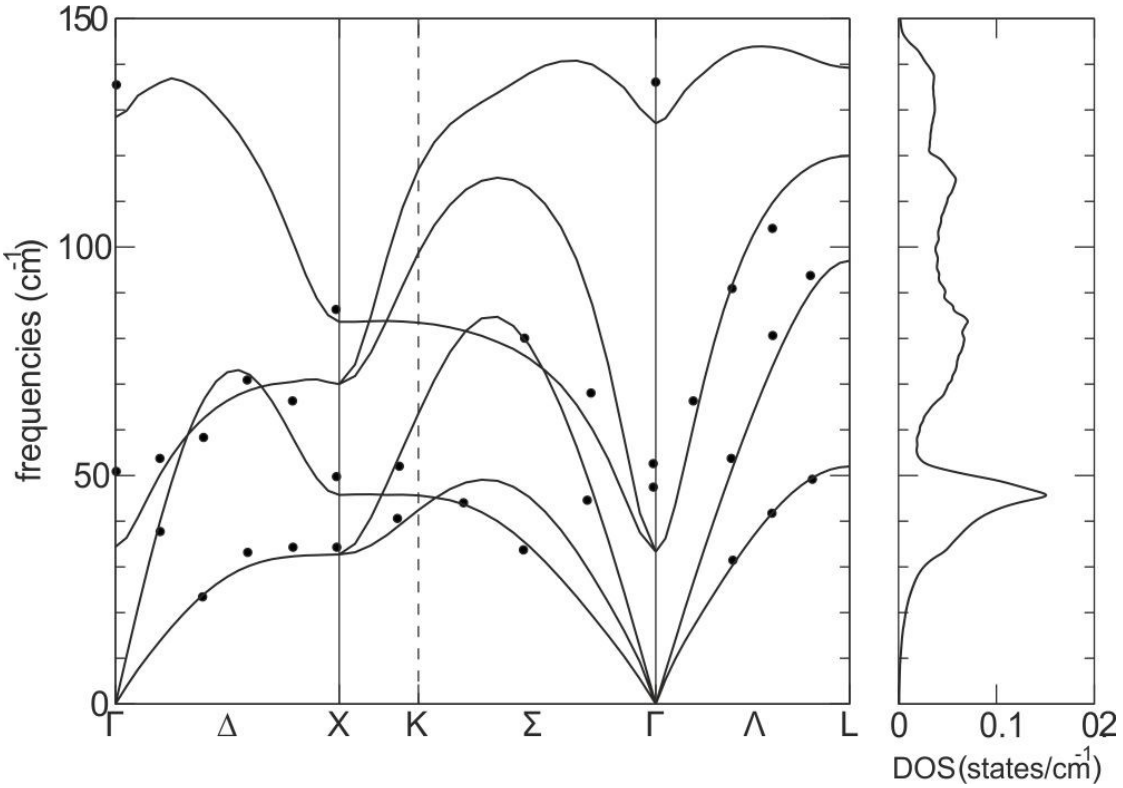

***Figure III.2**: Calculated phonon dispersion relation of lead selenide (PbSe) lines in comparison with experimental data (Ref.[19]) dots.*

In spite of the large dielectric screening, the LO/TO splitting is strongly pronounced due to the very large effective charges. Consequently, the TO mode at has a very low frequency. This frequency depends sensitively on the lattice constant. E.g., for PbSe, an artificial increase in the lattice constant by 0.1 Å leads to a softening of the TO-mode frequency below 0, i.e., toward imaginary values which means that the fcc phase would no longer be the stable one. This is a clear manifestation of the near-ferroelectric character of the lead chalcogenides. All three phonon dispersions exhibit a significant frequency drop of the LO mode at Γ. Cowley and Dolling[23] proposed that this phenomenon is caused by the screening of the macroscopic electric field accompanying the LO mode by free carriers which may have their origin by doping from impurities. We have done our calculations without the presence of additional free carriers, yet we have reproduced the LO anomaly.

Free-carrier doping can contribute to the LO dip but seems not to be its primary cause. Our calculations are in accordance with the theory of Maksimenko and Mischenko[23] who explained the LO anomaly as due to a strong electron-phonon interaction of pseudo-Jahn-Teller type in absence of free-carrier doping. We explain this dip as a "near Kohn anomaly." The notion of a Kohn anomaly[25] is known from metallic systems; the vibrations of the ionic cores are partially screened by the surrounding electron gas. The screening can be strongly enhanced for vibrations with a wave vector $\vec{q}$ that connects two points on the Fermi surface. The enhanced screening then leads to a dip in the phonon dispersion at those values of $\vec{q}$. Recently, two Kohn anomalies were found in the semimetal or "zero-gap semiconductor" graphene[26]. The band structure in the first Brillouin zone of graphene displays two conical intersections (linear crossings) of the π and π^* bands at the Fermi level. The Fermi surface is thus reduced to two points and Kohn anomalies can be found at Γ ($\vec{q} = \vec{0}$) and at K.

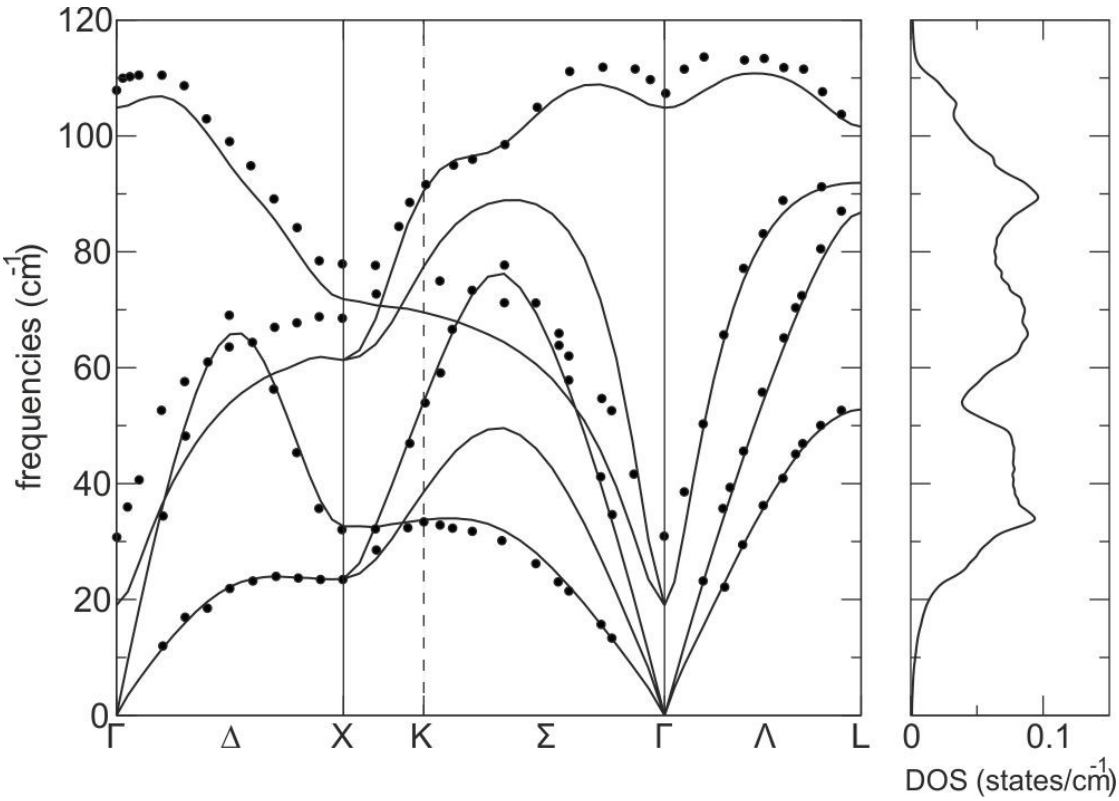

***Figure III.3**: Calculated phonon dispersion relation of lead telluride (PbTe) lines in comparison with experimental data (Ref.[23]) dots.*

The lead chalcogenides are semiconductors. Thus there are - *a priori* - no Kohn anomalies in their phonon dispersions. However, the direct band gap at the high-symmetry point L is small and, by compressing the lattice, it can be brought down to zero. The situation is demonstrated for the case of PbS in Figure III.4. We show the band structure along the high-symmetry lines Γ→L→W for three different values of the lattice constant. The highest valence band around L is

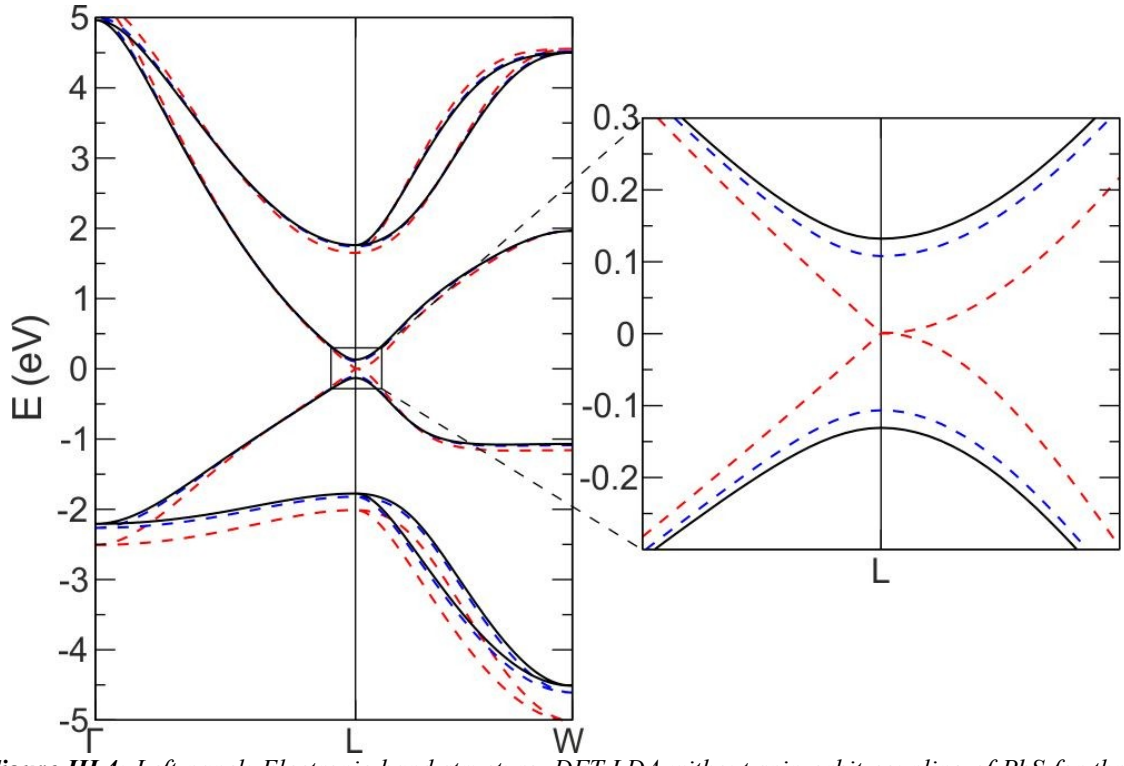

***Figure III.4**: Left panel: Electronic band structure DFT-LDA without spin-orbit coupling of PbS for three different values of the lattice constant a. (black solid lines): experimental lattice constant at 300 K; (blue dotted lines): experimental lattice constant at 30 K; (red dashed lines): a=5.801 Å (squeezed lattice constant which reduces the gap to zero). The Fermi level is at 0 eV. Right panel: A zoom for the region around the direct gap at L.*

composed of S *3p* orbitals. The lowest conduction band has a Pb *6p* character with an admixture of S *4s* orbitals. When calculated with the experimental lattice constant at 300 K, the LDA-density-functional theory (DFT) band gap is 267 meV. It decreases to the

value of 216 meV for the 30 K experimental lattice constant. Artificially decreasing the lattice constant further reduces the band gap at L. Eventually, for a value of the lattice constant a=5.801 Å, the band gap becomes zero with a linear crossing of the bands in the direction L→Γ and a parabolic dispersion in the direction L→W (see right panel of Figure III.4). This situation is now quite analog to the situation in graphene; the system is semimetallic and the Fermi surface is pointlike, located at the high-symmetry points L. For the corresponding phonon dispersion relation one can expect a Kohn anomaly at Γ and at X (the wave-vector difference between two different points L corresponds to either Γ or X). We note in passing that a further reduction in the lattice constants reopens the gap at L. However, the character of valence and conduction bands is inverted and a real crossing of valence and conduction bands along the line L→W shows up. After our publication[128] a similar study on the pressure induced gap closure and the formation of a linear band crossing was presented in 2010[110]. The authors used a self-consistent GW approach which includes the effects of electron-correlation and usually allows a very accurate prediction of the band-gap. Furthermore, they included the effects of spin-orbit coupling which, in the case of the lead chalcogenides leads to a decrease of the band-gap[16]. The resulting band-gap at the experimental lattice constant is thus similar to our LDA calculation. In other words, our LDA value for the band-gap is almost correct due to the cancellation of two errors, the underestimation of the gap by DFT-LDA and the neglect of spin-orbit coupling. Not surprisingly, both study give rise to the same linear band crossing under pressure.

Figure [III.5] presents the phonon dispersion relations of PbS for the three different values of the lattice constant. As expected, shrinking the lattice constant leads to a stiffening of the bonds and thus to an increase in the phonon frequencies. In particular, the TO mode is strongly affected because shrinking the lattice constant makes the system “less ferroelectric.” The only mode which softens is the highest optical branch at Γ and at X where we observe two very sharp dips which correspond to the Kohn anomalies predicted above. Furthermore, LO and TO modes at Γ are degenerate for the squeezed lattice; ε tends to infinity in the limit of the semi-metallic squeezed lattice and the LO/TO splitting tends to zero according to equation [III.2]. Opening the electronic gap by enlarging the lattice

constant to its original value reinstalls the LO/TO splitting. However, a remnant of the Kohn anomaly remains visible in the form of a strong dip of the LO mode at Γ. For this reason, we interpret the LO dip as a near Kohn anomaly.

We note that the LO dip is considerably less pronounced in our calculated phonon dispersion of PbTe. This is due to the strong overestimation of the gap of this material* (see Table [III.3] for our values obtained on the DFT-LDA level and a comparison with the experimental values). At this point, we have to discuss if the inclusion of spin-orbit coupling (SOC) leads to an improvement of the phonon calculations. It has been shown by Hummer *et al.*[111] that SOC strongly reduces the electronic gap for the three lead chalcogenides. E.g., for PbTe, the gap is reduced to 60 meV. The inclusion of electron-correlation effects, e.g., on the level of the GW approximation, is needed in order to "reopen" the gap and to obtain values in good agreement with the experimental gaps[111]. For the calculation of the LO dip this means that inclusion of SOC does not necessarily yield better results unless electron-correlation effects are properly taken care of at the same time; the underestimation of the gap leads to an overestimation of the LO dip. Such an effect can be seen, e.g., in the PbTe phonon dispersion of Romero *et al.* (Fig. 3 of reference[24].)

	E_{gap} calc. meV	E_{gap} expt. meV
PbS	267	410
PbSe	244	280
PbTe	644	310

Table III.3*: Values of the band gaps of the lead chalcogenides. Calculations are performed on the DFT- LDA level with the experimental lattice constant at 300 K. Experimental data at 300 K.*

A recent *ab-initio* calculation of Cardona and Romero *et al.*[24,27] yielded

*In Ref[111], Table IV, a similar overestimation of the PbTe gap is observed, using the FP−APW+LO approach with the PBE functional.

considerably higher phonon frequencies for PbS than the experimental data. This is due to two reasons: they use the optimized lattice constant a=5.808 Å which underestimates the experimental lattice constant at 30 K by 1.7% and the room-temperature lattice constant by 2.2%. Furthermore, their use of a pseudopotential with the lead *5d* electrons in the core may lead to different phonon frequencies. Including SOC leads to a general softening of the phonons and improves the agreement with experimental data[24] (except for the LO dip at Γ). Our calculations with the experimental lattice constant at 300 K are in very good agreement with the acoustic branches of the experimental dispersions. Inclusion of SOC would probably lead to less agreement.

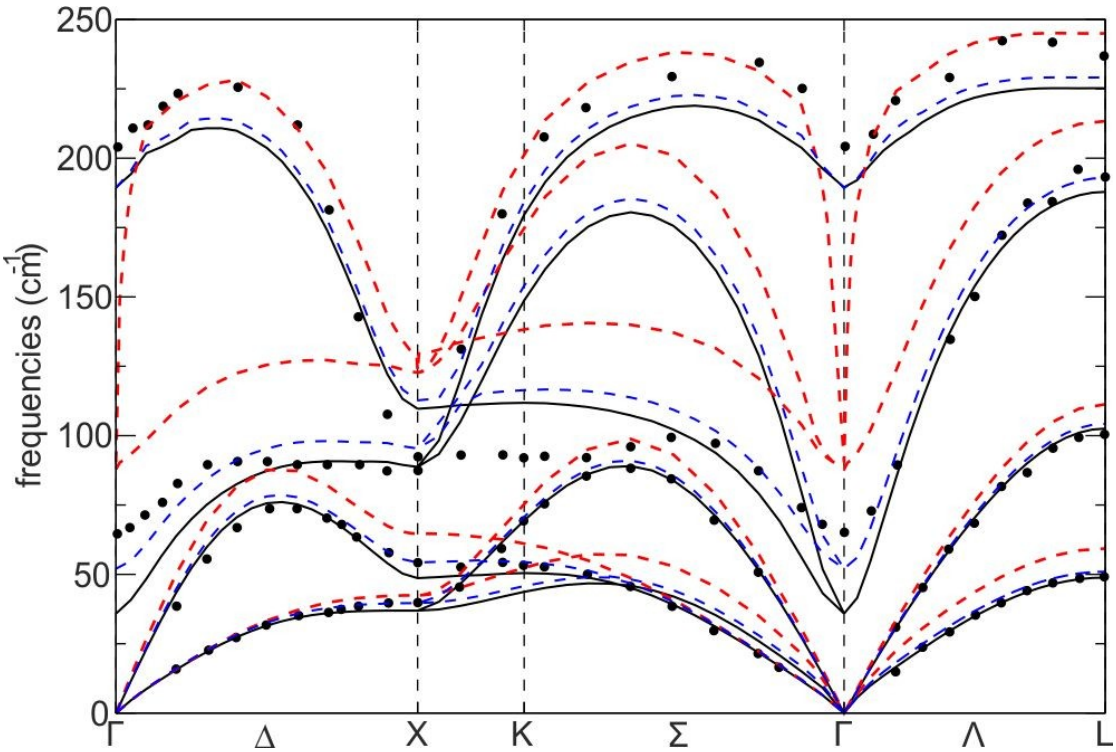

Figure III.5: *Color online Calculated phonon dispersion of PbS for three different values of the lattice constant a. (Black solid lines): experimental lattice constant at 300 K; (blue dotted lines): experimental lattice constant at 30 K; (red dashed lines): a=5.801 Å squeezed lattice constant which reduces the gap to zero. Circles: experimental data Ref.21.*

The optical phonons are in worse quantitative agreement with the experimental data points than the acoustic modes. In particular, for the TO mode around Γ, strong deviations

occur. This is not surprising, since our calculations take into account temperature effects only through the choice of the room-temperature lattice constant while phonon renormalization through phonon-phonon interaction[109] is neglected within the harmonic approximation. Due to the near ferroelectricity, the renormalization of the TO mode as a function of temperature will be particularly strong. E.g., the model calculation by Maksimenko and Mischenko[23] predicts for PbTe that the TO mode at room temperature stiffens by about 15 cm^{-1} with respect to its value at 4 K.

III.2 Specific Heat

Another test of the quality of our *ab-initio* phonon calculations is the comparison with available experimental data for the specific heat, c_v, of PbS, PbSe, and PbTe.[24,27,112,113] The specific heat depends on the phonon densities of states, $D(\omega)$ (right panels of Figures [III.1-III.3]). We calculate it numerically through the formula

$$c_v = N_A k \int_0^{\infty} \frac{\left(\frac{\hbar\omega}{kT}\right)^2 e^{\hbar\omega/kT}}{\left(e^{\hbar\omega/kT}-1\right)^2} D(\omega)\, d\omega$$

[III.3]

where k is the Boltzmann constant and N_A is the Avocado constant. Note that $D(\omega)$ is normalized to 6, i.e., the number of phonon branches.

The resulting specific heat as a function of temperature is plotted in the left panels of Figure [III.6]. All three curves display the typical convergence toward the Petit and Dulong value $6N_Ak$=49.9 J /mol K for a material with two atoms in the primitive cell. Following the discussion of Cardona et al. in Refs. [27] and [24], we also display c_v/T^3 in the low-temperature regime (right panels of Figure [III.6]). All three curves display a maximum between 8 and 12 K.

The agreement between the experimental and theoretical height of the maximum of c_v/T^3 was used in Ref.[27] as a critical test for the quality of the *ab-initio* phonon calculations. For PbS, they obtained a maximum height of the *ab-initio* curve at 1160 $J/mol.K^4$ while the experimental height is at 1520 $J/mol.K^4$. The deviation was tentatively assigned to the absence of SOC in the calculations. Recently, it was shown for elemental bismuth[114] and antimony[115] that inclusion of SOC in the phonon calculations leads to a lowering of the acoustic modes and thus to an increase in the maximum c_v/T^3 . Also for elemental lead, a lowering of the acoustic modes through the inclusion of spin-orbit coupling has been observed[107].

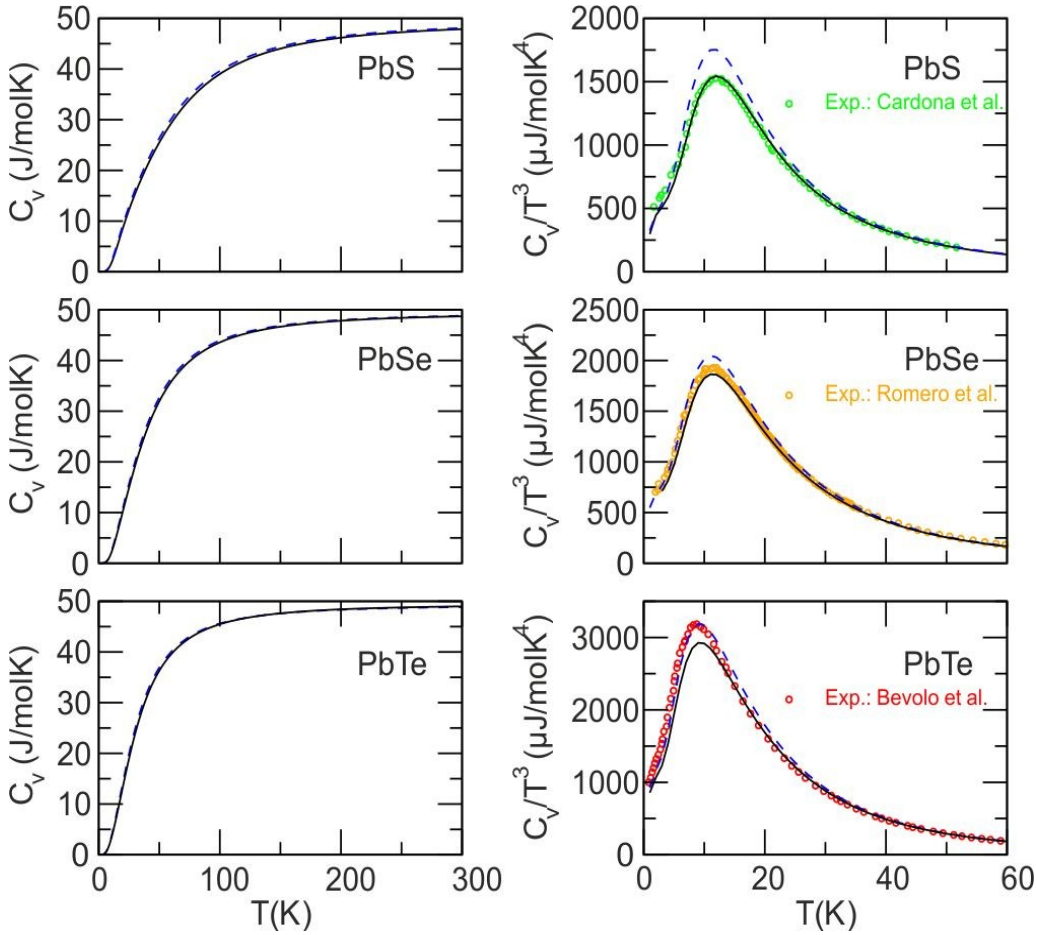

Figure III.6: *Color online Left panels: Specific heat of the three lead chalcogenides as a function of temperature. Right panels: Specific heat divided by T^3 in the low-temperature regime. Results from ab-initio phonon calculations using the respective lattice constants at 30 K solid line and at 300 K dashed lines. Symbols: Experimental data from Ref.[27] Cardona et al., Ref.[24] Romero et al., and Ref.[113] Bevolo et al.*

Since our dispersion relations have been calculated with the room-temperature lattice constants, we expect that we underestimate the frequencies of the acoustic phonons at very low temperature where the lattice constant shrinks and the interatomic force constants stiffen. Consequently, our computed c_v/T^3 for PbS should overestimate the measured one. Figure [III.6] blue dashed line shows that this is indeed the case; we obtain the maximum c_v/T^3 at 1750 $J/mol.K^4$. For a better assessment of the specific heat at low temperature, we have repeated the calculation of the phonon dispersion and the density of states DOS using the PbS lattice constant at 30 K see Table III.1. The resulting c_v/T^3 solid black line in Figure [III.6] is in excellent agreement with the measured data. For PbSe, the agreement with experiment is also fairly good. However, in the case of PbTe, the specific heat calculated with the phonons at the low- temperature lattice constant is somewhat lower than the experimental data. Consequently, spin-orbit coupling which has a stronger effect in PbTe than in PbSe and PbS Ref.[27] might be needed to yield good agreement with the experimental data. Further calculations of the phonon DOS including SOC effects and the *5d* electrons of Pb in the valence are needed to resolve this issue.

III.3 LO phonon confinement study in PbSe nanocrystals

The lead chalcogenide nanocrystals are a good medium (small gap, large exciton diameter and small effective carrier masses) for optical confinement studies[10,11]. In a similar way, one would expect the quantum-confinement to be effective also for the phonons in lead salt nanocrystals. One possible way to detect phonons in nanocrystals is Raman spectroscopy. In bulk lead salts, the LO mode at Γ is detected, probably through a resonant Fröhlich-coupling mechanism[116]. Few Raman spectroscopy studies were performed[117,118,119,120] and lead to contradictory results. The direction of the LO frequency shift (up/down), when switching from bulk to nanocrystals of various size, is unclear from these experiments. Recently a systematic Raman study of different diameter PbSe nanocrystals under constant experimental conditions was performed[28] in order to investigate the phonon confinement. Accompanying the experimental efforts, we performed ab-initio calculations of PbSe q-dots phonons.

For the modelization of Raman spectroscopy of nanocrystals, three levels of approximation have been used in the past (for an overview see Ref.[121]):

I) In the "*confinement model*" one assumes that the restriction of the phonon mode to a nanocrystal of diameter *d* leads to an uncertainty $\Delta q \approx \pi / d$ in the wave vector of a zone-center optical phonon which in turn leads to a shift and uncertainty (broadening) of its wavenumber.

II) In the "*continuum model*" (e.g. Refs.[122,123]) the vibrations of the spherical (or differently shaped) nanocrystal are obtained by solving the continuous equation of motion

which contains as input the bulk phonon dispersion relation in order to take into acount the atomic character of the vibrations. This equation of motion is coupled with the Poisson equation in order to take into account the coupling of the vibrations to the electric field that may result from the vibrations of a polar material.

III) Phonons of some nanocrystals, for example GaP[124], have been calculated on the atomistic level by diagonalizing the dynamical matrix which was calculated from force constants and effective charges fitted to the bulk phonon dispersion.

The quantum confinement model (I) has, e.g., been used to explain the Raman spectra of microcrystalline hexagonal boron nitride[125]: with decreasing crystal size, the Raman peak due to the TO phonon shifts upwards in wavenumber which corresponds to the fact that the TO mode of hBN has a pronounced local minimum at Γ as confirmed by calculations[126] and measurements[127] of the phonon dispersion. Thus a similar analysis may hold for the LO mode of PbSe which also displays a minimum at Γ[23,128] (Figure [III.2]).

The continuum model (II) was used by Krauss *et al.*[129] for the analysis of their Raman data of PbS nanocrystals with radii of 2 nm. Since it uses as input the bulk phonon dispersion which displays a dip for the LO mode at Γ[18], the model correctly predicts an up-shift of the Raman peak whith respect to the bulk LO model. Thus both the quantum confinement and the continuum model describe qualitatively correctly the up-shift of Raman peak with decreasing nanocrystal diameter. Nevertheless, both models do not take into account the changes of the electronic structure (band-gap, dielectric screening, effective charges) with decreasing crystal diameter. It would thus be desirable to perform microscopic lattice dynamical calculations (such as in Ref.[124] for GaP quantum dots). Due to the very peculiar electron and phonon dispersions, a good semi-empirical model for the interatomic force constants is not available (and would also not take into account the changes in dielectic screening and effective charges). In principle, one should therefore perform ab-initio calculations of the phonons. Since this is currently still not feasible for nanocrystals containing several hundreds or thousands of atoms, we performed ab-initio calculations of phonons on a slab geometry which allows to study the effect of a one-

dimensional quantum confinement.

We use density-functional theory[83] (DFT) in the local density approximation[78] (LDA) as implemented in the code Quantum Espresso[130]. The slabs consist of 6 to 15 layers in the (001) orientation. The slabs are arranged in a periodic supercell with a vacuum of a width of 14 a.u. (before geometry relaxation) between adjacent slabs. Wavefunctions are expanded in plane-waves with an energy cutoff at 30 Ry and the first Brillouin zone is sampled by a 10×10×2 k-point mesh. For Pb, we use a Vanderbilt ultrasoft pseudopotential with the 5d electrons in the valence and for Se we use a norm-conserving Bachelet-Hamann-Schlüter pseudopotential. For the in-plane lattice constant, we choose 6.124Å which is the experimental value at room temperature[1]. In the out-of-plane direction, the geometry is optimized, which leads to a 1.3% decrease in the nearest neighbor distance and to a surface rumpling ($z_{Se}-z_{Pb}$, where z denotes the coordinate perpendicular to the layer) of 0.072Å. The phonon frequencies are obtained from the equation [III.1]. The elements of the dynamical matrix are calculated by density functional perturbation theory[84] (DFPT).

Results and discussion:

The results of our calculations are displayed in Figure [III.7] and Table [III.4]. The calculations confirm the experimentally observed trend (and the qualitative expectations from the quantum-confinement model) that the LO frequency increases with decreasing nanocrystal radius. The absolute frequencies in our calculations are slightly higher (due to LDA approximation) than the experimental frequencies but the slopes of the experimental and theoretical curve agree very well. A further uncertainty in our comparison of calculations and experiment consists in the dielectric environment of the nanocrystals which can play an important role in the coupling of the induced macroscopic electric field with the LO mode. On the one hand, in our calculations, we use vacuum (with a dielectric constant of 1) in between the layers. On the other hand, the periodic stacking of PbSe-slabs leads to an average macroscopic dielectric constant (in the perpendicular direction)

between 4.1 (for the 6-layer slab) and 7.2 (for the 15-layer slab)* and thus to an effective dielectric environment which is probably not very far from the situation of a stacking of nanocrystals separated by layers of organic materials. Increasing the vacuum width between the slabs reduces the average dielectric constant but also reduces the effective charges such that the net influence of the vacuum width in our calculations is rather weak.

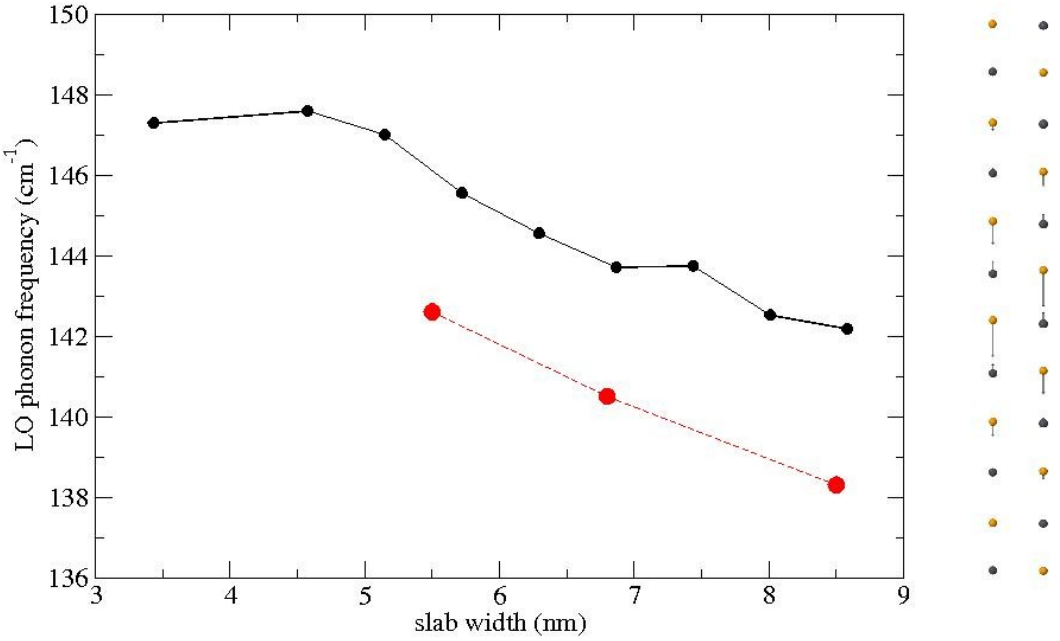

Figure III.7*: (Color online) Black: calculated frequencies of the LO mode for PbSe (100) slabs with a width varying from 6 layers up to 15 layers. Red: measured Raman frequencies. The right panel shows the vibrational pattern of the quantum confined LO mode (with polarization perpendicular to the slab) of a 12 layer slab. The double column of Pb (grey) and Se (orange) atoms represents the motive of the elementary unit-cell of the slab.*

The measured[18,19] and calculated[128] anomaly of the zone center LO phonon mode in the dispersion of bulk PbSe manifests itself also in the diameter dependence of the Raman spectra of PbSe nanocrystals. Contrary to most nanocrystaline materials, where the Raman active phonon modes shift down in frequency, we observe an upshift of the Raman peak with decreasing nanocrystal diameter. This behaviour can be qualitatively understood in

*For details of the dependence of the dielectric constant on the slab width and on the relation between the average macroscopic dielectric constant and the dielectric constant in the interior of the slabs, we refer the reader to the discussion in Ref.[131]

terms of quantum confinement of the LO mode because the phonon dispersion has a dip at the zone center. Decreasing the crystal diameter means increasing the value of the quantized wave-vector and thus leads to an increase of the frequency. This qualitative behaviour is confirmed by our ab-initio phonon calculations on PbSe slabs of various widths. These calculations take into account the changes in the electronic structure (band-gap opening) and the dielectric confinement.

PbSe diameter/slab thickness [nm]	Experimental LO frequency [cm-^{1}]	*Ab-initio* calculated LO frequency [cm-^{1}]
5.5	142.6	147
6.8	140.5	144.5
8.5	138.3	142.5

Table III.4: comparison of LO phonon frequencies as a function of nanocrystal diameter (slab equivalent) calculated ab-initio (this work[128]) and measured by Raman spectra experiment[28]

III.4 Influence of the *k*-point sampling on the LO-mode frequency at *Γ*

For most semiconductors, a 4x4x4 or 6x6x6 (shifted) Monkhorst-Pack *k*-point sampling[104] of the electronic structure is sufficient to reproduce the phonon dispersion, including the LO/TO splitting at Γ for polar materials. In this chapter, we show that for lead chalcogenides a much higher sampling is needed to properly reproduce the LO-mode dispersion around.

Figure [III.8a] shows the LO-mode dispersion of PbS close to Γ for different nxnxn Monkhorst-Pack samplings. We used here a Troullier-Martins pseudopotential with the *5d* electrons in the core (from the ABINIT webpage[106]). This allowed us to go to very high *k*-point samplings. With this pseudopotential, we obtain a gap of 231 meV which is close enough to the converged value of 267 meV see Table [III.3] to reproduce a similarly strong anomaly of the LO mode. The phonon frequencies marked by the symbols have been obtained by directly calculating the dynamical matrix for the corresponding phonon wave vector avoiding interpolation of the dynamical matrix. Obviously, it makes a big difference if *n* is even or odd. For *n* even, we obtain higher frequencies and for *n* odd, we obtain lower frequencies than in the limit $n \to \infty$. The difference between the 7x7x7 and the 8x8x8 sampling amounts to more than 40 cm^{-1} for the LO mode at Γ. For the TO mode—not shown here—the corresponding difference is less than 3 cm^{-1}. Even between the 19x19x19 sampling and the 20x20x20 sampling, there remains a difference of 2 cm^{-1} for the LO mode while the TO mode is converged to within 0.03 cm^{-1}. The origin of the even-odd discrepancy for the different *k*-point samplings lies in the electronic structure of the lead chalcogenides which all have a very small direct gap at the high-symmetry point L. The

small gap is among other factors responsible for the very high dielectric constants (ε>19) of the lead chalcogenides. The point L is included in the samplings when *n* is odd but not when *n* is even. Figure [III.8b] demonstrates that response-function calculations with odd samplings tend to strongly overestimate while the even samplings underestimate it. Similar even-odd oscillations for low *k*-point samplings are observed for the calculated effective charges [panel (c)]. The link between the dielectric screening, effective charges, and the LO/TO splitting is given by Eq. [III.2]. Panel (d) demonstrates that the ratio $(Z^*)^2/\epsilon$ also displays the even-odd oscillations and converges slowly with *n*. Obviously, Monkhorst-Pack grids with an even *n* lead to much faster convergence than grids with odd *n*.

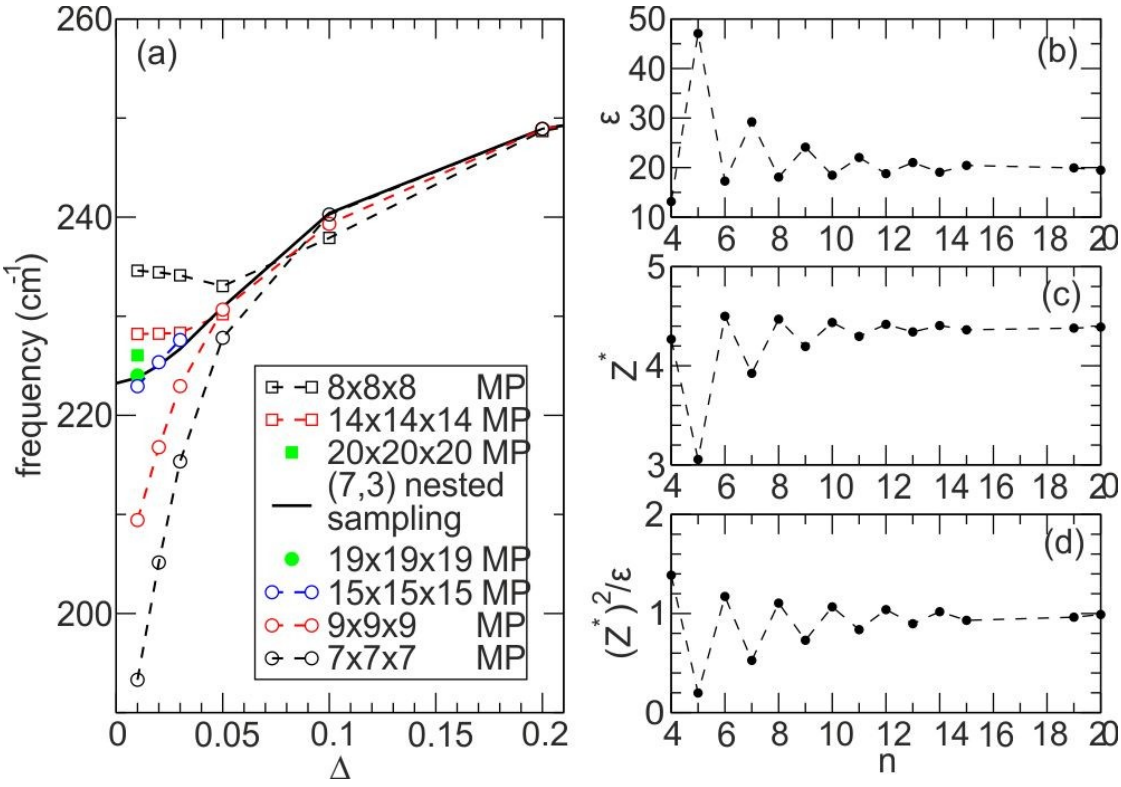

Figure III.8: *Color online* ***(a)*** *LO-mode dispersion in PbS for different MP samplings and a nested sampling see text. The dispersion is plotted along the line Δ(Γ→X) with 0 corresponding to Γ and 0.5 corresponding to X.* ***(b)*** *dielectric function as a function of n, where nxnxn denotes the Monkhorst-Pack sampling.* ***(c)*** *Effective charge Z as a function of sampling.* ***(d)*** $(Z^*)^2/\epsilon$ *as a function of sampling.*

Since a calculation of the full dispersion relation with a very dense Monkhorst-Pack grid (and with the *5d* electrons in the valence) was not feasible, we used a nested 7,3 grid (1476 k-points in the full Brillouin zone). This is a 7x7x7 MP grid where, in addition, the cubic volume element around the point L is sampled by a simple 3x3x3 grid. The high *k*-point density around L corresponds thus to the density in a uniform 21x21x21 grid and the solid line in Fig. [III.8a] demonstrates that we obtain the LO frequency in very good agreement with the 20x20x20 and 19x19x19 samplings.

Due to the pronounced dip, the calculation of the dispersion relation from a Fourier-interpolated dynamical matrix is not feasible for the LO mode around Γ. This is the reason, why in our dispersion relations Figures [III.1-III.3], we used interpolation for most of the Brillouin zone but added point-by-point calculations for the LO mode close to Γ.

IV. Conclusion

IV.Conclusion

Using DFT+DFPT with local density approach we have calculated ***the phonon dispersion relations of lead chalcogenides*** (Figures [III.1-III.3]). Strict convergence parameters and careful choice of the lead pseudopotential and the k-point sampling (TM lead pseudopotential with *5d* semi-core electrons in valance band and a L-point nested* M-P sampling grid), based on our profound investigations, enabled us to obtain ***good agreement with experimental phonon data***[17,18,19] and measurements of the ***specific heat***[24,27,112,113]. The acoustic phonon modes are reproduced almost exactly and thus our calculated specific heat (Figure [III.6]), depending mainly on acoustic phonons, agrees well with measurements. The optical phonon modes match qualitatively the experimental data but are in worse quantitative agreement with the measured points than the acoustic ones. This deviation was expected since our calculations take into account temperature effects only through the choice of the room-temperature lattice constant while phonon renormalization through phonon-phonon interaction[109] is neglected within the harmonic approximation. We also ***reproduced the pronounced dip of the LO mode at Γ.*** The LO mode dip at Γ is related to the narrow band gap and can be understood as a ***near Kohn anomaly***. In our ***PbS electronic bands study*** (Figure [III.4]) we demonstrate that compressed lead sulfide is a system with semi-metallic behavior similar to graphen (zero-gap at L, linear crossing in L→Γ direction, parabolic dispersion in L→W direction) and thus should exhibits a Kohn anomaly in phonon dispersion at Γ or X.

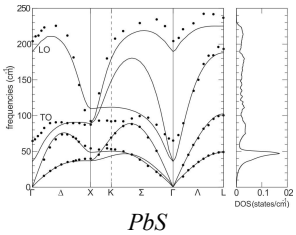

PbS

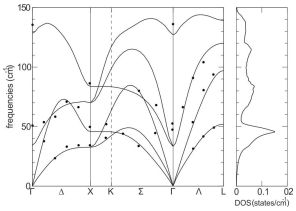

PbSe

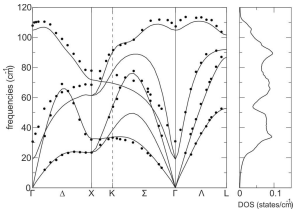

PbTe

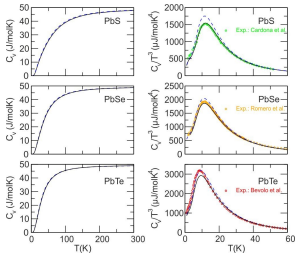

Specific Heat

We also calculated phonons on the nanocrystalline level

* See Influence of the k-point sampling on the LO-mode frequency at Γ (chapter III.4)

and ***calculated lead selenide Γ phonons for q-dots of various size*** (Figure [III.7]), furnishing results coherent with recent Raman spectroscopy experiments[28] investigating phonon confinement in PbS nanocrystals.

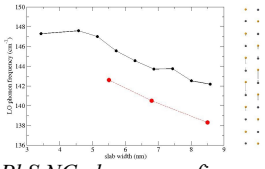

PbS NC phonon confinement

We have deeply investigated the phonon dispersion relations of lead chalcogenides, including the LO dip at Γ, and thus ***provided high quality data for further research***. In recent years promising electronic and optical properties of ***lead salts nanocrystals*** were discovered making them good candidates for modern opto-electronic devices, luminescent colorant dyes and especially ***high-efficient solar cells medium*** (PbS, PbSe). In order to exploit the potential applications many theoretical and experimental research efforts on optical and electronic properties was done, mainly focused on solar technology. However there are still gaps in the exact understanding of all properties. In particular, to fully ***understand the de-excitation of hot carriers*** it is necessary to learn more about the ***electron-phonon coupling in lead chalcogenides***. Our research provides necessary data for further investigations of the nanocrystalline phase.

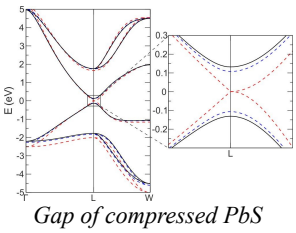

Gap of compressed PbS

Solar Panel

V. Résumé - Slovak

V.Résumé - Slovak

Olovnaté chalkogenidy (PbS, PbSe a PbTe) sú IV–VI polovodiče s úzkym zakázaným pásmom a kryštalickou štruktúrou kamennej soli. V nanokryštalickej fáze vykazujú nadpriemerné optické a elektrické vlastnosti, vďaka čomu majú široké použitie v mnohých aplikáciách. Majú úzke zakázané pásmo 280–410 meV pri izbovej teplote[1], veľký polomer excitónov (20 nm v PbS a 46 nm v PbSe)[10] a malú efektívnu hmotnosť elektrónov a dier, čo z nich robí veľmi dobré médium pre optoelektronické a fotovoltaické zariadenia, rovnako ako aj pre štúdium kvantového uväznenia[9,10]. Napríklad na báze PbSe/PbEuTe nanokryštálov bol skonštruovaný infračervený laser[14]. Nedávne štúdie[15] naznačujú, že PbSe nanokryštály by mohli tvoriť základ vysoko výkonných slnečných panelov. Vďaka impaktnej ionizácii sa silno energický pár elektrón-diera rozpadne na viaceré páry elektrón-diera s nižšou energiou. Dochádza tak k multiplikácii nosičov, čo by mohlo teoreticky viesť ku panelom s konverzným faktorom 60,3%[15]. Aby sme plne pochopili de-excitačný mechanizmus, je potrebné vedieť viacej o elektrón-fonónovej interakcii v olovnatých chalkogenidoch. Elektrónová pásová štruktúra je veľmi dobre preskúmaná a boli urobené vysoko kvalitné výpočty (Ref.[16] a odvolávky v nej). Napriek tomu fonónová disperzia olovnatých chalkogenidov nieje natoľko prebádaná. Experimentálne bola fonónová disperzia PbS, PbSe a PbTe meraná neutrónovým nepružným rozptylom[17,18,19]. Simulácie fonónovej disperzie sa doteraz pohybovali na úrovni semi-emirických modelov[20,21,22,23]. Všetky tri materiály vykazujú tú istú anomáliu v disperznom vzťahu; silný pokles longitudinálnej optickej (LO) vetvy v bode Γ. Pre LO pokles existujú rôzne vysvetlenia; Cowley a Dolling[22] pripisujú LO spád tieneniu voľnými nosičmi v kryštáli. V semi-empirických výpočtoch fonónov od Upadhyaya *et al.*[20] sa zaviedol termín dopovanie voľnými nosičmi. Maksimenko a Mishchenko[23] vysvetľujú LO pokles za pomoci pseudo-Jahn-Tellerovho efektu[21]. Nedávne ab-initio výpočty fonónov olovnatých chalkogenidov[24] ukázali minimum v LO móde u PbSe a PbTe, ktoré sa v kalkuláciách výrazne prehĺbi po zahrnutí spin-orbitálnej väzby. Dôvod poklesu ostával však stále nevysvetlený.

V tejto práci uvádzame systematickú *ab-initio* štúdiu disperzného vzťahu fonónov

olovnatých chalkogenidov. Vďaka úzkemu zakázanému pásmu a kvázi-ferroelektrickému správaniu týchto materiálov sme museli výpočtové parametre, ako je vzorkovacia sieť, alebo pseudopotenciály, vyberať veľmi opatrne. Naše výpočty kvantitatívne reprodukujú akustické fonóny. Anomálie v LO a TO módoch reprodukujeme kvalitatívne (keďže silno závisia od teploty[23], na to, aby sme kvantitatívne zreprodukovali merania pri izbovej teplote, museli by sme vziať do úvahy anharmonické efekty). Naše výpočty ukazujú, že obrátený pík LO módu v bode Γ je prítomný aj v čistom materiály bez dopovania voľnými nosičmi. Pokles vysvetľujeme v analógii s Kohnovými anomáliami[25], ktoré sa vyskytujú v semi-metalickom graféne[26]. Demonštrujeme, že *ab-initio* výpočty môžu veľmi dobre reprodukovať špecifické teplo PbS, PbSe a PbTe a porovnávame ich s nedávnymi výpočtami[24,27], v ktorých zahŕňajú do kalkulácií aj spin-orbitálny efekt. Ďalej predstavujeme *ab-initio* výpočty LO fonónových frekvencií pre PbSe dosky rôznych hrúbok. Naše výpočty vysvetľujú výsledky nedávnych experimentov, ktoré robili za pomoci Ramanovej spektroskopie[28] pri ktorých merali závislosť píku od diametru kryštálov a pozorovali modrý posun dominantného píku (previazaný s LO módom) pri zmenšujúcom sa polomere nanokryštálov.

I. Detaily výpočtov

Za použitia harmonickej aproximácie získame fonónové frekvencie, ako funkcie vlnového vektora $\vec{q}$ z nasledovnej rovnice:

$$\det\left|\frac{1}{\sqrt{M_s M_t}}\ \widetilde{C}_{st}^{\alpha\beta}(\vec{q})-\omega(\vec{q})^2\right|=0$$

[V.1]

Dynamická matica $\widetilde{C}_{st}^{\alpha\beta}(\vec{q})$ zodpovedá sile vyvinutej na atóm *t* v smere β vyvolanej posunom atómu *s* v smere α. Maticu sme vypočítali za pomoci poruchovej teórie funkcionálu hustoty* (DFPT)[83,84] implementovanej v programe ABINIT[106]. Pri tom sme

* Density Functional Perturbation Theory

využili aproximáciu lokálnej hustoty* na vyjadrenie funkcionálu** výmeny a korelácie[78]. Vlnové funkcie sú rozložené do rovinných vĺn a vnútorné elektróny nahradené pseudopotenciálmi.

Zistili sme, že fonónové frekvencie sú veľmi citlivé na výber pseudopotenciálu olova. Konkrétne je pri výpočtoch dôležité zahrnúť vnútorné elektróny z orbitálu *5d* medzi valenčné elektróny. (Na rozdiel od prípadov s čistým olovom, kde *5d* elektróny výrazne neovplyvňujú fonónové frekvencie[107]). Dôvodom k tomuto kroku je silný iónový charakter chalkogenidov olova; atómy olova majú tendenciu preniesť *6p* valenčné elektróny na anióny, následovne prekryv orbitálov zostávajúcich *6s* s *5d* elektrónov olova s *3p* orbitálom aniónu určuje kovalentnú časť PbX väzby (X = S, Se, Te). Keďže elektróny z *5d* orbitálu prispievajú k väzbe, ich hustotu treba počítať explicitne a nenahrádzať ich pseudopotenciálom. Vytvorili sme[98,99] a otestovali rôzne pseudopotenciály *Troullier-Martins*-ovho typu a overili, že pseudopotenciály z ABINIT[106] web-stránky dávajú konvergentné výsledky fonónových frekvencií. Na rozklad vlnových funkcií sme použili rovinné vlny po energiu 40 hartree.

Bolo pozorované, že *ab-initio* vypočítané fonónové frekvencie ferroelektrických materiálov sú v lepšej zhode s experimentálnymi hodnotami, ak sa v nich používa experimentálna mriežková konštanta (namiesto mriežkovej konštanty získanej z minimalizácie celkovej energie[108]). Dôvodom je, že LDA podhodnocuje mriežkovú konštantu a v skoro ferroelektrických materiáloch aj 1% podhodnotenie silne ovplyvňuje ferroelektrickú stabilitu. V našich výpočtoch sme používali experimentálne mriežkové konštanty zodpovedajúce teplote 300 K, uvedené v Tabuľke [V.1] spolu s hodnotami optimalizovaných mriežkových konštánt. Vzhľadom na to, že sme zanedbali anharmonické efekty, ktoré sú veľmi ťažko zahrnuteľné na *ab-initio* úrovni[109], nepredpokladáme, že plne reprodukujeme tepelnú závislosť fonónových frekvencií.

* Local-Density Approximation

**exchange-correlation functional

	DFT-LDA (Å)	Expt. 30 K (Å)	Expt. 300 K (Å)
PbS	5.810	5.909	5.936
PbSe	6.012	6.098	6.124
PbTe	6.318	6.428	6.462

***Tabuľka V.1**: Porovnanie vypočítaných mriežkových konštánt s experimentálnymi hodnotami (Ref.[1]) pri teplote 30K a 300K.*

Na to, aby sme získali konvergentné výsledky sme na vzorkovanie elektronických *k* bodov z prvej Brilliouin-ovej zóny používali takzvanú (7,3) *vhniezdenú* sieť*, to znamená 7x7x7 (posunutá) Monkhorst-Pack[104] sieť s 3x3x3 zahusteným vzorkovaním okolo bodu symetrie L. Aby sme dostali fonóny pre ľubovoľný fonónový vlnový vektor $\vec{q}$, spočítali sme explicitne dynamickú maticu $\widetilde{C}_{st}^{\alpha\beta}(\vec{q})$ na 8x8x8 sieti a ľubovoľný vektor obdržali Fourierovskou interpoláciou. Aby sme dôkladne reprodukovali LO pokles v blízkosti Γ, spočítali sme explicitne dynamickú maticu pre body pozdĺž línií vysokej symetrie Δ, Σ, a Λ v blízkosti bodu Γ.

II. Disperzný vzťah fonónov.

Na obrázkoch [V.1,V.2,V.3] predstavujeme nami vypočítané fonónové disperzné krivky pre chalkogenidy olova v porovnaní s experimentálnymi dátami získanými nepružným rozptylom neutrónov. Zároveň ukazujeme vypočítanú hustotu stavov fonónov, ktorú sme potrebovali na výpočet špecifického tepla. Vo všetkých troch prípadoch dosahujeme výbornú zhodu s experimentom pre tri akustické módy. Keďže atómy Pb sú oveľa ťažšie ako atómy S, Se a Te, akustické vetvy zodpovedajú skoro výlučne vibráciám olovnatých iónov. Následkom toho disperzia akustických módov je veľmi podobná pre všetky chalkogenidy olova. Hlavným rozdielom je malý pokles frekvencie zodpovedajúci

* nested grid

zväčšujúcej sa mriežkovej konštante v sériách PbS, PbSe a PbTe. Tri optické vetvy zodpovedajú aniónovým vibráciám. Maximálna frekvencia sa škáluje ako $1/\sqrt{M_X}$, kde X predstavuje prislúchajúci anión. V prípade PbS majú optické módy tak vysokú energiu, že nedochádza ku kríženiu s akustickými vetvami, v prípade PbSe a PbTe ku kríženiu dochádza.

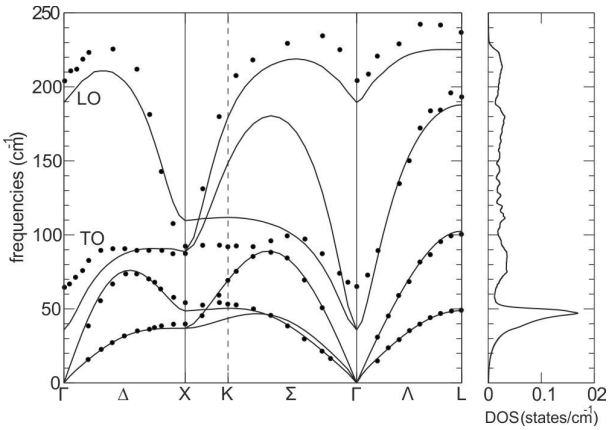

***Obrázok V.1**: Ľavý panel: vypočítaná fonónová disperzná krivka pre PbS (plné čiary) v porovnaní s experimentálnymi dátami[18] (bodky). Pravý panel: hustota stavov fonónov.*

Vo všetkých troch prípadoch pozorujeme značný LO/TO rozštep v Γ. Pre kubické systémy je rozštep daný:

$$\omega^2_{\mathrm{LO}} - \omega^2_{\mathrm{TO}} = \frac{4\pi e^2}{\mu\Omega}\frac{(Z^*)^2}{\epsilon}$$

[V.2]

kde Z^* je efektívny náboj, ε je dielektrická konštanta, e je náboj elektróna, Ω je objem jednotkovej bunky a $\mu = \frac{M_{Pb}M_X}{M_{Pb}+M_X}$ je efektívna hmotnosť. Hodnoty pre Z^* udávame v Tabuľke [V.2].

	ϵ	Z*
PbS	19.6	±4.5
PbSe	24.1	±4.9
PbTe	31.7	±6.1

***Tabuľka V.2**: Hodnoty dielektrickej konštanty a efektívneho náboja pre tri olovnaté chalkogenidy. Výpočty boli robené na úrovni DFT-LDA s experimentálnou mriežkovou konštantou pri teplote 300 K.*

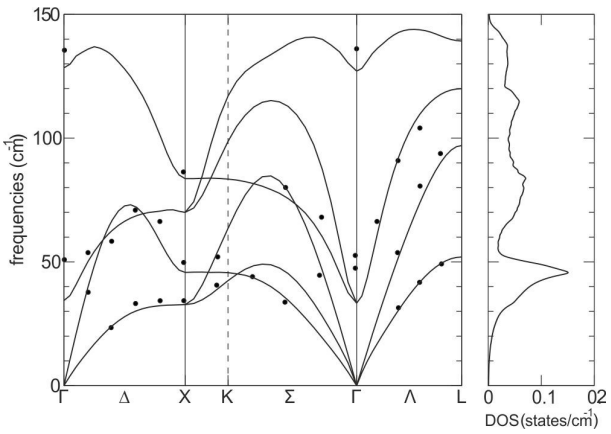

***Obrázok V.2**: Ľavý panel: vypočítaná fonónová disperzná krivka pre PbSe (plné čiary) v porovnaní s experimentálnymi dátami[19](bodky). Pravý panel: hustota stavov fonónov.*

Vďaka veľkým efektívnym nábojom je napriek silnému dielektrickému tieneniu LO/TO rozštep silno prehĺbený. Konzekventne TO mód dosahuje veľmi nízku frekvenciu v bode Γ, ktorá je veľmi citlivá na mriežkovú konštantu. Napríklad umelé zväčšenie mriežkovej konštanty pre PbSe o 0.1 Å vedie k poklesu frekvencie TO módu pod nulu, teda smerom k imaginárnym hodnotám, čo znamená že fcc fáza by už nebola stabilnou. Toto je jasný prejav kvázi ferroelektrického charakteru olovnatých chalkogenidov. Vo všetkých troch prípadoch zaznamenávame významný pokles frekvencie LO módu v oblasti Γ. Cowley z Dolling[22] vyjadrili predpoklad, podľa ktorého by tento jav mohol byť spôsobený tienením makroskopického elektrického poľa sprevádzajúci LO mód voľnými nosičmi, ktoré by mohli pochádzať z dopovania od nečistôt. Naše výpočty sme robili bez pridania voľných nosičov, napriek tomu sme zreprodukovali LO anomáliu. Dopovanie voľnými nosičmi môže prispievať k LO poklesu, ale nezdá sa byť jeho primárnou príčinou. Naše výpočty sú skôr v zhode s teóriou Maksimenka a Mischenka[23], ktorí LO anomáliu vysvetľujú na základe silnej elektron-fonónovej interakcie pseudo-Jahn-Teller-ovho typu bez prítomnosti dopovania voľnými nosičmi. LO pokles vysvetľujeme ako kvázi Kohnovú anomáliu*. Kohnová anomália[25] je pojem známy z metalických systémov, v ktorých sú vibrácie iónových jadier čiastočne odtienené okolitým elektrónovým plynom. Tienenie môže byť pre vibrácie o vlnového vektoru $\vec{q}$, ktorý spája dva body Fermiho plochy, silno znásobené. Zosilnené tienenie potom vedie k poklesu vo fonónovej disperzii hodnôt $\vec{q}$. Nedávno boli objavené dve Kohnové anomálie v graféne[26]. Elektronická pásová štruktúra prvej

*near Kohn anomaly

Brillouinovej zóny grafénu vykazuje dva kónické prieseky[**] pásu π a π^* na Fermiho úrovni. Fermiho plocha je takto zredukovaná na dva body, tým pádom môžeme pozorovať Kohnové anomálie v bode Γ a v bode K.

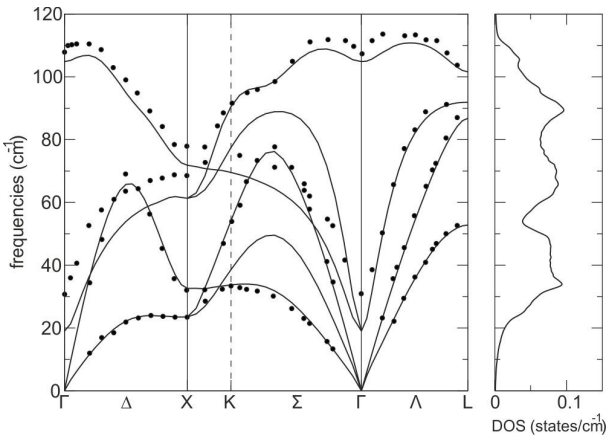

***Obrázok V.3**: Ľavý panel: vypočítaná fonónová disperzná krivka pre PbTe (plné čiary) v porovnaní s experimentálnymi dátami[17] (bodky). Pravý panel: hustota stavov fonónov.*

Olovnaté chalkogenidy sú polovodiče a teda v ich disperziách fonónov niesu *–a priori–* Kohnové anomálie. Avšak priame zakázané pásmo v bode vysokej symetrie L je malé a stlačením mriežky ho vieme dostať na nulu. Prípad PbS je znázornený na Obrázku [V.4], kde prezentujeme elektronickú pásovú štruktúru pozdĺž čiar vysokých symetrií Γ→L→W pre tri rôzne hodnoty mriežkovej konštanty. Najvyššie valenčné pásmo v oblasti L pozostáva z *3p* orbitálov síry (S). Najnižšie vodivostné pásmo má charakter *6p* orbitálu olova (Pb) s prímesou *4s* orbitálu síry. Šírka zakázaného pásma počítaného DFT-LDA s experimentálnou mriežkovou konštantou pri teplote 300 K je 267 meV. Jeho hodnota klesne na 216 meV, keď použijeme experimentálnu mriežkovú konštantu pri teplote 30 K. Umelým zmenšením mriežkovej konštanty redukujeme zakázané pásmo v bode L. Keď mriežkovú konštantu stlačíme na hodnotu a=5.801 Å, zakázané pásmo je nulové s lineárnym skrížením[*] pásov v smere L→Γ a parabolickou disperziou v smere L→W (viď pravý panel Obrázku [V.4]). Situácia je analogická k situácii v graféne; systém je semi-metalický a Fermiho plocha je ostrá, lokalizovaná v bodoch vysokej symetrie L. Pre prislúchajúce fonóny môžeme očakávať Kohnovú anomáliu v Γ a X (rozdiel vlnových vektorov medzi dvomi bodmi L zodpovedá buď Γ alebo X). Je dôležité poznamenať, že ďaľšie zmenšovanie mriežkovej konštanty znovu otvorí zakázané pásmo v bode L, pričom charakter vodivostného a valenčného

**linear crossings

*linear crossing

pásma je obrátený a dochádza tak k reálnemu skríženiu pásov v smere L→W. Neskoršia, podobná štúdia zakázaného pásma pri umelom stlačení kryštálu (Svane *et al.* 2010[115]), využívajúca QSGW teóriu pre *ab-initio* výpočty, potvrdzuje naše výsledky o uzavretí zakázaného pásma a lineárneho skríženia.

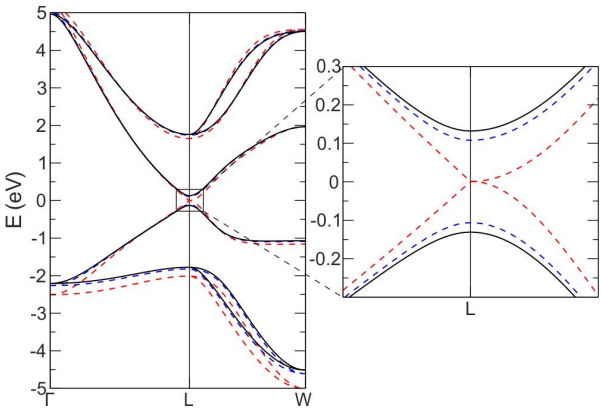

Obrázok V.4: *Ľavý panel: elektronická pásová štruktúra PbS (DFT-LDA bez spin-orbitálnej väzby) pre tri rôzne hodnoty mriežkovej konštanty a. (čierné plné čiary): experimentálna mriežková konštanta pri teplote 300 K; (modré bodkované čiary): experimentálna mriežková konštanta pri teplote 30 K; (červené prerušované čiary): a=5.801 Å stlačená mriežková konštanta pri ktorej sa uzavrie zakázané pásmo. Fermiho hladina je na 0 eV. Pravý panel: priblíženie oblasti okolo priameho zakázaného pásma v bode L*

Na Obrázku [V.5] predstavujeme disperzný vzťah fonónov PbS pre tri rôzne hodnoty mriežkovej konštanty. Ako sme predpokladali, stlačením mriežkovej konštanty dochádza k stvrdnutiu väzieb a teda k náraste fonónových frekvencií. Zmenšením mriežkovej konštanty sa systém stáva „menej ferroelektrickým“, čo najviac ovplyvňuje TO mód. Najvyššia vetva optického módu poklesne v bodoch Γ a X kde pozorujeme ostré obrátené píky zodpovedajúce predpovedanej Kohnovým anomáliám. V ďalšom pozorujeme, že LO a TO módy sú pri stlačenej mriežkovej konštante degenerované v bode Γ; v semi-metalickom priblížení stlačenej mriežkovej konštanty ide ε do

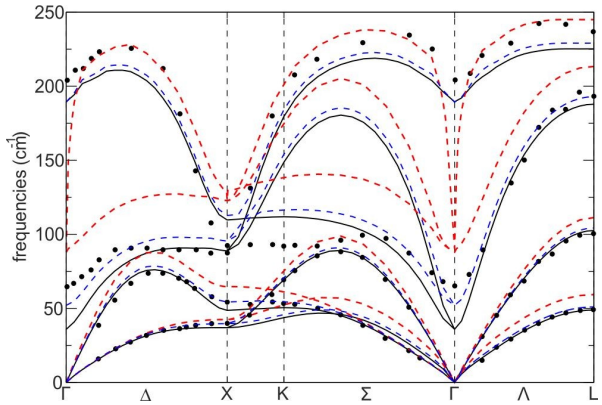

Obrázok V.5: *Farebné čiary: Vypočítané fonónové disperzie PbS pre tri rôzne mriežkové konštanty a. (čierné plné čiary): experimentálna mriežková konštanta pri teplote 300 K; (modré bodkované čiary): experimentálna mriežková konštanta pri teplote 30 K; (červené prerušované čiary) a=5.801 Å stlačená mriežková konštanta pri ktorej sa uzavrie zakázané pásmo Bodky: experimentálne dáta[17].*

nekonečna a LO/TO rozštep ide k nule, podľa rovnice [V.1]. Rozšírením zakázaného pásma na jeho pôvodnú hodnotu (zväčšením mriežkovej konštanty) sa vráti LO/TO rozštep do pôvodného stavu. Avšak viditeľný pozostatok Kohnovej anomálie ostáva vo forme silného obráteného píku LO módu v bode Γ. Na základe toho interpretujeme LO pokles ako kvázi Kohnovú anomáliu.

III. Špecifické teplo

Špecifické teplo materiálov závisí od hustoty stavov fonónov *D(ω)* (pravý panel na Obrázkoch [V.1-V.3]) a dá sa numericky spočítať podľa nasledovnej formuly:

$$c_v = N_A k \int_0^{\infty} \frac{\left(\frac{\hbar\omega}{kT}\right)^2 e^{\hbar\omega/kT}}{\left(e^{\hbar\omega/kT}-1\right)^2} D(\omega)\, d\omega$$

[V.3]

kde *k* je Boltzmannova konštanta a N_A je Avogadrova konštanta*. Kvalitu našich *ab-initio* vypočítaných fonónov môžeme preveriť porovnaním takto spočítaného špecifického tepla (c_v) s experimentálnymi dátami pre PbS, PbSe, a PbTe.[24,27,112,113].

V ľavom panely Obrázka [V.6] je znázornené špecifické teplo ako funkcia teploty. Všetky tri krivky konvergujú k typickej hodnote Petit a Dulonga $6N_Ak$=49.9 J /mol.K pre materiály s dvoma atómami v primitívnej bunke. V pravom panely Obrázka [V.6] sú znázornené závislosti c_v/T^3 v nízko-teplotnom režime. Všetky tri krivky vykazujú maximum v rozmedzí 8 až 12 K.

*D je normalizované na počet fonónových vetiev (6)

Vzhľadom na to, že sme fonónovú disperziu počítali s použitím mriežkovej konštanty pri izbove j teplote, očakávame, že podhodnotíme frekvencie akustických fonónov pri veľmi nízkych teplotách, pri ktorých sa mriežková konštanta zmenší a interatómové silové konštanty narastú. Následovne, nami spočítané c_v/T^3 pre PbS by malo nadhodnotiť experimentálne údaje. Na obrázku [V.6] (modrá prerušovaná čiara) môžeme overiť, že naozaj dochádza k predpokladanému prípadu; maximum c_v/T^3 dosahuje hodnotu 1750 J/mol.K^4. Pre lepšie ohodnotenie špecifického tepla pri nízkej teplote sme zopakovali výpočet hustoty stavov pre PbS s mriežkovou konštantou pri teplote 30 K (pozri Tabuľka [V.1]). Výsledné c_v/T^3 (plné čierne čiary na Obrázku [V.6]) je v perfektnej zhode s nameranými dátami. Pre PbSe máme dobrú zhodu s experimentálnymi hodnotami. V prípade PbTe je špecifické teplo, spočítané na základe fonónov pri nízko teplotnej mriežkovej konštante, nižšie ako namerané dáta. Predpokladáme, že by sme na dosiahnutie lepšej zhody s nameranými hodnotami museli do výpočtov zahrnúť spin-orbitálnu väzbu, keďže v prípade PbTe má s-o väzba silnejší vplyv ako u PbSe a PbS[24].

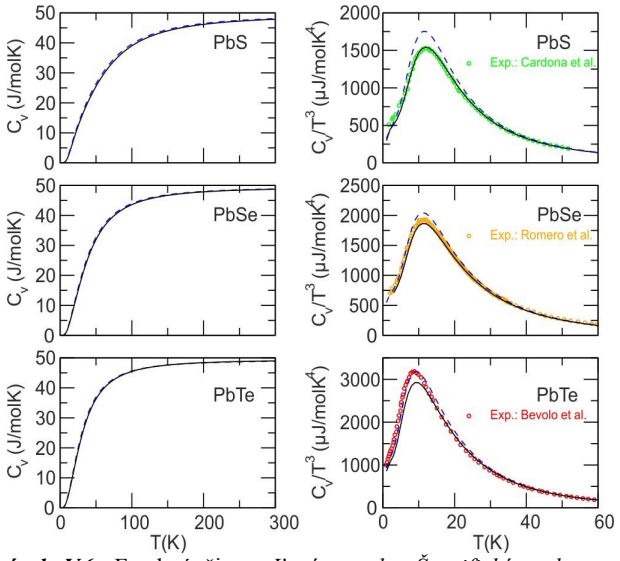

Obrázok V.6: Farebné čiary: *Ľavé panely: Špecifické teplo pre tri olovnaté chalkogenidy ako funkcia teploty. Pravé panely: Špecifické teplo predelené T^3 v nízko teplotnom režíme. Výsledky ab-initio fonónových výpočtov za použitia mriežkovej konštanty pri teplote 30 K (plné čiary) a 300 K (prerušované čiary).* Symboly: *Experimentálne dáta od Cardona et al.[27], Romero et al.[24] a Bevolo et al.[113]*

IV. Štúdia priestorového uväznenia LO fonónov v nanokryštáli PbSe

Nanokryštály olovnatých chalkogenidov sú vďaka svojim vlastnostiam (úzke zakázané pásmo, veľký excitonický polomer a malá efektívna hmotnosť nosičov) vhodné na štúdium optického uväznenia*[10,11]. Analogicky sa očakáva, že sa kvantové uväznenie prejaví aj na fonónoch. Jednou z metód ako detekovať fonóny v nanokryštáloch je Ramanova spektroskopia. V masíve vieme detekovať LO mód v bode Γ, pravdepodobne vďaka Fröhlichov mechanizmu[116]. Na tému Ramanovej spektroskopie nanokryštálov bolo zameraných len niekoľko štúdií[117,118,119,120] a vykazovali protichodné výsledky. Z prevedených experimentov bolo nejasné v ktorom smere (hore/dole) dochádza k posunu frekvencii pri prechode z masívu na nanokryštáli rôznych veľkostí. V nedávnej práci Habinshuti *et al.*[28] prezentovali systematickú štúdiu Ramanovou spektroskopiou, kde sledovali uväznenie fonónov v nanokryštáloch PbSe. V súlade s experimentálnou štúdiou a na doplnenie celkového obrazu sme vypočítali *ab-initio* fonóny PbSe nanokryštálov.

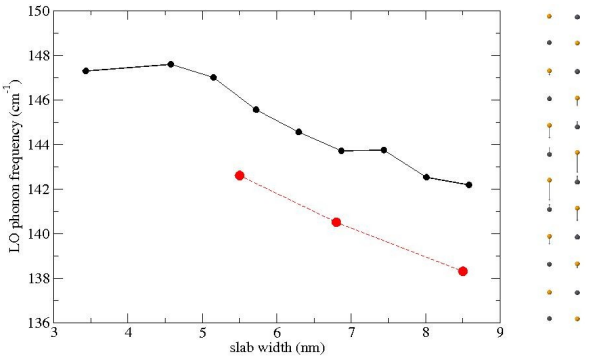

***Obrázok V.7**: Farebné čiary: (čierná): výpočítané frekvencie LO módu pre (100) PbSe dosky s hrúbkou od 6 po 15 vrstiev. (červená): namerané Ramanové frekvencie. Pravý panel znázorňuje vibračné vzory kvantovo uväzneného LO módu (s polarizáciou kolmou na dosku) pre 12 vrstvovú dosku. Dva stĺpce Pb (šedé) a Se (oranžové) atómov predstavujú motív elementárnej bunky v doske.*

Fonóny PbSe nanokryštálov sme vypočítali za pomoci teórie funkcionálu hustoty[83] (DFT) v priblížení lokálnej hustoty[78] (LDA) implementovanej v programe Quantum Espresso[130]. Dosky nanokryštálov sa skladali z 6 až 15 vrstiev s orientáciou (001). Dosky sme zoradili do periodickej superbunky s 14 a.u. vákua medzi jednotlivými doskami (pred relaxáciou). Vlnové funkcie sme rozložili do rovinných vĺn s maximálnou energiou 30 Ry

* optical confinement

a prvú Brillouinovú zónu vzorkujeme 10×10×2 sieťou. Pre olovo sme použili Vanderbiltov ultrajemný pseudopotenciál s *5d* elektrónmi vo valenčnom pásme, pre selén sme použili Bachelet-Hamann-Schlüter pseudopotenciál. V smere roviny dosiek sme použili experimentálnu mriežkovú konštantu pri izbovej teplote 6.124Å[1]. Geometriu v smere kolmom na rovinu dosiek sme optimalizovali, čo viedlo k 1.3% skráteniu vzdialeností medzi susediacimi atómami a ku zvlneniu povrchu dosky o 0.072Å (rozdiel medzi kolmou vzdialenosťou Pb a Se atómov od roviny dosky). Fonónové frekvencie sme vypočítali z rovnice V.1 a elementy dynamickej matice za pomoci poruchovej teórie funkcionálu hustoty[84] (DFPT).

Výsledky sú zhrnuté na Obrázku [V.7] a v Tabuľke [V.3]. Naše výpočty potvrdzujú nárast LO frekvencii pri zmenšujúcom sa priemere nanokryštálu, ako bolo pozorované pri experimente a očakávané na základe modelu kvantového uväznenia. Vypočítané frekvencie sú čiastočne vyššie ako namerané, čo je zapríčinené LDA priblížením, avšak kvalitatívny priebeh kriviek sa veľmi dobre zhoduje s nameranými hodnotami. Ďalšia nepresnosť, pri porovnávaní našich hodnôt v s experimentálnymi, spočíva v dielektrickom okolí nanokryštálov, ktoré môže silno ovplyvniť na interakciu medzi indukovaným makroskopickým elektrickým poľom a LO módom.

PbSe diameter/hrúbka dosky [nm]	Experimentálne LO frekvencie [cm-[1]]	*Ab-initio* vypočítané LO frekvencie [cm-[1]]
5.5	142.6	147
6.8	140.5	144.5
8.5	138.3	142.5

Tabuľka V.3*: porovnanie ab-initio vypočítaných (táto práca128) LO fonónových frekvencii a nameraných Ramanovou spektroskopiou[28] v závislosti od priemeru nanokryštálu (hrúbka dosky ako ekvivalent)*

Zaznamenali sme, že anomália LO módu fonónovej disperzií v masíve PbSe (nameraná [18,19] a vypočítaná[128]) sa prejavuje aj v závislosti Ramanovho spektra nanokryštálov od ich priemeru. Kontrastne k väčšine materiálov v nanokryštalickej fáze, kde frekvencia Ramanovskyaktívných fonónononových módov poklesne, v prípade PbSe

zaznamenávame nárast Ramanovho píku so zmenšujúcim sa priemerom kryštálu. Kvalitatívne to vysvetľujeme v rámci kvantového uväznenia LO módu, keďže fonónová disperzia má pokles v centre zóny. Zmenšenie polomeru kryštálu znamená nárast hodnoty kvantovaného vlnového vektora a čo vedie k nárastu frekvencie. Toto správanie sme kvalitatívne potvrdili ab-initio výpočtom fonónov PbSe dosiek rôznych hrúbok. Výpočty zohľadňovali aj zmenu v elektrónovej štruktúre (zväčšenie zakázaného pásma) a dielektrické okolie.

Záver:

Využitím DFT+DFPT v aproximácii lokálnej hustoty sme vypočítali disperzný vzťah fonónov olovnatých chalkogenidov (Obrázky [V.1-V.3]). Použitie striktných konvergentných kritérií a premysleného výberu pseudopotenciálu olova a vzorkovania k-bodov (T-M pseudopotenciál olova s *5d* elektrónmi vo valenčnom páse a vhniezdená M-P vzorkovacia sieť), nám umožnilo dosiahnuť veľmi dobrú zhodu s experimentálnymi fonónovými dátami[16,17,18,19] a meraniami špecifického tepla[24,27,112,113]. Akustické módy sme reprodukovali skoro exaktne a nami vypočítané špecifické teplo (Obrázok [V.6]), závislé prevažne od akustických fonónov, sa dobre zhoduje s meraniami. Optické módy fonónov sa zhodujú kvalitatívne s experimentálnymi dátami, ale sú v horšej kvantitatívnej zhode s nameranými hodnotami ako akustické. Odchýlku sme očakávali, keďže naše výpočty zahŕňali vplyv teploty len cez výber mriežkovej konštanty meranej pri izbovej teplote, zatiaľ čo renormalizácia cez fonón-fonónovú interakciu[109] bola v rámci harmonického priblíženia zanedbaná. Naše výpočty reprodukujú silný pokles LO módu v bode Γ. LO pokles v Γ súvisí s úzkym zakázaným pásmom a dá sa vysvetliť ako kvázi Kohnová anomália. V našej štúdii elektrónovej pásovej štruktúry PbS (Obrázok [V.4]) ukazujeme, že stlačené PbS je semi-metalický systém správajúci sa podobne ako grafén (nulové zakázané pásmo v bode L, lineárne prekríženie v smere L→Γ, parabolická disperzia v smere L→W) a preto by mal vykazovať Kohnové anomálie vo fonónovej disperzií v bode Γ alebo X.

Taktiež sme vypočítali fonóny na nanokryštalickej úrovni a Γ fonóny selenidu

olovnatého pre kvantové bodky rôznych veľkostí (Obrázok [V.7]), doplňujúc výsledky v súlade s nedávnymi experimentami Ramanovou spektroskopiou[28], kde skúmali priestorové uväznenie fonónov v nanokryštáli PbSe.

Detailne sme preskúmali disperzný vzťah fonónov olovnatých chalkogenidov, vrátane LO poklesu v bode Γ, a tak sme poskytli veľmi kvalitné dáta pre ďalší výskum. V posledných rokoch boli objavené veľmi perspektívne elektrické a optické vlastnosti nanokryštálov olovnatých solí, vďaka čomu by sa mohli stať dobrým médiom pre moderné opto-elektronické zariadenia, luminiscenčné organické farbivá a obzvlášť vysoko-účinné slnečné kolektory (PbS, PbSe). Veľa výskumných projektov, teoretických a experimentálnych, sa zameralo na optické a elektrické vlastnosti nanokryštálov, obzvlášť v oblasti slnečnej konverzie. Napriek tomu máme stále medzery v úplnom pochopení všetkých ich vlastností. Predovšetkým je nevyhnutné hlbšie preskúmať elektrón-fonónovú interakciu v olovnatých chalkogenidoch na to, aby sme dostatočne pochopili de-excitačný mechanizmus horúcich nosičov. Náš výskum poskytuje nevyhnutné dáta pre ďalšie skúmanie nanokryštalickej fázy.

VI. Résumé - French

VI.Résumé - French

Les chalcogénures de plomb (PbS, PbSe et PbTe) sont des semi-conducteurs de groupe IV-VI à faible gap fine et la structure cristalline du sel gemme. Dans la phase nanocristalline ils ont des propriétés électriques et optiques supérieurs et sont donc potentiellement intéressantes pour de nombreux dispositifs. Les chalcogénures de plomb ont la bande interdite de 280–410 meV à la température ambiante[1], un grande diamètre des excitons (20 nm v PbS a 46 nm v PbSe)[10] et la masse effective des porteurs est petite. Ces caractéristiques font de lui un matériau privilégié pour les dispositifs opto-électroniques et photovoltaics, aussi que pour des études de confinement quantique[9,10]. Par exemple un laser infra-rouge de haut performance sous la base des PbSe/PbEuTe nanocristeaux a été construit[14]. Des investigations[15] récents indiquent que les PbSe nanocristeaux pourraient servir comme la base pour des collecteurs solaires de haut performance. Grâce à l'ionisation par impacte un paire électron-trou de grande énergie se décompose en plusieurs paires électron-trou avec l'énergie inférieur. Cette multiplication pourrait théoriquement mener à des panneaux solaire avec une conversion de 60,3%[15]. Pour bien comprendre le mécanisme de de-excitation il faut savoir plus de l'interaction électron-phonon dans les chalcogénures de plomb. La structure de bandes est très bien examinée et des calcules de bonne qualité ont été présenté (Réf.[16] Et des références dedans). Quand même la dispersion des phonons des chalcogénures de plomb n'est pas si profondément sondé. La dispersion des phonons de PbS, PbSe et PbTe a été mésurée par la diffraction inélastique des neutrons[17,18,19]. Les simulations de la dispersion des phonons ont été faite au niveau des modèles semi-empiriques[20,21,22,23]. Les trois matériaux montrent la même anomalie dans la relation de dispersion; un chute abrupte dans la branche longitudinale optique (LO) dans le point Γ. Plusieurs propositions pour expliquer l'abaissement du mode LO ont été présentés; Cowley et Dolling[22] l'attribuent à l'écrantage par porteur libres dans le cristal. Dans les calcules semi-empiriques de Upadhyaya *et al.*[20] l'anomalie est associée à la dopage par des porteur libres. Maksimenko et Mishchenko[23] l'expliquent à l'aide de le pseudo-effet de Jahn-Teller[21]. Les calcules *ab-initio* récents de phonons des chalcogénures de plomb[24] ont montrés un minimum dans le mode LO pour PbSe et PbTe lequel c'est approfondi en ajoutant au calcules la liaison spin-orbitale. Quand même la cause de cet anomalie est inconnue.

VI.Résumé - French

On présente une étude *ab-initio* systématique de la relation de dispersion des phonons des chalcogénures de plomb. On reproduit quantitativement les phonons acoustiques, les anomalies de mode LO et TO sont reproduites qualitativement. Les anomalies dépendent fortement de la température[23] et donc pour une description quantitative on devrait inclure des effets anharmoniques. Nos calcules démontrent que le pic inverse de mode LO dans le point Γ et présente aussi dans le matériel pure sans des porteurs libres. On explique l'abaissement comme analogue à celui des anomalies de Kohn[25], présentes dans le graphène semi-métalique[26]. On démontre que les calculs *ab-initio* peuvent très bien reproduire la chaleur spécifique de PbS, PbSe et PbTe et on les compare avec des calculs récents[24,27] (incluant l'effet spin-orbitale). Ensuit on présent calculs *ab-initio* des phonons LO pour des films de PbSe d'épaisseur différente. Nos calculs servent notamment à confirmer des expériences récents[28] effectués par la spectroscopie de Raman. Ces expériences montrent la dépendance du spectre de Raman de diamètre des nanocristeaux et ont observé une décalage bleu du pic principale (relié avec le mode LO) en diminuant le diamètre des nanocristeaux.

I. Les détails des calculs.

En utilisant l'approximation harmonique on obtient les phonons en fonction du vecteur d'onde $\vec{q}$ de l'équation suivante:

$$\det\left|\frac{1}{\sqrt{M_s M_t}}\ \widetilde{C}_{st}^{\alpha\beta}(\vec{q})-\omega(\vec{q})^2\right|=0$$

[VI.1]

La matrice dynamique $\widetilde{C}_{st}^{\alpha\beta}(\vec{q})$ correspond à la force exercée sur l'atome *t* dans la direction β causée par le déplacement de l'atome *s* dans la direction α. On a calculé la matrice en utilisant la théorie de perturbation de la fonctionnelle de la densité* (DFPT)[83,84] implémentée dans le logiciel ABINIT[106]. Pour la fonctionnelle de l'échange et de la

* Density Functional Perturbation Theory

corrélation**[78] on a utilisé l'approximation de la densité locale*. Les fonctions d'onde sont décomposées sous forme d'ondes planes (jusqu'à l'énergie 40 hartree) et les électrons intérieurs été remplacés par des pseudopotentiels. On a constaté que les fréquences des phonons sont très sensibles au choix du pseudopotentiel de plomb. Il est essentiel d'inclure des électrons intérieurs d'orbitale *5d* entre les électrons de valence, et donc de calculer leur densité directement, car les chalcogénures de plomb ont un caractère fortement ionique et les électrons d'orbitale *5d* de plomb participent à la part covalente de liaison PbX (X = S, Se, Te). On a généré et testé[98,99] plusieurs pseudopotentiels du type *Troullier-Martins* et vérifié que les pseudopotentiels présentés sur la page web ABINIT[106] fournissent des résultats convergents.

Dans nos calcules on a utilisé les constantes de maille expérimentales à 300K (voir Tableaux [VI.1]) car les constants de maille calculées *ab-initio* en utilisant LDA sont sous-estimées et dans les matériaux ferroélectriques même une déviation de 1% suffit à influencer sensiblement les fréquences de phonons[108].

	DFT-LDA (Å)	Expt. 30 K (Å)	Expt. 300 K (Å)
PbS	5.810	5.909	5.936
PbSe	6.012	6.098	6.124
PbTe	6.318	6.428	6.462

Tableaux VI.1*: Comparaison de constants de maille calculées avec de valeurs expérimentales (Réf.[1]) à 30K et 300K.*

Pour obtenir des résultats convergents on a utilisé pour échantillonnage des point électroniques *k* de la première zone de Brillouin un réseaux de Monkhorst-Pack[104] 7×7×7 avec un réseaux supplémentaire 3×3×3 autour de point de haut symétrie L.

**exchange-correlation functional

* Local-Density Approximation

II. La dispersion des phonons

On présente les courbes de dispersion des phonons des chalcogénures de plomb calculées *ab-initio* en comparaison avec des données expérimentales obtenues par spectroscopie par diffraction inélastique de neutrons [VI.1,VI.2,VI.3]. On montre aussi la densité d'état des phonons qu'on a utilisé pour calculer la capacité thermique spécifique. On a obtenu dans les trois cas un très bon accord avec des données expérimentales pour les branches acoustiques. Les branches acoustiques correspondent presque uniquement aux vibrations des ions de plomb qui sont plus lourds que les atomes S, Se, Te. Pour cela les modes acoustiques sont très similaires pour les trois chalcogénures et la majeure différence est dans le faible abaissement des fréquences correspondant à la diminution de la constante de maille dans la série PbS, PbSe a PbTe. Les branches optiques correspondent aux vibrations des anions; le fréquence maximale se comporte comme $1/\sqrt{M_X}$, ou X représente l'anion correspondant. Dans le cas de PbS les modes optiques ont une si grande énergie qu'on n'observe pas de croisement avec les branches acoustiques, dans le cas de PbSe et PbTe on observe le croisement.

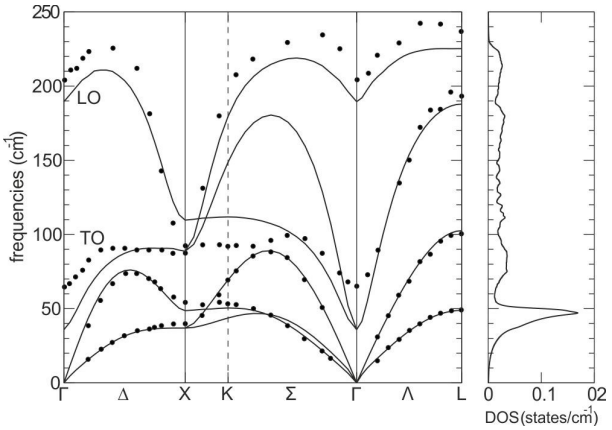

***Image VI.1**: Panneau gauche: courbe de dispersion calculée de phonons de PbS (lignes noirs pleins) en comparison avec des donnés experimentalles[18](points). Panneau droit: densité d'état des phonons*

Dans les trois cas on observe une séparation LO/TO considérable au le point Γ. Pour un système cubique la séparation est décrite par:

$$\omega^2_{\mathrm{LO}} - \omega^2_{\mathrm{TO}} = \frac{4\pi e^2}{\mu\Omega}\frac{(Z^*)^2}{\epsilon}$$

[VI.2]

d' où Z^* (voir Tableaux [VI.2]) est la charge effective, ε est la constante diélectrique, e est la charge d'électron, Ω est le volume de la cellule unitaire et $\mu = \frac{M_{Pb} M_X}{M_{Pb} + M_X}$ est la masse effective.

	ϵ	Z*
PbS	19.6	±4.5
PbSe	24.1	±4.9
PbTe	31.7	±6.1

Tableaux VI.2*: Les valeurs de la constante diélectrique e et de la charge effective pour les trois chalcogénures de plomb. Les calculs ont été fait au niveau de DFT-LDA avec la constante de maille expérimentale à 300 K*

La séparation LO/TO est grâce aux charges effectives très grandes considérablement approfondie même qu'on a une forte écrantage diélectrique. Donc le mode TO atteint des fréquences basses au point Γ, lesquelles sont très sensibles à la constante de maille. Une diminution artificielle de la constante de maille de 0.1 Å pour le PbSe a pour conséquence une abaissement de fréquence TO au dessous de zéro, donc des valeurs imaginaires, ce que signifie que la phase fcc* ne sera plus stable. Cela est une démonstration du caractère presque ferroélectrique des chalcogénures de plomb.

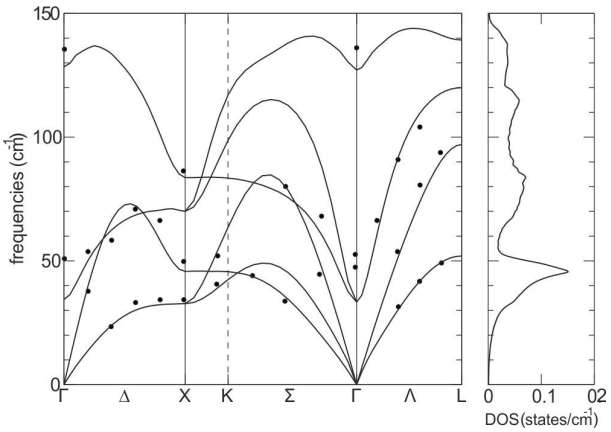

Image VI.2*: Panneau gauche: courbe de dispersion calculée de phonons de PbS (lignes noirs pleins) en comparison avec des donnés experimentalles[19](points). Panneau droit: densité d'état des phonon*

*Réseau à faces centrées

Dans les trois cas on observe un abaissement profond de la fréquence du mode LO au point Γ. Par le passe, cette baisse était associée a l'écrantage du champs électrique (associe au mode LO) par des porteurs libres suite a la présence d'impuretés (Cowley z Dolling[22]). Mais nos calculs montrent que cela persiste même dans le cas de cristaux parfaits de chalcogenures de plomb. Nos calculs sont plustôt en accord avec la théorie de Maksimenka et Mischenko[23], qui l'expliquent à l'aide d'une forte intéraction de électron-phonon de type pseudo-Jahn-Teller sans la présence des porteurs libres. Nous expliquons cette chute comme une "quasi-Anomalie de Kohn"* associée au faible gap électronique au point de haute symétrie L.

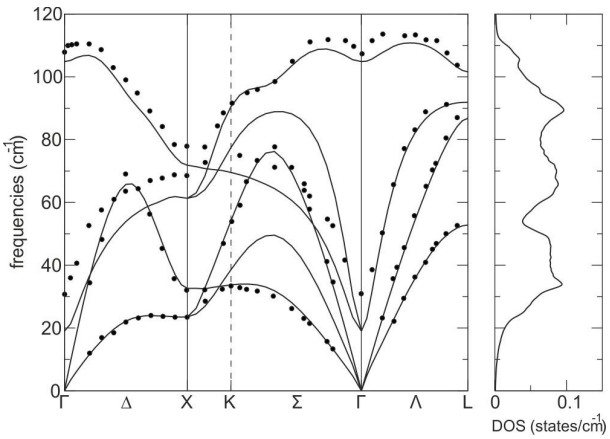

***Image VI.3**: Panneau gauche: courbe de dispersion calculée de phonons de PbS (lignes noirs pleins) en comparison avec des donnés experimentalles[17](points). Panneau droit: densité d'état des phononsi*

L'anomalie de Kohn[25] est une notion connue dans les systèmes métalliques, dans lesquelles les vibrations des ions sont partialement écrantées par le gaz des électrons. L'écrantage peux être fortement augmenté pour les vibrations du vecteur d'onde $\vec{q}$ qui connecte deux points de surface de Fermi. Les chalcogénures de plomb sont des semi-conducteurs donc leur dispersion de phonons ne présente *–a priori–* pas des anomalies de Kohn. Cependent leur bande interdite au point de haut symétrie L est petite et peut être fermée par une compression de la maille. Sur l' Image [VI.4] on présente une étude de structure de bandes de PbS pour trois valeurs de la constante de maille dans la direction Γ→L→W. La bande interdite est maximale pour la constante de maille expérimentale à 300K, elle diminue pour la constante à 30K et pour la maille artificiellement comprimée à la valeur a=5.801 Å la bande interdite devient nulle avec un croisement linéaire* dans la

*near Kohn anomaly

*linear crossing

direction L→Γ et la dispersion parabolique pour la direction L→W (voir le panneau droit sur l' Image [VI.4]). Cette situation est analogue au graphène[26] qui exhibe deux anomalies de Kohn; le système est semi-métalique et la surface de Fermi est pointue, localisée aux points de haut symétrie L. Pour les phonons correspondane on peut obtenir une anomalie de Kohn dans Γ et X. Il faut remarque que si on continue de diminuer la constante de maille on réouvre la bande interdite au point L et le caractère de la bande de valence et de la bande de conduction devient inversé. Récemment une étude similaire de la bande interdite de cristal sous pression, présenté par Svane *et al.* 2010[115], utilisant la théorie QSGW pour des calcules *ab-initio* vérifie nos résultats de la fermeture de la bande interdite et du croisement linéaire.

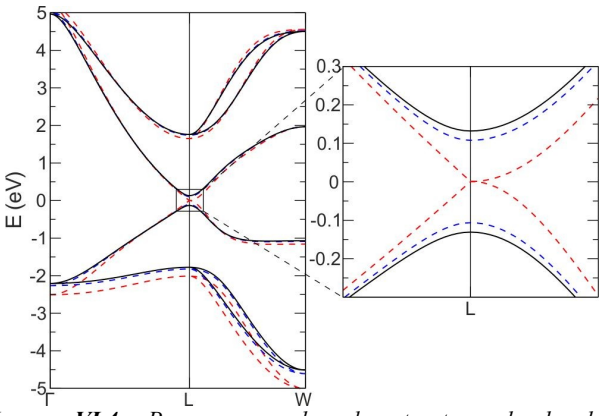

Image VI.4: *Panneau gauche: la structure de bandes électronique de PbS (DFT-LDA sans la liaison spin-orbitale) pour trois valeurs de la constante de maille a. (lignes noirs pleins): la constante de maille expérimentale à 300 K; (lignes bleu):la constante de maille expérimentale à 30 K; (lignes rouges interrompues): la constante de maille comprimées a=5.801 Å tels que la bande interdite est fermée. Niveau de Fermi à 0 eV. Panneau droit: agrandissement de la région de la bande interdite en point L*

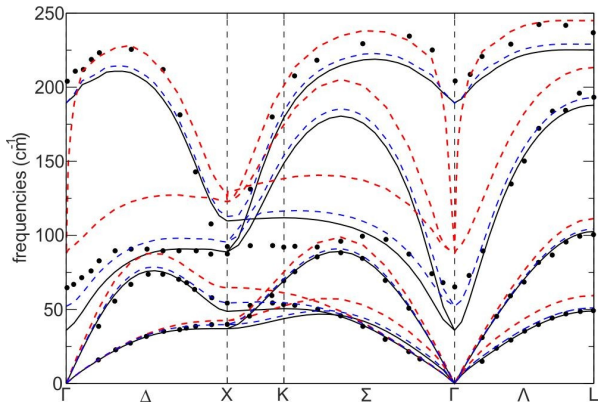

Obrázok VI.5: *Lignes en couleur: courbe de dispersion calculée de phonons de PbS pour trois valeurs de la constante de maille a. (lignes noirs pleins): la constante de maille expérimentale à 300 K; (lignes bleu):la constante de maille expérimentale à 30 K; (lignes rouges interrompues): la constante de maille comprimées a=5.801 Å tels que la bande interdite est fermée. Points: donnés expérimentales[17].*

On présente sur l' Image [VI.5] la dispersion des phonons de PbS pour trois constantes de maille différentes. D'après notre supposition en comprimant la constante de maille

les liaisons devient plus dures et donc les fréquences des phonons augmentent. Par la diminution de la constante de maille le système devient « moins ferroélectrique » ce que influence principalement le mode TO. La haute branche du mode optique est abaissée aux points Γ et X ou on observe des pics inverses correspondantes aux anomalies de Kohn. Ensuite on a observé que les modes LO et TO sont dégénérés an point Γ lorsqu'on compresse le cristal; dans l'approximation semi-métalique en diminuant la constante de maille la constante diélectrique ε tend vers l'infini et la séparation LO/TO tend vers zéro, d'après l'équation [VI.1]. Quand on reouvre la bande interdite à sa valeur initiale (par rélargir la constante de maille) la fissure LO/TO revient dans son état initiale mais il reste un résidu de l'anomalie de Kohn visible sous forme d'un pic inverse du mode LO en point Γ. En raison de ce phénomène on interprète l'abaissement du mode LO comme la quasi-anomalie de Kohn.

III. La chaleur spécifique

La capacité thermique spécifique des matériaux dépend de la densité d'état des phonons D(ω) (panneau droit sur les Images [VI.1-VI.3]) et peut être calculée numériquement en utilisant la formule suivante:

$$c_v = N_A k \int_0^\infty \frac{\left(\frac{\hbar\omega}{kT}\right)^2 e^{\hbar\omega/kT}}{\left(e^{\hbar\omega/kT}-1\right)^2} D(\omega)\, d\omega$$

[VI.3]

où k est la constante de Boltzmann et N_A est la constant d' Avogadro*. On peut donc vérifier la qualité de nos phonons calculés *ab-initio* en comparant la chaleur spécifique calculée (c_v) avec les donnée expérimentaux pour PbS, PbSe et PbTe[24,27,112,113].

**D* est normalisée aux nombre des branches des phonons (6)

Dans le panneau gauche d' Image [VI.6] on représente la chaleur spécifique comme une fonction de la température. Les trois courbes convergent vers la valeur typique de Petit et Dulong $6N_Ak=49.9$ J /mol.K pour des matériaux avec deux atomes dans la cellule primitive. Dans le panneau droit d' Image [VI.6] on représente la dépendance c_v/T^3 dans le régime de basse température. Les trois courbes ont un maximum dans l'intervalle de 8-12 K. Lorsqu'on avait calculé la dispersion de phonons en utilisant la constante de maille à 300K on a prévu qu'on sous-éstime les fréquences des phonons acoustiques à des températures basse où la constante de maille diminue et les constantes de forces interatomiques augmentent. En suite nôtre c_v/T^3 de PbS calculé devrait sure-éstimer les valeurs expérimentales (voir l' Image [VI.6] la ligne bleu interrompue)

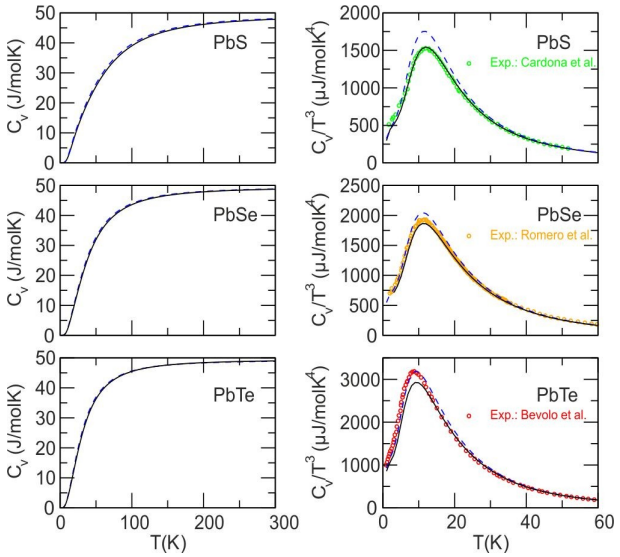

***Image VI.6**: Lignes en couleur: Panneau gauche: Chaleur spécifique des trois chalcogénures de plomb en fonction de la température. Panneau droit: Chaleur spécifique divisée par T^3 dans le régime de basse température calculée à la base des phonons calculés ab-initio uilisant la constante de maille à 30K (lignes pleins) et à 300K (lignes interrompues). Symboles: Valeurs expérimentales. Cardona et al.[27], Romero et al.[24] a Bevolo et al.[113]*

Pour une meilleure évaluation de la chaleur spécifique à des températures basse on a recalculé la densité d'état pour PbS avec la constante de maille à 30K (voir Tableau [VI.1]). Le c_v/T^3 résultant (ligne noirs plaines sut l' Image [VI.6]) est parfaitement en accord avec des données expérimentaux. Pour PbSe on constate un bon accord avec des valeur expérimentalles. La chaleur spécifique de PbTe, calculée en utilisant les phonons à constante de maille à 30K, est plus bas que les donnée experimentaux. On suppose que pour obtenir un bon accord il faudra inclure la liaison spin-orbitale dans les calculs, car dans le cas de PbTe la liaison spin-orbitale a une influence plus forte que dans le cas de PbSe et PbS[24].

IV. Étude de confinement quantique du phonon LO dans les nanocristeaux PbSe.

Les nanocristeaux des chalcogénures de plomb ont des propriétés interessantes (bande interdite fine, grand diamètre excitonique et petite masse effective des porteurs) pour les études du confinement optique*[10,11]. De manière analogue on s'attend à ce que le confinement quantique influence les phonons. Une des méthodes pour détecter des phonons dans les nanocristeaux est la spectroscopie Raman. Grâce au mécanisme de Fröhlichov[116] (probablement) on peut détecter le mode LO à G dans le massif. Plusieurs travaux adressaient la spectroscopie de Raman des nanocristeaux[117,118,119,120] mais les résultats étaient contradictoires. Concrètement le sans de la décalage en fréquence de ce mode en fonction du diamètre des nanocristaux. Récemment Habinshuti *et al.*[28] présentait une étude systématique par la spectroscopie de Raman du confinement quantique des phonons dans les nanocristaux de PbSe. On a calculé *ab-initio* les phonons dans les nanocristeaux de séléniur de plomb ce qui apporte un support théorique pour l'interprétation des spectres Raman mésurés par Habinshuti *et al.*

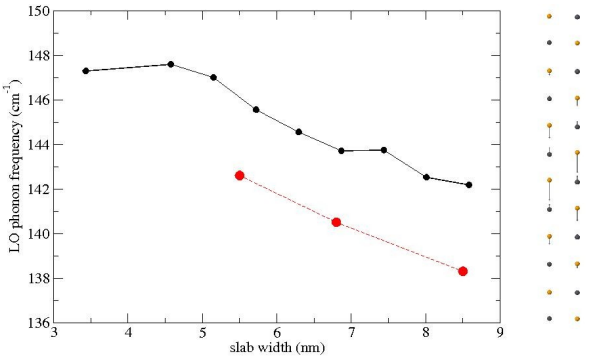

***Image VI.7**: Lignes en couleur: (noir): fréquences calculées pour le mode LO du film (100) PbSe avec l'épaisseur de 6 à 15 couches. (rouge): fréquences Raman mesurées. Panneau droit représente la structure de vibration du mode LO confiné (polarisation perpendiculaire au film) pour un film à 12 couches. Deux collones des atomes Pb (gris) et Se (orange) représentent le motive de la cellule élementaire.*

On présente les phonons des nanocristeaux PbSe calculé *ab-initio* dans le cadre DFT+LDA[83,78] implémenté dans le code Quantum Espresso[130]. On a utilisé la géométrie des films crées par une super-cellule composée de 6 à 15 couches, orientés (001), de PbSe et 14 a.u. de vide. Les fonctions d'ondes été décomposées à des ondes planes d'énergie maximale de 30 Ry et on a échantillonné la première zone de Brillouin par un réseau

* optical confinement

10×10×2. Pour le plomb on a utilisé un pseudopotentiel ultra léger* de Vanderbilt avec des *5d* électrons dans la bande des valences et pour sélénium on avait un pseudopotentiel de Bachelet-Hamann-Schlüter. Dans la direction du plan on a calculé avec la constante de maille expérimentale à température ambiante (6.124Å[1]), la géométrie dans le sens perpendiculaire a été optimisée. Les phonons ont été calculés utilisant l'équation VI.1 et les éléments de la matrice dynamique par la théorie de la perturbation du fonctionelle de la densité[84] (DFPT).

Les résultats sont totalisés sur l'Image [VI.7] et dans le Tableau [VI.3]. Nos calculs vérifient la tendance de la fréquence du mode LO de croitre avec la diminution de la taille du cristal, correspondant à des observation expérimentales et en accord avec le modèle du confinement quantique. Les fréquences calculées sont un peu au dessus des fréquences mesurées à cause de l'approximation de la densité locale, mais qualitativement les courbes de dispersion correspondent aux donné expérimentales.

PbSe diamètre [nm]	Fréquences LO expérimentales [cm-^{1}]	Fréquences LO calculées *ab-initio* [cm-^{1}]
5.5	142.6	147
6.8	140.5	144.5
8.5	138.3	142.5

Tableau VI.3*: comparaison des fréquences LO calculées ab-initio (cette travail[128]) et mesurées par la spectroscopie Raman[28] en fonction de diamètre du nanocristal (épaisseur du film).*

On a observé que l'anomalie du mode LO de la dispersion des phonons dans le massif de PbSe (mesurée [18,19] et calculée[128]) se manifeste aussi dans la dépendance du spectre de Raman du diamètre des nanocristeaux. Par opposition à la majorité des matériaux sous forme nanocristalline, où la fréquence des phonons Ramman actives diminue, dans le cas de PbSe on observe une croissance du pic de Ramman. On l'explique qualitativement dans le cadre du confinement quantique du mode LO où la dispersion montre un pic inverse au centre de la zone. Diminution du diamètre du nanocristale signifie

* ultra soft

une augmentation de la valeur du vecteur d'onde quantique et donc la fréquence augmente. On a vérifié ce comportement qualitativement par des calculs *ab-initio* des phonons de films d'épaisseur variable.

Conclusion:

En utilisant DFT+DFPT et l'approximation locale de la densité on a calculé des dispersions de phonons des chalcogénures de plomb (l'Images [VI.1-VI.3]). Appliquant des critères strictes pour la convergence et pour des pseudopotentiels on a obtenu des résultats en bon accord avec des valeurs des phonons expérimentales[16,17,18,19] et avec des mesures de la chaleur spécifique[24,27,112,113]. On a reproduit des phonons acoustiques presque exactement et la chaleur spécifique calculée (l' Image [VI.6]), qui dépend principialement des phonons acoustiques, est en accord avec des données expérimentales. Les phonons optiques son en accord avec les valeur mesurées qualitativement mais l'accord quantitative devient plus mauvaise ce que nous avions anticipé car les effet thermique été incorporé seulement au niveau du choix de la constante de maille à température ambiante. On a reproduit le forte chut du mode LO au point Γ. L'abaissement des fréquences LO est relié avec la bande interdite étroite et peut être expliqué comme une quasi anomalie de Kohn. On montre par des calculs de la structure de bandes de PbS (l' Image [VI.4]) que le PbS comprimé est un système semi-métalique similaire de graphène (la bande interdite fermée dans le point L, croissement linéaire L→Γ et dispersion parabolique L→W) et devrait manifester une anomalie de Kohn dans la dispersion des phonons dans le point Γ ou X. On a aussi calculé des phonons en point Γ pour des nanocristeaux de PbSe de différente taille (l' Image [VI.7]). Nos résultats sont complémentaires au récent expérience par la spectroscopie de Raman[28] de confinement spatiale des phonons dans les nanocristals de PbSe.

Nous avons profondément étudié la relation de dispersion des phonons des chalcogénures de plomb y compris le chut abrupte de mode LO au point Γ, fournissant des données de hauet qualité pour la future recherche. Ces dernières années, de nombreuses perspectives intéressantes ont été attribuées aux nanocristaux de chalcogénures de plomb.

On envisage notamment de les utiliser dans des dispositifs opto-électroniques dernière génération, dans des colorants organiques luminescents et des pilles solaires efficaces (PbS, PbSe). Malgré des nombreux projets de recherche dédicacés aux propriétés électriques et optiques, spécialement la conversion solaire, des nanocristeaux on ne comprends pas encore toutes leurs propriétés. Notamment il faut étudier plus profondément l'interaction électron-phonon dans les chalcogénures de plomb pour bien comprendre le mécanismes de de-excitation des porteurs. Nos recherches fournissent les donnée nécessaires pour la future investigation de la phase nanocristalline.

VII. References

[1]*Semiconductors: Group IV Elements, IV-IV and III-IV Compounds*, Landolt-Börnstein, New Series, Group III, Vol. **41**, Pt. A, edited by MADELUNG O., RÖSSLER U., SCHULZ M., Springer- Verlag, Berlin (2005)
[2]LOPEZ-OTERO A., *Hot-wall epitaxy*, Thin Solid Films, **49**, 3 (1978)
[3]CUSHMAN R.J., *Film-type infrared photoconductors*, Proceedings of IRE **47,** 1471 (1959)
[4]ZEMEL J.N., JENSEN J.D., SCHOOLAR R.B., *Electrical and Optical Properties of Epitaxial Films of PbS, PbSe, PbTe, and SnTe*, Phys. Rev., **140**, A330 (1965)
[5]COCHRAN W., *Crystal stability and the theory of ferroelectricity*, Adv. Phys., **9**, 387 (1960); COCHRAN W., *Dielectric constant of lead telluride*, Phys. Lett., **13**, 193 (1964)
[6]DIMMOCK J.O, MELNAGAILIS I., STRAUSS A.J., *Band Structure and Laser Action in* $Pb_xSn_{1-x}Te$, Phys, Rev. Lett., **16**, 1193 (1966)
[7]JANTSCH W., BAUER G., KROST A., LOPEZ-OTERO A., *Anomalies of the static dielectric constant of* $Pb_{1-x}Ge_xTe$, Z. Phys. B – Condensed Matter, **41**, 287 (1981)
[8]EKIMOV A.I., ONUSHCHENKO A.A., *Quantum size effect in three-dimensional microscopic semiconductor crystals*, JETP Lett., **34**, 345. (1981)
[9]ROSSETTI R., NAKAHARA S., BRUS L.E., *Quantum size effects in the redox potentials, resonance Raman spectra, and electronic spectra of CdS crystallites in aqueous solution*, J. Chem. Phys., **79**, 1086 (1983)
[10]WISE F.W., *Lead Salt Quantum Dots: the Limit of Strong Quantum Confinement*, *Acc. Chem. Res.*, **33**, 773 (2000)
[11]WEHRENBERG B.L., WANG C., GUYOT-SIONNEST P., *Interband and Intraband Optical Studies of PbSe Colloidal Quantum Dots*, J. Phys. Chem. B, **106**, 10634 (2002)
[12]MOREELS I., LAMBERT K., SMEETS D., *et al.*, *Size-Dependent Optical Properties of Colloidal PbS Quantum Dots*, AcsNano, **3**, 10, 3023 (2009)
[13]CADEMARTIRI, L., BERTOLOTTI J., SAPIENZA R., *et al.*, *Multigram Scale, Solventless, and Diffusion-Controlled Route to Highly Monodisperse PbS Nanocrystals*, J. Phys. Chem. B, ***110***, 671 (2006)
[14]SPRINGHOLZ G., SCHWARZL T., HEISS W., *et al.*, *Midinfrared surface-emitting PbSe/PbEuTe quantum-dot lasers*, Appl. Phys. Lett., **79**, 1225 (2001)
[15]SCHALLER R. D., KLIMOV V. I., *High Efficiency Carrier Multiplication in PbSe Nanocrystals: Implications for Solar Energy Conversion*, Phys. Rev. Lett., **92**, 186601 (2004)
[16]HUMMER K., GRÜNEIS A., KRESSE G., *Structural and electronic properties of lead chalcogenides from first principles*, Phys. Rev. B, **75**, 195211 (2007)
[17]COCHRAN W., COWLEY R.A., DOLLING G., *The Crystal Dynamics of Lead Telluride*, Proc. R. Soc. London A, **293**, 433 (1966)
[18]ELCOMBE M.M., *The Crystal Dynamics of Lead Sulfide*, *Proc. R. Soc. London Ser. A*, **300**, 210 (1967)
[19]VIJAYARAGHAVAN P.R., SINHA S.K., IYENGAR P. K., *Proc. Nucl. Phys. Solid State Phys. Symp. C*, **16**, 208 (1973)
[20]UPADHYAYA K.S., YADAV M., UPHADHYAYA G.K., *Lattice Dynamics of IV–VI Ionic Semiconductors: An Application to Lead Chalcogenides*, Phys. Status Solidi B, **229**, 1129 (2002)
[21]GEHRING G.A., GEHRING K.A., *Co-operative Jahn-Teller effects*, Rep. Prog. Phys., **38**, 1 (1975)
[22]COWLEY R.A., DOLLING G., *Conduction Electrons and Optic Modes of Ionic Crystals*, Phys. Rev. Lett., **14**, 549 (1965)

[23]MAKSIMENKO O. B., MISHCHENKO A.S., *On the nature of the phonon dispersion relations anomalies of IV-VI compounds*, J. Phys.: Condens. Matter, **9**, 5561 (1997)
[24]ROMERO A.H., CARDONA M., KREMER R.K., *et al.*, *Lattice properties of PbX (X=S, Se, Te): Experimental studies and ab initio calculations including spin-orbit effects*, Phys. Rev. B, **78**, 224302 (2008)
[25]KOHN W., *Image of the Fermi Surface in the Vibration Spectrum of a Metal*, Phys. Rev. Lett., **2**, 393 (1959)
[26]PISCANEC S., LAZZERI M., MAURI F., et al., *Kohn Anomalies and Electron-Phonon Interactions in Graphite*, Phys. Rev. Lett., **93**, 185503 (2004)
[27]CARDONA M., KREMER R.K., LAUCK R., et al., *Heat capacity of PbS: Isotope effects*, Phys. Rev. B, **76**, 075211 (2007)
[28]HABINSHUTI J., *Du nanocristal de PbSe a l'hetero-nanostructure PbSe/CdSe : Synthese chimique et caracterisation des proprietes physiques*, Thesis #40467, IEMN, USTL, Lille 1, France, (2011)
[29]*Handbook of mineralogy*: http://rruff.info/
[30]SWANSON H.E., FUYAT R.K., NAT C.S., *Standard X-ray diffraction powder patterns: carbonate*, Bur. Stand. Circ., *539*, U.S. CPO, Washington D.C., **2**, 18 (1953)
[31]MCCANN P.J., FUCHS J., FEIT Z., *et al.*, *Optical properties of ternary and quaternary IV–VI semiconductor layers on (100) BaF_2 substrates*, *J. Appl. Phys.*, **62**, 2994 (1987)
[32]SZE S.M., *Physics of Semiconductor Device*, New York, Wiley Interscience Publication, 848 (1981)
[33]HARDY A, WALTON R, VAISHNAV R., *Composition of eye cosmetics (kohls) used in Cairo*, *Int J Environ Health Res.*, **14**(1), 83 (2004)
[34]HARDY A.D., VAISHNAV R., AL-KHARUSI S.S., *et al.*, *Composition of eye cosmetics (kohls) used in Oman*, Jurnal of Ethnopharmacol, **60**(3), 223 (1998)
AL-HAZZAA S.A., KRAHN P.M., *Kohl: a hazardous eyeliner*, *Int Ophthalmol.*, **19**(2), 83 (1995)
PARRY C., EATON J., *Kohl: a lead-hazardous eye makeup from the Third World to the First World,* Environ Health Perspect, **94,** 121 (1991)
[35]LAWSON W. D., NIELSON S., PUTLEY E. H., *et al.*, *Preparation and properties of HgTe and mixed crystals of HgTe-CdTe*, J. Phys. Chem. Solids, **9**, 325 (1959)
[36]ROGALSKI A., *Infrared detectors: status and trends*, Progress in Quantum Electronics, **27**, 59 (2003)
[37]*Characteristics and use of IR detectors,* Hamatsu Photonics K.K. technical information SD-12, (2004)
[38]BLITZ H., BUSSMANN-HOLDER A., JANTCH W., *et al.*, *Dynamical Properties of IV-VI Compounds,* Springer-Verlag Berlin, Heiderberg, New York, Tokyo (1983)
[39]DALVEN R., *Electronic Structure of PbS, PbSe, and PbTe*, Sol. Stat. Phys., **28**, 171 (1974)
[40]RAVICH YU.I., EFIMOVA B.A., TAMARCHENKO V.I., *Scattering of Current Carriers and Transport Phenomena in Lead Chalcogenides,* Phys. Status Solidi (b), **43**, 11; **43**, 453 (1971)
[41]JANTSCH W., ROZENBERG J., HEINRICH H., *High field transport in PbTe*, Solid-State Electronics, **21**, 103 (1978)
[42]GERLACH E., GROSSE P., *Festkörpenprobleme*, **17**, 157 (1977)
[43]BAUER G., *Proc. Int. Conf. on the Application of High Magnetic Fields in Semiconductor Physics* (Clarenon, Oxford), 153 (1978); BAUER G., *Narrow Gap Semiconductors, Physic and Applications, Lecture Notes in Physics*, (Springer, Berlin,

Heidelberg, New York) **133** , 407 (1980); BAUER G., *Applications of High Magnetic Fields in Semiconductor Physics, Lecture Notes in Physics*, **177**, 259 (1980)
[44]HEINRICH H., *Narrow Gap Semiconductors, Physic and Applications, Lecture Notes in Physics*, (Springer, Berlin, Heidelberg, New York) **133**, 407 (1980)
[45]LISCHKA K., *Bound defect states in IV–VI semiconductors*, Appl. Physics, **A29**, 177 (1982)
[46]PREIER H., *Recent advances in lead-chalcogenide diode lasers*, *Appl. Phys.*, **20**, 189 (1979)
[47]HOLLOWAY H., *IV-VI Semi Conductor Photodiode*,Thin Solid Films, **11**, 105 (1980)
[48]HAAS D., HEINRICH H., JANTSCH W., *et al.*, *Comparison of PbTe diodes fabricated by epitaxial growth and by ion implantation of epitaxial layers*, Critical Reviews in Solid State Sciences, **5**, 547 (1975)
[49]BORRELLI, N. F., SMITH D.W., *Quantum confinement of PbS microcrystals in glass, J. Non-Cryst. Solids*, **180**, 25 (1994)
[50]KANE R.S., COHEN R.E., SILBEY R., *Theoretical Study of the Electronic Structure of PbS Nanoclusters*, J. Phys. Chem., **100**, 7928 (1996)
[51]SOMERS R.C., MOUNGI G. BAWENDI G., *et al.*, *CdSe nanocrystal based chem-/bio-sensor*, Chem. Soc. Rev., **36**, 579 (2007)
[52]TALAPIN D.V., ROGACH A.L., KORNOWSKI A., et al., *Highly Luminescent Monodisperse CdSe and CdSe/ZnS Nanocrystals Synthesized in a Hexadecylamine−Trioctylphosphine Oxide−Trioctylphospine Mixture*, Nano Lett., **1**, 207 (2001)
[53]DABBOUSI B.O., RODRIGUEZ-VIEJO J., MIKULEC F.V., *et al.*, *(CdSe)ZnS Core−Shell Quantum Dots: Synthesis and Characterization of a Size Series of Highly Luminescent Nanocrystallites*, J. Phys. Chem. B, **101**, 9463 (1997)
[54]BRUCHEZ M., MORONNE M., GIN P., *et al.*, *Semiconductor Nanocrystals as Fluorescent Biological Labels*, Science, **281**, 2013 (1998)
[55]CHAN W.C.W., NIE S., *Quantum Dot Bioconjugates for Ultrasensitive Nonisotopic Detection*, Science, **281**, 2016 (1998)
[56]JAISWAL J.K., SIMON S.M., *Potentials and pitfalls of fluorescent quantum dots for biological imaging*, Trends Cell Biol., **14**, 497 (2004)
[57]NAKAMURA S., SENOH M., NAGAHAMA S., *et al., InGaN-Based Multi-Quantum-Well-Structure Laser Diodes*, Japan J. Appl. Phys., **35,** L74 (1996)
[58]NAKAMURA S., FASOL G., PEARTON S.J., "*The Blue Laser Diode : The Complete Story"*, Springer (2000)
[59]http://www.blu-raydisc.com/
[60]ELLINGSON R.J., BEARD M.C., JONSON C.J., et al., *Highly Efficient Multiple Exciton Generation in Colloidal PbSe and PbS Quantum Dots*, Nano Lett., **5**, 865 (2005)
[61]SCHALLER R.D., KLIMOV V.I., *Non-Poissonian Exciton Populations in Semiconductor Nanocrystals via Carrier Multiplication*, Phys. Rev. Lett., **96**, 097402 (2006)
[62]SHOLIN V., BREEZE A.J., ANDERSON I.E.*et al.*, *All-inorganic CdSe/PbSe nanoparticle solar cells*, Solar Energy Materials ans Solar Energy Cells, **92**, 1706 (2008)
[63]CHOI J.J., LIM Y., SANTIAGO-BERRIOS M.B., *et al.*, *PbSe Nanocrystal Excitonic Solar Cells*, Nano Lett., **9**, 3749 (2009)

[64]ALLAN G., DELERUE C., *Confinement effects in PbSe quantum wells and nanocrystals*, Phys. Rev. B, **70**, 245321 (2004)

[65]ALLAN G., DELERUE C., *Role of impact ionization in multiple exciton generation in PbSe nanocrystals*, Phys. Rev. B, **73**, 205423 (2006)

[66]DELERUE C., ALLAN G., PIJPERS J.J.H., *et al.*, *Carrier multiplication in bulk and nanocrystalline semiconductors: Mechanism, efficiency, and interest for solar cells*, Phys. Rev. B, **81**, 125306 (2010)

[67]NOZIK A.J., *Spectroscopy and hot electron relaxation dynamics in semiconductor quantum well and quantum dots*, Annu. Rev. Phys. Chem., **52**, 193 (2001); NOZIK A.J., *Quantum dot solar cells*, Physica (Amsterdam), **14E**, 115 (2002)
[68]SCHALLER R.D., PIETRYGA J.M., GOUPALOV S.V., *et al.*, *Breaking the Phonon Bottleneck in Semiconductor Nanocrystals via Multiphonon Emission Induced by Intrinsic Nonadiabatic Interactions*, *Phys. Rev. Lett.*, **95**, 196401 (2005)
[69] SZENDREI K., GOMULYA W., YAREMA M.,*et al.*, *PbS nanocrystal solar cells with high efficiency and fill factor*, Appl. Phys. Lett., **97**, 203501 (2010)
[70]DE CICCO D., JOHNSON F. A., *The Quantum Theory of Lattice Dynamics. IV*, Proc. R. Soc. London Ser. A, **310**, 111 (1969)
[71]PICK R.M., COHEN M.H., MARTIN R.M., *Microscopic Theory of Force Constants in the Adiabatic Approximation*, Phys. Rev. B, **1**, 910 (1970)
[72] HELLMANN H., *Einführung in die Quantenchemie* Leipzig: Franz Deuticke. p.285 (1937); FEYNMAN R.P., *Forces in Molecules*, Phys. Rev., **56**, 4 (1939)
[73]SCHRÖDINGER E., *An Undulatory Theory of the Mechanics of Atoms and Molecules*, Phys. Rev. **28** , 1049 (1926)
[74]HARTREE D.R.: *The Wave Mechanics of an Atom with a Non-Coulomb Central Field. Part I. Theory and Methods*, Math. Proc. Camb. Phil. Soc., **24**, 89
The Wave Mechanics of an Atom with a Non-Coulomb Central Field. Part II. Some Results and Discussion, Math. Proc. Camb. Phil. Soc., **24**, 111
The Wave Mechanics of an Atom with a Non-Coulomb Central Field. Part III. Term Values and Intensities in Series in Optical Spectra, Math. Proc. Camb. Phil. Soc., **24**, 426
FOCK V., *Näherungsmethode zur Lösung des quanten-mechanischen Mehrkorperproblems*, Z. Physik., **61**, 126 (1930)
[75]SLATER J., VERMA H.C, *The Theory of Complex Spectra*, *Phys. Rev.*, **34**, 1293 (1929)
[76]PAULI W., *Über den Zusammenhang des Abschlusses der Elektronengruppen im Atom mit der Komplexstruktur der Spektren*, Z. Physik., 31, 765 (1925)
[77]FIOLHAIS C., NOGUEIRA F., MARQUES M., *A Primer in Density Functional Theory*, Springer-Verlag Heidelberg, Germany (2003)
[78]KOHN W., SHAM L.J., *Self-Consistent Equations Including Exchange and Correlation Effects*, Phys. Rev., **140**, A1133 (1965)
[79]HOHENBERG P., KOHN W., *Inhomogenous Electron Gas*, Phys. *Rev.*, **136**, B864 (1964)
[80]CEPERLEY D.M., ALDER B.J., *Ground State of the Electron Gas by a Stochastic Method*, Phys. Rev. Lett., **45**, 566 (1980)
[81]LANGRETH D.C., MEHL M.J., *Beyond the local-density approximation in calculations of ground-state electronic properties*, Phys. Rev. B, **28**, 1809 (1983); BECKE A.D., *Density-functional exchange-energy approximation with correct asymptotic behavior*, Phys. Rev. A, **38**, 3098 (1988)
[82]PERDEW J.P., CHEVARY J.A., VOSKO S.H., *et al.*, *Atoms, molecules, solids, and surfaces: Applications of the generalized gradient approximation for exchange and correlation*, *Phys. Rev. B*, **46**, 6671 (1992); PERDEW J.P., CHEVARY J.A., VOSKO S.H., *et al.*, *Erratum: Atoms, molecules, solids, and surfaces: Applications of the generalized gradient approximation for exchange and correlation*, Phys. Rev. B, **48**, 4978(E) (1993)
[83]DFPT: ZEIN N.E., Sov. Phys. Solid State, 26, 1825 (1984); BARONI S., GIANNOZZI P., TESTA A., *Green's-function approach to linear response in solids*, Phys. Rev. Lett., **58**,

1861 (1987); GONZE X., *Adiabatic density-functional perturbation theory*, Phys. Rev. A, **52**, 1096 (1995)
[84]BARONI S., GIRONCOLI S., DAL CORSO A., *Phonons and related crystal properties from density-functional perturbation theory*, Rev. Mod. Phys., **73**, 515 (2001)
[85]MESSIAH A., *Quantum Mechanics* (North-Holland, Amsterdam), p. 686 (1962)
[86]IHM J., ZUNGER A., COHEN M.L., *Momentum-space formalism for the total energy of solids*, C: Solid State Phys., **12**, 4409 (1979); IHM J., ZUNGER A., COHEN M.L., *Momentum-space formalism for the total energy of solids*, C: Solid State Phys., **13**, 3095 (1980)
[87]IHM J., *Total energy calculations in solid state physics*, Rep. Prog. Phys., **51**, 105 (1988)
[88]PICKETT W.E., *Pseudopotential methods in condensed matter application*, Comp. Phys. Rep., **9**, 115 (1989)
[89]PHILLIPS J.C., KLEINMAN L., *New Method for Calculating Wave Functions in Crystals and Molecules*, Phys. Rev., **116**, 287 (1959)
[90]PHILLIPS J.C., KLEINMAN L., *Crystal Potential and Energy Bands of Semiconductors. III. Self-Consistent Calculations for Silicon*, Phys. Rev., **118**, 1153 (1960)
[91]ANTONČÍK E., *Approximate formulation of the orthogonalized plane-wave method*, J. Phys. Chem. Solid, **10**, 314 (1959)
[92]TOPP W.C., HOPFIELD J.J, *Chemically Motivated Pseudopotential for Sodium*, Phys. Rev. B, 7, 1295 (1973)
[93]ABARENKOV I.V., HEINE V., *The model potential for positive ions*, Phil. Mag., **12**, 529 (1965)
[94]ABARENKOV I.V., HEINE V., *A new method for the electronic structure of metals*, Phil. Mag., **9**, 415 (1964)
[95]ANIMALU A.O.E, HEINE V., *The screened model potential for 25 elements*, Phil. Mag., **12**, 1249 (1965)
[96]ASHCROFT N.W., *Electron-ion pseudopotentials in metals*, Phys. Lett., **23**, 48 (1966)
[97]ASHCROFT N.W., LANGRETH D.C., *Compressibility and Binding Energy of the Simple Metals*, Phys. Rev., **155**, 682 (1967)
[98]ZUNGER A., COHEN M.L., *First-principles nonlocal-pseudopotential approach in the density-functional formalism: Development and application to atoms*, Phys. Rev. B, **18**, 5449 (1978)
[99]BACHELET G.B., HAMMAN D.R., SCHLÜTER, *Pseudopotentials that work: From H to Pu*, Phys. Rev B, **26**, 4199 (1982)
[100]TROULLIER N., MARTINS J.L., *Efficient pseudopotentials for plane-wave calculations*, Phys. Rev. B, **43**, 1993 (1991)
[101]TROULLIER N., MARTINS J.L., *A straightforward method for generating soft transferable pseudopotentials*, Solid State Commun., **74**, 613 (1990)
[102]http://www.fhi-berlin.mpg.de/th/fhi98md/fhi98PP/
[103]FUCHS M., SCHEFFLER M., *Ab initio pseudopotentials for electronic structure calculations of poly-atomic systems using density-functional theory*, Comput. Phys. Commun., **119**, 67 (1999)
[104]MONKHORST H.J., PACK J.D., *Special points for Brillouin-zone integrations*, Phys. Rev. B, **13**, 5188 (1976)
[105]CHADI D.J., COHEN M.L., *Special Points in the Brillouin Zone*, Phys. Rev. B, **8**, 5747 (1973)
[106]GONZE X., BEUKEN J.-M., CARACAS R., *et al.*, *First-principles computation of material properties: the ABINIT software project*, Comput. Mater. Sci., **25**, 478 (2002)

The ABINIT code results from a common project of the Université Catholique de Louvain, Corning Incorporated, and other collaborators *http://www.abinit.org*
[107]VERSTRAETE M. J., TORRENT M., JOLLET F., *et al.*, *Density functional perturbation theory with spin-orbit coupling: Phonon band structure of lead*, Phys. Rev. B, **78**, 045119 (2008)
[108]RESTA R., *Ab initio simulation of the properties of ferroelectric materials*, Modell. Simul. Mater. Sci. Eng., **11**, R69 (2003)
[109]BONINI N., LAZZERI M., MARZARI N., *et al.*, *Phonon Anharmonicities in Graphite and Graphene*, Phys. Rev. Lett., **99**, 176802 (2007)
[110]SVANE A., CHRISTENSEN N.E., CARDONA M., *et al.*, *Quasiparticle self-consistent GW calculations for PbS, PbSe, and PbTe: Band structure and pressure coefficients*, Phys. Rev. B, **81**, 245120 (2010)
[111]HUMMER K., GRÜNEIS A., KRESSE G., *Structural and electronic properties of lead chalcogenides from first principles*, Phys. Rev. B, **75**, 195211 (2007)
[112]PARKINSON D.H., QUARRINGTON J.E., *The Molar Heats of Lead Sulphide, Selenide and Telluride in the Temperature Range 20°K to 260°K*, Proc. Phys. Soc., London, Sect. A, **67**, 569 (1954)
[113]BEVOLO A.J., SHANKS H.R., ECKELS D.E., *Molar heat capacity of GeTe, SnTe, and PbTe from 0.9 to 60 K*, Phys. Rev. B, **13**, 3523 (1976)
[114]DÍAZ-SÁNCHEZ L.E., ROMERO A.H., CARDONA M., *et al.*, *Effect of the Spin-Orbit Interaction on the Thermodynamic Properties of Crystals: Specific Heat of Bismuth*, Phys. Rev. Lett., **99**, 165504 (2007)
[115]SERRANO J., KREMER R.K., CARDONA M., *et al.*, *Specific heat of Sb: Isotopic and spin-orbit effects from measurements and ab initio calculations*, Phys. Rev. B, **77**, 054303 (2008)
[116]SMITH G.D., FIRTH S., CLARK R.J.H., *et al.*, *First- and second-order Raman spectra of galena (PbS)*, J. Appl. Phys., **92**, 4375 (2002)
[117]KRAUSS T.D., WISE F.W., TANNER D.B., *Observation of Coupled Vibrational Modes of a Semiconductor Nanocrystal*, Phys. Rev. Lett., **76**, 1376 (1996)
[118]NANDA K.K., SAHU S.N., SONI R.K., *et al.*, *Raman spectroscopy of PbS nanocrystalline semiconductors*, Phys. Rev. B, **58**, 15405 (1998)
[119]MANCIU F.S., SAHOO Y., CARRETO F., *et al.*, *Size-dependent Raman and infrared studies of PbSe nanoparticles*, J. Raman Spectrosc., **39**, 1135 (2008)
[120]KIGEL A., BRUMER M., MAIKOV G., *et al.*, Superlatt. Microstruc. 46, 272 (2009)
[121]ARORA A.K., RAJALAKSHMI M., RAVINDRAN T.R., *et al.*, *Raman spectroscopy of optical phonon confinement in nanostructured materials*, J. Raman Spectrosc., **38**, 604 (2007)
[122]ROCA E., TRALLERO-GINER C., CARDONA M., *Polar optical vibrational modes in quantum dots*, Phys. Rev. B, **49**, 13704 (1994)
[123]Rolo A.G., Vasilevskiy M.I., *Raman spectroscopy of optical phonons confined in semiconductor quantum dots and nanocrystals*, J. Raman Spectrosc., **38**, 618 (2007)
[124]FU H., OZOLINŠ V., ZUNGER A., *Phonons in GaP quantum dots*, Phys. Rev. B, **59**, 2881 (1999)
[125]NEMANICH R.J., SOLIN S.A., MARTIN R.M., *Light scattering study of boron nitride microcrystals*, Phys. Rev. B, 23, 6348 (1981).
[126]KERN G., KRESSE G., HAFNER J., *Ab initio calculation of the lattice dynamics and phase diagram of boron nitride*, Phys. Rev. B 59, 8551 (1999)
[127]SERRANO J., BOSAK A., ARENAL R., *et al.*, *Vibrational Properties of Hexagonal*

Boron Nitride: Inelastic X-Ray Scattering and Ab Initio Calculations, Phys. Rev. Lett., **98**, 095503 (2007)
[128]KILIAN O., ALLAN G., WIRTZ L., *Near Kohn anomalies in the phonon dispersion relations of lead chalcogenides*, Phys. Rev. B, **80**, 245208 (2009)
[129]KRAUSS T.D., WISE F.W., TANNER D.B., *Observation of Coupled Vibrational Modes of a Semiconductor Nanocrystal*, Phys. Rev. Lett., **76**, 1376 (1996).
[130]GIANNOZZI P., BARONI S., BONINI N., *et al., QUANTUM ESPRESSO: a modular and open-source software project for quantum simulations of materials*, J. Phys. Condens. Matter, **21,** 395502
[131]MOREELS I., ALLAN G., DE GEYTER B., *et al.*, *The Dielectric Function of Colloidal Lead Chalcogenide Quantum Dots Obtained by a Kramers-Kronig Analysis of the Absorbance Spectrum*, Phys. Rev. B, **81**, 235319 (2010)